An investigation of the influence of radiographic malpositioning and image processing algorithm selection on ICU/CCU chest radiographs

AN INVESTIGATION OF THE INFLUENCE OF RADIOGRAPHIC MALPOSITIONING AND IMAGE PROCESSING ALGORITHM SELECTION ON ICU/CCU CHEST RADIOGRAPHS

AHMED M S B ELHAIN

Submitted for the degree of Master of Philosophy

UNIVERSITY OF BRADFORD

2013

Abstract

Key words: ICU/CCU chest radiography, chest tubes and lines malpositioning, image processing algorithm.

Mobile chest radiography remains the most appropriate test for critical care patients with cardiorespiratory changes and with patients who have chest tubes and lines as a monitoring tool, and to detect complications related to their use.

However, one of the most frequent issues recognized radiographically with patients in critical care is chest tubes and lines malposition. This can be related to technical quality reasons which can affect their appearance in the chest radiography.

This research considers how the technical quality of the ICU/CCU chest radiography can impact upon the appearance of chest tubes/lines and how that appearance can impact on the decision making.

Results show that the methods used in the chest phantom experiment to estimate the degree of angulation have a large effect upon the appearance of anatomical structures, but it does not have a particularly large effect upon the apparent changes of tube/line position central venous catheter and endotracheal tube (CVC, ETT).

The study also shows that there was a little difference between the two image processing algorithms, apart from the visualisation of sharp reproduction of the trachea and proximal bronchi, which was significantly better using the standard algorithm compared to the inverted algorithm.

The two methods used to estimate the degree of angulation and the apparent position of the CVC/ETT on 17 mobile chest radiographs provide limited useful information to the image interpreter in estimating the degree of angulation and degree of malpositioning of the tube and line.

Acknowledgements

First and foremost I would like to offer my sincerest thanks to both of my supervisors, Andy Scally for his invaluable academic, patient, and constructive guidance from the commencement of my research. Also to my second supervisor Professor Neil Small for his kind supervision and continuous encouragement. Without their extensive assistance and unlimited support this research would not have been completed.

I would also like to extend my thanks to Professor Maryann Hardy who supported me at the first stage of my research journey.

I would like to offer my thanks and my love to my parents and my wife Hajer for their patience, moral support and prayers. I will never forget my lovely children Abdulrahman, Rahaf and Yusuf with sincere apologies for my long absence.

Special thanks to Dr Beverley Snaith, Gary Culpan and all my colleagues at School of Health Studies University of Bradford.

Table of Contents

List of Tables

List of Figures

List of Graphs

1 Chapter One: Introduction

The human chest contains important anatomical structures (heart, lungs, diaphragm, trachea, ribs, scapula, breast, hila, and aortic knuckle). Many signs of diseases can be found in the chest through radiographic imaging (Briggs, 2004). The natural contrast (i.e. different tissue densities) of the thoracic cavity enables the clinicians, through chest imaging, to assess numerous disorders; thoracic abnormalities involving the heart, pleura, lungs, tracheal tree, oesophagus, thoracic lymph nodes, thoracic vertebrae, chest wall and upper abdomen (Mehta et al., 2010).

Many tubes and lines (endotracheal tube, central venous line, Swan-Ganz catheter, thoracostomy tube and Nasogastric tube) are passed through the chest of the intensive care unit patient (ICU) and coronary care unit (CCU), for many purposes. For example, feeding tubes, fluid infusions, drug admission, mechanical ventilation, and monitoring atrial pressure (Moskowitz, 2010).

However, because the patients in the ICU often have many devices, tubes, and lines connected to them to keep monitoring their status, it is often difficult to transport the patient to the radiology department (Rubinowitz et al., 2007). Therefore, mobile chest radiography is one of the simplest tests used in the ICU to assess the cardiopulmonary condition of the patient, detecting the appropriate position of tubes and lines, as well as monitoring devices (Eisenhuber et al., 2012).

As a result of the use of tubes and lines, many complications can occur during and after the insertion of chest tubes and lines (Aronchick and Miller, 1997). The malposition of chest tubes and lines is one of the issues that can negatively impact on patients, especially in ICUs and surgical departments (Aronchick and Miller, 1997). A study by Tolsma et al (2011) found that 33.5 % of 534 ICU chest radiographs showed abnormalities such as pleural effusion, atelectasis, consolidation, a widened mediastinum, and malposition of invasive devices.

This research considers how the technical quality of the intensive care unit chest radiography can impact upon the appearance of chest tubes and lines and how that appearance can impact on the decision making with regard to patients' clinical situations.

The report of this research will include seven chapters:

Chapter one will include an introduction to chest radiography, methodology of the study and a short description about the chest phantom experiment, a comparison between two methods to estimate the degree of angulation for rotation, kyphosis and lordosis on 17 mobile chest radiographs and observer study.

Chapter two will include evidence relevant to the study, what has been studied before this study, complications of chest tube and line malposition, technical considerations, technology, changes in work patterns due to developing of radiographic image acquisition**,** and how the geometry of technique employed can influence the radiographic image (distortion). It will also offer a justification for the study and will identify the gaps in the literature in relation to this study.

Chapter three will include background literature on the history of x-ray, image technology and changing from analogue to digital, and image processing of film/screen and digital image. It will also include a background on chest anatomy, chest tubes/lines.

Chapter four will include an identification of degree of angulation (rotation, kyphosis and lordosis) and also to identify apparent movement of tube/ line position with degree of rotation and kyphotic/lordotic angulation. It will describe details of conducting the experiment, supported by figures, will extract the results of the experiment and discuss them.

Chapter five will include a comparison between two methods to estimate the degree of angulation for rotation, kyphosis and lordosis on 17 mobile chest radiographs. It will include a report of materials and methods, results and discussion.

Chapter six will include an introduction to the observer study on the chest tubes/lines algorithms. Materials and methods, results and discussion will be presented.

Chapter seven will include general conclusion and suggestions for further work.

1.1 General introduction and methodology of study

1.1.1 Chest radiography

Until recently, the conventional chest radiograph had remained the most common performed examination for chest imaging (Mehta et al., 2010). The natural contrast of the thoracic cavity enables the clinicians through chest imaging to assess numerous disorders, thoracic abnormalities involving the heart, pleura, lungs, tracheal tree, oesophagus, thoracic lymph nodes, thoracic vertebrae, chest wall and upper abdomen.

The chest radiography allows detection of chest diseases and monitoring of their responses to therapy in both acute and chronic illnesses. For these reasons, the standard chest radiography should almost always be the first radiologic study requested for evaluation of diseases of the thorax (Mehta et al., 2010).

In addition, obtained at the time of admission to hospital and in the preoperative setting has been a common practice and essential diagnostic tool to help direct the optimal care of critically ill patients (Tarrac, 2009).

1.1.2 Mobile chest radiography

Mobile chest radiography remains one of the simplest tests used in the intensive care unit (I.C.U) to assess the cardiopulmonary condition of the patient, to detect the appropriate position of tubes and lines and to monitor devices(Moskowitz, 2010). Because the patients usually have many serious and complicated medical issues many devices, tubes, and lines are connected to patients to keep monitoring their status and, as a result, it is difficult to transport the patient to the radiology department (Rubinowitz et al., 2007).

Therefore, other imaging modalities such as computed tomography (CT), ultrasound (US), magnetic resonance imaging (MRI) and nuclear medicine are limited in their use for examining patients in the intensive care unit in order to avoid any morbidity resulting from moving the patients from the intensive care unit

into radiology department or disconnecting any life supporting device such as automatic ventilation, pulmonary artery pressure by the central venous catheter (Tocino, 1996).

In addition, for patients who are undergoing mechanical ventilation, who are unstable hemodynamically or who are under invasive procedures, mobile chest X-rays are cost-effective compared with other imaging modalities like computed tomography (CT) or magnetic resonance imaging (MRI) (De Lacey et al., 2008).

Moreover, conventional chest radiography it is valuable time investment through reducing the delay in timely delivery of care compared with other imaging procedures such as (CT) or (MRI)(Mehta et al., 2010). Furthermore, the radiation dose received from the conventional chest imaging is one hundred times less than the dose received from computed tomography. A conventional chest CT scan with slice thickness of about 5 mm would give about 2 mSv (200 mrem) and a helical CT of the chest about 8 mSv (800 mrem) as compared with a standard CXR's effective dose of 0.06 mSv (6 mrem) (Mehta et al., 2010) .

However, one of the most frequent issues recognized in relation to radiography with patients in the intensive care unit is the assessment of chest tubes and lines malposition (Aronchick and Miller, 1997). It can be related to technical quality reasons which can affect the appearance of the tubes and lines in the mobile chest radiography (Foos et al., 2011). Difficult positioning of patients in the critical care can lead to rotation the patient(De Lacey et al., 2008) and that can produce distortion in the cardiac shadow and other anatomical structures such as ribs, clavicles and trachea shadow (Moskowitz, 2010).

Kyphotic and lordotic patients in the intensive care unit can lead to overlapping (I.e. apart or portion of anatomical structure extend over another) (Leroux et al., 2002) therefore, the anatomical features of the chest structures will change in the radiographic image. Because most of the patients in the intensive care unit are not able to co-operative by virtue of their anaesthetised state, the anterior posterior supine position is the typical position (Eisenhuber et al., 2012)and that can make it difficult to evaluate heart size due to the short distance between the source of

radiation and the image receptor and also because the gravity factor, which can make the heart size appear larger than in the posterior anterior position (Moskowitz, 2010).

In addition, there are limitations in detecting diseases by supine mobile chest radiography. Many complications in the intensive care unit occur commonly as (consolation, pulmonary oedema, aspiration, infection and haemorrhage), radiographic information with such complications is not sufficient to justify treatment for the patient.

Another issue of disease detection by mobile chest imaging is the difficulty of distinguishing pleural effusion from consolidation or collapse in the posterior lung base. This is common in supine position and leads to increase radio opacity at the lung bases (Savoca et al., 1978).

1.2 Philosophical approach of radiology

1.2.1 Epistemology

"Epistemology (from the Greek episteme= knowledge) is the theory of knowledge, and epistemological questions are those which concern what can be known about the world" (Wulff et al., 1986). Ladyman (2002:5) defines epistemology as "a branch of philosophy that an inquiry into knowledge and it is justification". With more explanation Bakker and Clark (1988:5) have said that "epistemology has, through the centuries, attempted to clarify not only the meaning of explanation but also the meaning and relationships of concepts such as knowing, truth, validity and the like".

Alternatively, epistemology has focused on what is required for knowledge rather than focus only on what it is to claim the truth "it is a defining characteristic of knowing" (Greetham, 2006). Specifically, Ladyman (2002:6) states that "knowledge is a justified true belief".

Subjectively, belief based on psychological experience, could be admitted as approaching knowledge. But truth is the objective part we have acquired as a knowledge based on real facts without any effects like personal belief or the subjective sense we make of things (Greetham, 2006).

Accordingly the main questions which are addressed by the epistemological approach are: What is knowledge? how is knowledge acquired and how do we know what we know? (Greetham, 2006). So, in this regard, the answer related to clinical radiology could be that knowledge is what is seen in the radiographic image (shadows of bones, soft tissues, organs, gases, fluids, calcifications). All this information, and a belief that observational information or shadows are true, is used to make a correct diagnosis for the case of the patient, who has been examined.

Secondly, what is seen in the radiological image is based on the experience acquired. For example, radiologists have studied anatomy of the human body, physiology, pathology, histology and medical physics. They have seen many normal and abnormal radiographic images and therefore they have become experts in their field.

Medical practitioners do not rely on direct observation. They use sense-extending instrument, like X-ray, CT scan and MRI to observe unseen causes which cannot be directly observed(Gifford, 2011).

Also sense is used to obtain information, which is used to make judgments about the truth of the diagnosis. For example, in the radiographic images, the radiologists utilize the image present on the radiograph in order to give a distinct and clear description about the inside of the body (Marwede and Fielding, 2005).

1.2.2 Objectivity

"Objectivity in simple terms refers to a lack of bias or prejudice. Objectivity is associated with claims to authority, universality and detachment. It typically is linked with an empiricist use which assumes that facts and values can or should be separated from each other" (Robson, 2002).

As a result, to achieve truth-based on objective components requires testing using methods of natural science either to find proofs to support the result or to approach the truth or to find a generalisable theory. "Theory is a proposed explanation for phenomena, or sets of occurrences, or relationships. It is a statement describing how some part of the world works. To be a scientific theory, it has to be testable" (Robson, 2002) without any prejudice. Additionally, interpretation and reflection are methods that can be used to approach the subjective truth (Wulff et al., 1986).

In addition, O'Hear (1980) suggested that our experience and objectivity is based on an inductive approach, from collecting observations to generalized conclusion. "The inductive approach is the process of making conclusions from the specific and concrete to the general and abstract" (Robson, 2002), or using what is known from prior knowledge to recent or future knowledge; while deduction moves from more general to more specific approaches (Bakker and Clark, 1988). Therefore, it seems to be that deduction and induction approaches can be used together to achieve the truth (Greetham, 2006).

However, using an inductive approach based on the method of observation to generalise conclusions, can produce a false truth. The following example (Bakker and Clark, 1988) illustrates this, the induction that all swans are white due to the observation that each swan that you have seen is white, becomes false due to the discovery of a black swan.

1.2.3 Objectivity related to clinical radiology

According to the objective approach to the truth in clinical radiology, the radiographic image, which is observed by the radiologists in the medical field in order to produce accurate diagnosis it based on the inductive theory. Sarvazyan et al. (1991:327) stated that "following signal processing, the image information is displayed to the eye and, fundamentlly, the process which takes place is the transfer of information from within the body of the patient to the mind of the radiologist, whose other principal task is to interpret and convey the information".

The result of what the radiologists has seen (by observation) in the radiographic image, using their prior knowledge (previous experience) and without any influence from feeling or common sense, is used to describe what they found in the recent image and to write their report or results. That is the knowledge or information which they need to generalise.

Therefore, this process starts from more general knowledge, what radiologists have acquired during their work (observing a lot of radiographic image) for a period of time (previous experience) and moves to more specific knowledge, which is the diagnosis they established to be the result of the recent radiographic image (Bakker and Clark, 1988).

In order for the radiologists to write a report for a leg X-ray they should have background about what findings should be normal and what findings abnormal (is this a fracture or not, is this lesion or normal anatomical feature?), so that, based on this experience, they can draw out the final result or report to help the other medical staff to give the appropriate treatment for the patient.

Alternatively, to be only relying on the previous experience (background about normal and abnormal anatomical radiographic images) through the observation activity could be false. Because simply what the radiologists have decided and believe is normal or abnormal, could after a period of time be false.

There may be new findings that would appear in the radiographic images and face the radiologists with something that does not connect with their previous experience.

Therefore, there is a limit to the use of observation to achieve the result of the clinical exam. Consequently, induction may be used. Russell (1927) said that, imagine A and B have always been seen together, so if A is present again, B will probably also be present. For example, related to clinical radiology, it is not necessary when the radiologists have found a fracture in the calcaneus bone to find a compression fracture in the lumbar vertebras because they usually have seen a calcaneus fracture associated with lumbar spine vertebral compression fractures (Mattu, 2010).

The effectiveness of the modern methods of imaging does not just rely on the quality of the device but, in addition, on the intuition and skills of the radiologists (Sarvazyan et al., 1991). Therefore, to find an appropriate solution for a problem they should refer to differential diagnosis by using either radiological equipments like CT scan (Computed Tomography scan), MRI (Magnetic Resonance Imaging), ultrasound (US) or laboratory tests to discover new findings. They then should justify those findings by observing this phenomena and finally they can establish the new findings and generalise new knowledge in order to improve health care services.

1.2.4 Justification

“In the standard analysis knowledge is defined to be justified true belief. A justification involves three components, namely the foundational as a statements that form the premises of justification, the collection of acceptable logical procedures or rules of inference from the foundational statements and a non-logical and non-linguistic rational authority that establishes the truth of the foundational statements”(Jarvie et al., 2006).

In this sense, identify that a belief is true based on justification from the support of gathering evidence and making observations (Ladyman, 2002). Greetham (2006: 62) maintained that “the reasons must support, or be evidence for, the truth of what you believe”. Consequently, justification as a part of epistemology seeks to make logic knowledge in order to achieve truth. In contrast, not all we believe can be true and also it is not necessary that all we do not believe is not true (Greetham, 2006). That is what science seems to provide, a systematic way to develop and test theories, even if it is not true, and the promise of real explanation of a phenomena (O'Hear, 1980).

1.2.5 Justification related to clinical radiology

In the medical field clinical radiology has tried to find the difference between normal and abnormal information in the radiographic image. The radiographic image, which we use in the medical field in order to diagnosis diseases, contains many items of information, or shadows of anatomical parts. The radiologist believes what they have seen in the radiographic image because it is truth related to them from evidence and observations (Greetham, 2006).

The source of evidence in clinical radiology has been produced as a result of experience and logical knowledge, based on observations. For example, in the chest X-ray the radiologists have the ability to identify the shadow of the heart or lungs because it is logical knowledge for them and they have studied the anatomy of the human body, and they know the normal position for every anatomical part in the human body.

Therefore, the radiologists could describe the reason for many diseases based on what they believe in the radiographic image. This is the epistemological approach. In addition, in medical imaging research, a significant focus is often on exploring, using an appropriate quantitative methodology, the degree to which an imaging system can achieve some reference standard in which we have a greater degree of trust, or that we think is close to the truth.

1.2.6 Empiricism theory

"A school of thought claiming that experience via the senses is the source of all knowledge. It is characteristic of positivism generally (i.e. positive data obtained through the senses) (Comte and Lenzer, 1998) . However, empiricism is also the basis for phenomenology which relies on the observation of evidence" (Robson, 2002). It is based on sensory experience with observation, to justify the knowledge (Greetham, 2006). Related to the philosophy of medicine Wulff et al (1986) have stated that clinicians in the medical field have been influenced by empiricism theory and their knowledge has been developed from a sequence of observations.

The number of empiricists increased in the seventeenth and eighteenth centuries and the theory of empiricism has been used widely in all scientific fields (Wulff et al., 1986). Empiricists stated that only by our experience we can make claims for what we are acquainted with (Bakker and Clark, 1988). This scientific notion is also stated by Popper, "Popper's account of scientific theories is based on the idea that our general theories are tested by making particular observations" (O'Hear, 1980).

In addition, Popper has suggested that the first stage in investigating any phenomena is not by observation but by making testing hypotheses to be examined by experiments and observations (Wulff et al., 1986). However, observation is not enough of a source to claim the validity of empiricism (Popper, 1963). Moreover, Popper (1963) maintained that most assertions are not based on our observations, but on all kinds of other sources, for example by reading.

1.2.7 Empiricism theory related to clinical radiology

In this sense, and related to clinical radiology via observing the phenomena in the radiographic image, experience is very important in producing the final report or diagnosis by the radiologists. So, "radiologists are required to describe the complexes of shadows, densities and contrast enhancements subsequently providing what amounts to the appearance of a body structure in a clinical context and what those appearance represent in reality" (Marwede and Fielding, 2005).

However, there is a limit to the degree to which any kind of observation relates to an underlying 'truth'. The aim in radiological science is to close this gap. Moreover, a medical imaging (radiography) does not provide us with direct information (by direct observation) of patient anatomy or pathology. It is obtained by using certain physical principles (properties of x-rays, sound waves, radio waves, etc) in order to produce a visual pattern that provides information of underlying anatomy, pathology etc and that what is believed to be true or close to truth and therefore, it is used to diagnosis the case of the patient.

1.2.8 Positivism

The result of using sense experience to justify knowledge, which is the result of reading or observing the radiographic image, leads us to a concept that was developed in the early 19th century by the philosopher and founding sociologist, Auguste Comte. The concept is called positivism. The purpose of this school of thought was to put more emphasis on direct experience, and build on the positive data obtained through the senses (Comte and Lenzer, 1998).

Positivism has been defined by Robson (2002:550) as "A school of thought seeing reality as the sum of sense impressions, equating social sciences with natural sciences, employing a deductive logic and quantitative research methods. An extremely influential intellectual trend from the mind-nineteenth century, forming, until recently, the generally accepted view of science.

Although some social scientists still take this position, it is widely discredited by methodologists and philosophers of science". Social scientists are critical of the range of perspectives and philosophies that holds that positivism is the best approach to detect and describe physical and human events.

In addition, there is a trend in the philosophy which declares natural (experimental) sciences to be the only source of true knowledge and refuses to value the knowledge of philosophical study (Bakker and Clark, 1988). As a result, positivism is apart from empiricism theory, in dealing with 'positive facts' without any intuition

or revelation (Comte and Lenzer, 1998). Greetham (2006) has stated that in the seventeenth, eighteenth and nineteenth centuries philosophers have turned their attention to the study of the human mind to consider its ability to reason.

Consequently, this approach leads to a concept called 'logical positivism' or 'logical empiricism'. This concept has risen from the work of a group called 'Vienna Circle' (Greetham, 2006). Greetham (2006) maintained that logical positivism is also recognised as logical empiricism or scientific empiricism, because it is a notion in philosophy that has combined empiricism theory and the observational approach necessary to a achieve knowledge with the notion of rationalism This argues that not all our knowledge has been acquired only by the observational approach.

1.2.9 Positivism philosophy related to clinical radiology

Regarding clinical radiology, the truth should be based on sense experience from what has been seen in the radiographic images and from this we establish that knowledge as truth. For example, we use our senses to obtain information which we then use to make judgments about truth.

Alternatively, this truth is what we have seen in radiographic image. For example, an abdomen X-ray could show that there is no lesion (a sign for disease in the film) but in fact the patient is still suffering. In this case, to rely only on this experience or this exam, is not enough to approach the truth, which is the proper diagnosis to the patient.

1.2.10 Conclusion of the philosophical approach

In clinical radiology, it seems to be that we cannot rely only on the experience through the observational approach in the radiographic image and also we cannot rely only on the radiographic image or the information on it to diagnosis the diseases for achieving the truth. And as a result we are sometimes deceived by imaging system, because for example pathology there are signs and symptoms are

very clear, but the imaging system does not generate any information produced by it and therefore it is difficult to detect them.

In addition, to approach the truth by using an experienced view could not be enough, especially when the radiologists observe new findings in the radiographic image and these findings were not related to their previous experience. Therefore, medical practitioners have preferred to do differential diagnosis either by using radiological equipments like CT scan (Computed Tomography scan), MRI (Magnetic resonance Image), ultra sound or laboratory tests to discover the new findings and justifying those findings by observing this phenomenon. They can then establish the new findings and generalise new knowledge in order to improve health care services.

1.3 Methodology and research questions:

1.3.1 Introduction

Mobile chest radiography remains the most appropriate test for critical care patients with cardiorespiratory changes and for patients who have chest tubes and lines as a monitoring tool, and to detect complications related to the use of supporting devices (Wallace , 1997).

Because the patient in the intensive care unit is connected often to the bedside by life supporting devices, it is difficult to transport the patients from the intensive care unit to the radiology department (Rubinowitz et al., 2007). Therefore, mobile chest radiography can reduce morbidity which may occur due to patient transport and to disconnecting the monitoring devices from the patient (Tocino, 1996).

However, one of the most frequent issues recognized radiographically with the patients in the intensive care unit is chest tubes and lines malposition (Aronchick and Miller, 1997).

Difficult positioning of patients who are not able to co-operate by virtue of their anaesthetised state can lead to rotation of the patient (De Lacey et al., 2008) and that can produce distortion in the cardiac shadow and other anatomical structures such as ribs, clavicles, trachea shadow (Moskowitz, 2010). In addition,

kyphotic/lordotic patients in the intensive care unit can lead to overlapping in the radiographic image (Leroux et al., 2002).

Therefore, the technical quality of mobile chest radiography might have an impact upon the appearance of the anatomical structures and the chest tubes and lines in the mobile chest radiography (Foos et al., 2011).

Because most of the patients in the intensive care unit are not able to co-operate by virtue of their anaesthetised state the anterior posterior supine position is the typical position and that can make it difficult to evaluate heart size due to gravity (Moskowitz, 2010).

Digital imaging has developed rapidly recently with many advantages such as a wide dynamic range of the recording system to postprocess the images by adjusting the window level to enhance the image (i.e. to allow the clinician to change contrast to lighter or darker, enhancement of superimposed various textures on images and enlarge images), more efficient data storage, elimination of the photographic process (dark room), make possible image acquisition in real time and communication with other practitioners by using the picture archiving and communications system (PACS) (Bacher et al., 2006).

Although digital imaging has improved some aspects of technical quality (for example, optimisation of image density and contrast), the ease of distribution of the image, through the PACS system, has led to decision making taking place without consulting face to face with those with expertise (Larsson et al., 2007). Clinicians action can be poor as a result of less communication (Watkins et al., 2000).

Many studies have been published about digital imaging developing (De Boo et al., 2011), (Hamer et al., 2005), (Strotzer et al., 2002), and the impacts of digital imaging upon the work place, chest image quality and radiation dose. However there is no study that has evaluated how the technical quality of the mobile chest radiography can impact on the appearance of chest tubes and lines.

1.3.2 The primary research question

How the technical quality of the ICU chest radiography can impact on the appearance of chest tubes and lines. Does that appearance impact on decision making?

1.3.3 The secondary research question

Do the alternative algorithms designed for ICU chest radiography impact on the appearance of chest tubes and lines? Do the alternative algorithms allow different decision making?

1.3.4 An identification of degree of angulation (rotation, kyphosis and lordosis) and apparent of chest tube/line movement on chest phantom

The purpose of conducting this experiment will be to identify the measurements of rotation, kyphotic and lordotic degrees related to the chest anatomical structures, chest tubes and lines. Therefore, the experiment will quantify the degrees of angulation (rotation, kyphosis and lordosis) by identifying measurements of anatomical symmetry on the chest phantom and their consistency with one another. In addition, to identify apparent movement of tube/ line position with degree of rotation and kyphotic lordotic angulation.

1.3.5 A comparison between two methods to estimate the degree of angulation for rotation, kyphosis and lordosis on 17 mobile chest radiographs

Seventeen ICU/CCU mobile chest radiographs have been collected to apply the measurements used in the chest phantom experiment. The methods used on the chest phantom were compared with those used on the 17 mobile chest radiographs to estimate the degree of malpositioning (rotation, kyphosis and lordosis) in the 17 chest mobile radiographs and their assistance to measure the malpositioning in clinical practise to inform interpretation.

1.3.6 Observer study

This stage will be an experiment on 17 digital mobile chest radiographs for patients in critical care who have at least 2 inserted tubes or lines. The chest radiographs should be of good quality. In this study because lungs field and pulmonary diseases are the most evaluated in the chest images and that may not appropriate to visualize chest tubes and lines (Nodine et al., 1996).

Therefore the goal of this stage is to compare two algorithms for localizing chest tubes and lines and standard CEC image quality criteria in the 17 mobile chest radiographs.

2 Chapter Two: Literature review

2.1 Introduction

In order to understand and answer the research question mentioned in the introduction chapter, it is imperative to do an extant literature review on this discipline. This chapter will therefore discuss the key topics in the subject area, namely- complications of chest tube and line malposition, technical considerations, evaluation of x-ray imaging technology, changes in work patterns due to developing of radiographic image acquisition. The chapter will conclude by justifying the study by identifying the research gap in the field.

2.2 Complications of chest tube and line malposition

Yilmazlar et al (1997) researched into the complications of 1303 central venous catheter canulations (CVC), and found that 68 (5.2 %) of patients had an arterial puncture. There was arrthymias in 21 (1.6 %) patients, cardiopulmonary arrest in 1 (0.1 %) and pneumothorax in 5 (0.5 %). The study also showed that the tip of the CVC was incorrectly located in 149 (11.2 %) patients, where 117 patients had it malpositioned in the right ventricle, 18 in the right atrium and 14 in the external or internal jugular vein.

However, Yilmazlar et al.'s (1997) discussion was very brief and failed to link data on the malposition of the lines and patients' complications, so there is a difficulty in recognizing which complication has occurred due to which malposition. The study also mentioned that posterior-anterior chest radiographs were obtained for all patients in the ICU and operating room. The question needs to be asked if all the patients are able and willing to adopt the position for a posterior-anterior chest radiograph. The radiographic positioning references state that the anterior posterior position is the appropriate position for patients in a critical situation, when they cannot stand to do a posteroanterior view (Henschke et al., 1997).

Moskowitz (2010) mentioned that if the catheter tip is located in the proximal third of the superior vena cava it can lead to thrombus and if the tip is located too distally it can enter the atrium, potentially producing ventricular arrhythmias or even cardiac perforation.

Vahid et al (2007) outlined a case report about the malposition of central venous catheters in left superior intercostal veins, as detected by chest radiography (anterior-posterior on admission to the ICU showed the catheter in a left paramedian position and lateral showed the catheter to curve posteriorly) and confirmed by chest computed tomography with intravenous contrast Figure (2-1).

Figure 2-1: Malposition of central venous catheter in left superior intercostal vein.

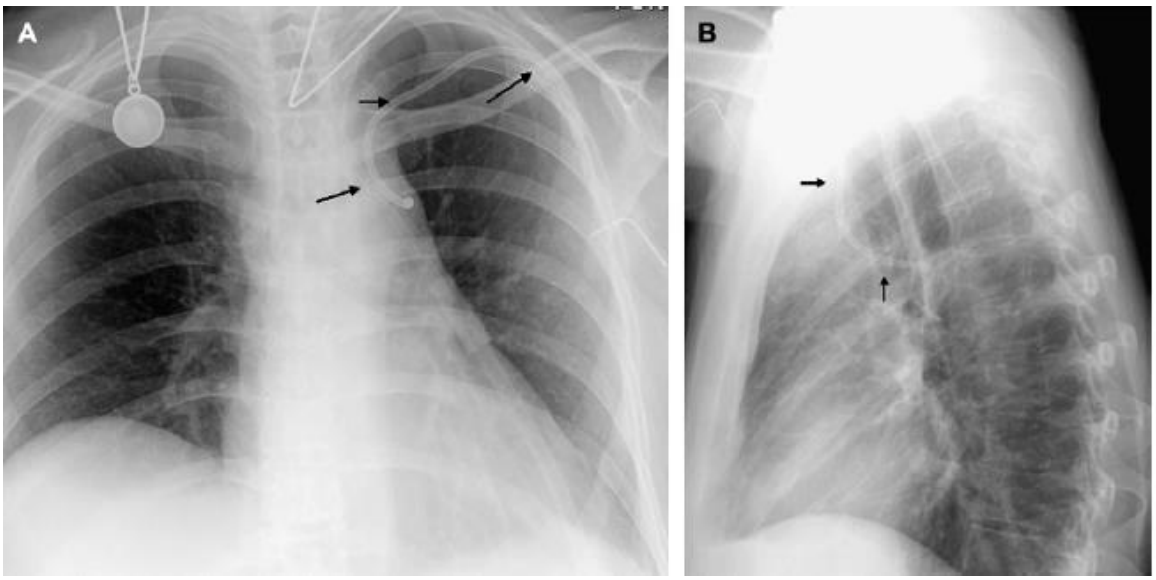

(A) Chest radiography anterior view showing the in the left paramedian position. (B) Chest lateral view showing the catheter to curve position.

Zaman et al (1990) looked at cases where the central venous catheter was malpositioned during the insertion in the left pericardiacophrenic vein. They also stated that using an anterior-posterior chest radiograph the CVC can be seen lying along the left pericardial border, but with lateral chest radiography the CVC can be seen superimposed on the middle mediastinum.

Orme and McSwiney (2007) found an example of a fatal cardiac tamponade that occurred due to peripherally inserted central venous catheters. The catheter migrated from the right atrium within 24 hours of the insertion, which led to the release of the solutions into the pericardial space, leading to less pulse activity and subsequently, ventricular fibrillation. On the fourth postoperative day the patient died. The study recommended chest radiography to confirm the location of the catheter tip before the infusion of any fluids.

However, Vahid et al (2007), Zaman et al (1990) and Orme and McSwiney (2007) were addressing unusual cases, which give information which is very rare, and as a result provides little basis for generalisation (Greenhalgh, 2001). Another weakness is that there is no explanation of how technical quality can impact upon the appearance of the CVC and lead to misinterpretation of the chest radiograph.

A study by Bankier et al (1997)found that in 16 (1.2%) of 1287 chest radiographs the central venous catheter was malpositioned in the azygos arch, and in three cases of this 16, there were venous perforation complications. The study suggested that the frequency of the azygos arch cannulation is dependent on the anatomical site of the catheter insertion.

A study by Haygood et al (2011) aimed to check the accuracy with which radiologists reading posteroanterior chest radiographs differentiate between whether a central venous line is in the superior vena cava or the azygos vein. This study also looked at the circumstances in which radiologists may omit lateral views when determining the position of a central venous catheter. The study addressed the important technical point that, on anterior posterior chest radiographs, because the azygos vein mouth is superimposed on the superior vena cava, the malpositioning of the tip of the central venous line can be misinterpreted.

However, this study used a process that was not robust because all the observers were radiologists. The interpretation experience of clinicians or radiographers is lower than that of radiologists who are the most experienced medical staff in reading radiographic images (Foos et al., 2011). Another problem with this study is that it was conducted in two locations with two different image station tools used for reviewing the images; this can impact on the technical quality of the visualization of the chest image and therefore the diagnosis.

A study by Kearney and Shabot (1995) was conducted to determine the incidence rate, risk factors, and proper management protocols for pulmonary artery ruptures associated with the Swan-Ganz catheter. The study involved 32,442 in-patients requiring hemodynamic monitoring with a Swan-Ganz catheter, in the period 1975-1991. Ten patients sustained pulmonary artery rupture. However, the authors did not provide data about the malpositioning of the catheter, which might have been the cause of the pulmonary artery rupture. Although these results were based on data from 18 years ago, they are still relevant.

Tocino (1996) stated that there are two complications that can occur due to ETT intubation. Malpositioning of the ETT within the right main bronchus can lead to the most common complication; inadequate ventilation of the left lung. This occurs in approximately 10% of malpositioning cases. The second complication is the long term effects after the insertion of the ETT, such as nosocomial infection, atelectasis and sinusitis.

A study by Brunel et al(1989) looked at 219 patients in a critical situation to examine the accuracy of chest radiography and physical examination in assessing the proper position of the endotracheal tube. The results showed that 14 % of patients needed repositioning of the endotracheal tube. Brunel al recommended post intubation chest radiography for all ICU patients because physical examination is unreliable.

A study by Marik and Janower(1997) mentioned that in 24% of 174 ICU chest radiographs the ETT was repositioned as a therapeutic intervention.

However, both Brunel et al(1989) and Marik and Janower(1997) did not consider the head position, which can move the ETT up or down by about 2 cm, and how this can affect the flexion and extension (De Lacey et al., 2008). Another point of note is that with Brunel et al(1989) all the images were reviewed by radiologists who have advanced experience. The assessment of the ETT may be different if the images were reviewed by clinicians or radiographers.

A study by Hegde and Raghavendra Rao(2010) addressed a case study of a nasogastric tube malpositioned in the left main bronchus of the trachea. An urgent chest radiograph (anterior-posterior view) was obtained to reveal the malposition. After a few hours the condition worsened with progressive respiratory failure, requiring tracheal intubation and mechanical ventilation, but after 24 hours the condition failed to respond and the patient expired.

In this study the discussion was focussed on the nature of the NGT malposition and the complications, however the study failed to explain the role of the chest radiograph in detecting the NGT malposition and why the chest radiograph was requested urgently rather than following the insertion (Eisenhuber et al., 2012). A standard post-insertion chest radiograph could reduce the incidences of malpositioning and complications which can lead to morbidity.

Kawati and Rubertsson(2005) addressed three case studies of the malpositioning of fine bore feeding tubes and their complications. In all three cases the feeding tube was malpositioned in the right main bronchus. The authors identify the nature of the malpositioning, the complications and role of the chest radiograph in confirming the malposition. As a result of the radiograph, clinical intervention occurred, with the removal of the feeding tube. As a result, the complications were reduced in all three cases.

Chan et al (1997) looked at the complication rate of tube thoracostomy in an emergency department (ED), operating room (OR) and inpatient ward (IW). Of 373 tube thoracostomies, in 269 patients, the percentage of complications was ED - 14%, OR - 9.2% and IW - 25%. The study tried to compare the rate of complications related to thoracostomy tube placement in ED, OR and IW. The potential of chest radiography to detect complications was missed in the study. The study also failed to address the possible malfunctioning of the thoracostomy tube as a result of its malpositioning.

Chahine-Malus et al (2001) found that routine chest radiographs had a low value for management changes in the intensive care unit (ICU). One hundred twenty-seven (19.7%) patients out of 645 in the medical ICU had one or more management changes. The majority of changes were related to monitoring medical devices such as the endotracheal tube and central venous catheter. However, 19.7% is a high value compared with the total number of patients, and decision making by the clinicians should consider the morbidity that can result from malpositioning.

A study by Webb and LaBerge(1984) attempted to identify chest tube malpositioning in the major fissure. The data found that on 12 patients a chest x-ray was used to confirm the clinical evidence of the chest tube placement. In three patients from the 12 it was found the malposition in the major fissure was identified by an anteroposterior view. One patient was examined by taking both views, posteroanterior and a lateral chest x-ray, and the malposition was detected in both views. On three out of eight patients the malpositioning was not identified by taking an anteroposterior view. Of the other five patients the diagnosis was made only by taking posteroanterior and lateral x-ray views.

Although the study was about radiographic recognition of chest tube malpositioning in the major fissure, it relied on clinical evidence of chest tube malfunctioning, and only then used chest radiograph as a form of confirmation. The appearance of the chest tube in the radiographs was affected by the patient's position. In some cases the tube appears to be in a good position in the posterior

anterior view but in the lateral view appears to be placed in a major fissure figure (2-2).

Figure 2-2: Chest tube located within major fissure with tip near to left hilum

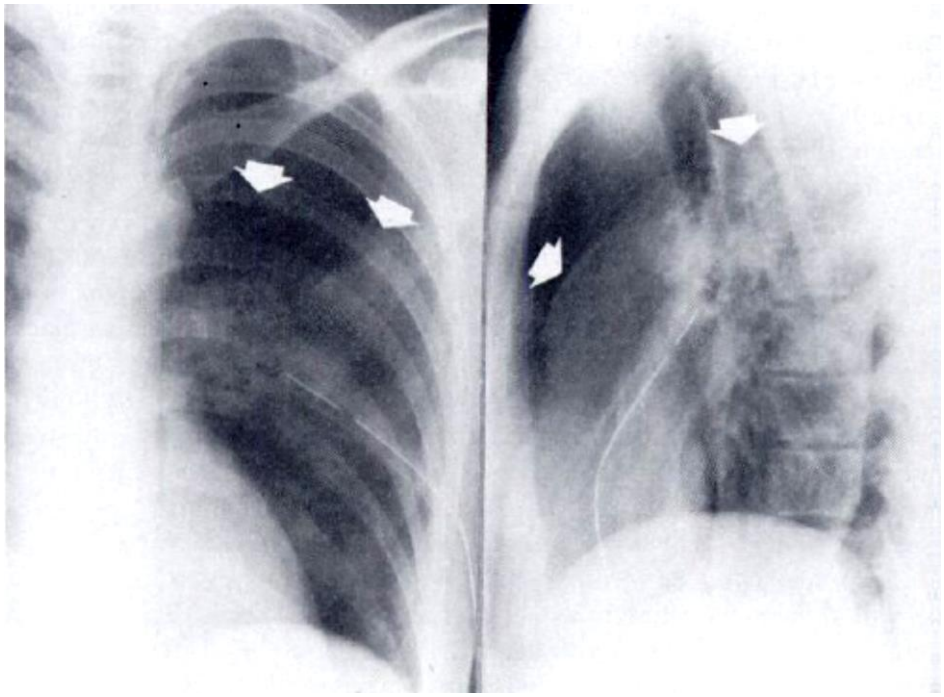

source: (Webb and LaBerge, 1984a)

Left anterior posterior view with pneumothorax (arrows), right lateral position showing tube to be within major fissure with tip near to left hilum, pneumothorax (arrows).

The study failed to associate the complications from the malposition as due to misinterpretations in the chest radiography, which explains why in the study the clinicians rely on the clinical evidence rather than understanding how the technical factors of the chest radiograph can impact on the appearance of the chest tube.

2.3 Technical considerations:

There have been many studies looking at the technical considerations and limitations of mobile chest radiography in the ICU/CCU, but little attention has been paid to the technical adequacy of the patient position, which can be rotated, kyphotic (chest tilted forward) and lordotic (chest tilted backward) due to the patients' condition in the ICU/CCU, and how that can impact on the visualisation of the chest tubes and lines in chest radiography.

Normally chest radiography uses the posterior anterior erect view, which is seen as the most reliable view (De Lacey et al., 2008). The patient is positioned against an upright Bucky with their shoulders rolled forward to move the scapular bodies from the lung field. The X-ray is centred at the level of the 7^{th} thoracic vertebra. The distance between the X-ray tube and the image receptor is 180 cm. The image receptor size is 35x45 cm. The patient needs to hold their breath for better inspiratory effort.

Consequently, when these techniques are employed the patient will be without rotation, kyphosis or lordosis. The radiation dose to the patient and the heart magnification will be reduced. There will be adequate visualization of at least 10 posterior ribs (Briggs, 2004).

However, in the intensive care unit the environment is not organized and structured to adequately replicate and duplicate the techniques of the posterior anterior view. In fact the anterior posterior view is the most performed in the ICU (Rubinowitz et al., 2007).

Wallace (1997) has stated that because the patients in the intensive care unit usually have many serious and complicated medical issues many devices, tubes, and lines are connected to them. This makes it difficult to transport the patient to the radiology department. Therefore, mobile chest radiography remains one of the simplest tests used in the intensive care unit. However, no attempt was made to address the patient's position, the cooperation of the patients (who might be

unconscious so they cannot move), and the morbidity which can occur due to disconnected life support devices.

The position of the patient in the ICU, which depends on the patient's condition, might be supine, erect or semi erect. Positioning the patient, who might be unconscious, is very difficult. Consequently, it is difficult to roll the shoulders forward to avoid the lungs being superimposed on the scapular bodies and to hold the breath for better inspiratory effort to avoid crowding of the vessels at the lung base and heart and to avoid mediastinum shadow enlargement (McQuillen-Martensen, 1996).

In addition, the distance of the ICU chest radiograph between the X-ray tube and the image receptor of about 100 cm can affect the appearance of the heart shadow, causing it to appear enlarged , because the heart in the AP view is located at the front, away from the image receptor and the X-ray beam diverges the margins of the heart, causing magnification(De Lacey et al., 2008). However, the whole chest will appear magnified, not just the heart shadow. There is a gap in the radiology literature with regard to recognizing how narrow the shadows of the chest anatomical structures appear as the distance is changed, and therefore it is difficult to know the exact impact of the distance.

Moreover, as focus distance detector (FDD) is reduced (for example, from 180 cm to 100 cm) the radiation dose to parts of the patient closer to the x-ray tube increases, relative to parts of the patient closer to the detector, due to inverse square law effects. For a constant dose to the detector, overall patient dose is therefore higher at lower FDD's, even though the mAs is reduced to compensate for increased intensity of the x-ray beam (Carlton and Adler, 2006).

The radiographic factors are not always standardised, and the distance between the X-ray tube and the image receptor is not fixed, so considerable variations in exposure levels and image density can occur. Therefore, the image produced can have a loss of contrast and resolution, and therefore there can be degradation of the quality of the mobile chest radiography. Consequently, there are difficulties in

detecting and interpreting important information such as the tip of tubes and lines' locations in mobile chest radiography (Moskowitz, 2010).

Tocino (1996) has mentioned that use of other imaging modalities, such as computed tomography (CT), ultrasound (US), magnetic resonance imaging (MRI) and nuclear medicine, is limited for intensive care patients, in order to avoid morbidity resulting from moving the patients from the intensive care unit to the radiology department, or disconnecting any life support devices such as automatic ventilation and central venous catheters.

A comparative study between the key imaging modalities in the ICU (CXR, CT, US and MRI) by Porté et al (2009) maintained that CTs and MRIs are too large and less suitable for the ICU, and transporting a patient out of the ICU is not without its complications.

However, both Tocino, (1996) and Porté et al (2009) pay far too little attention to the cost effectiveness of chest radiography compared with the CT and MRI. Another problem with Porté et al (2009) study is that it does not take into account the fact that chest radiography is easy and quick. Although they have paid attention to the cheap cost of US and it having no ionizing radiation, there is no mention of exposure doses of CT which are substantially higher than chest radiography (Rubinowitz et al., 2007).

Rubinowitz et al (2007) looked at the uncooperative patient who is connected to numerous life support devices. This type of patient is a unique challenge to the quality of ICU chest radiography, due to the difficulty of moving and positioning them adequately for the film. It is also difficult to control scatter radiation in obese patients, where exposure takes a long time due to the large size of the patient and the possibility of the patient moving while the exposure is being taken which can result in rotation artifact.

Rubinowitz et al (2007) have failed to consider the difficulties of moving and positioning the patient and the impact of this on the life support devices and chest radiography. Another weakness of Rubinowitz et al is that they have not connected the reasons for the increasing scatter radiation with the increasing of the exposure time in obese patients.

The nature of the ICU environment is one of the most challenging factors for ICU chest radiography (Tocino, 1996). In normal X-ray department practice the X-ray tube can be fixed at an optimum distance between the tube and the image receptor (chest 180 cm) and the X-ray beam is perpendicular to the image receptor.

However, in the ICU there are limitations which mean that the X-ray tube and image receptor cannot be perpendicular to each other. Firstly, the patient's position may be semi erect, erect decubitus or supine, depending on their situation. Secondly, there are no straight edges to support the image receptor, due to the soft patient bed, so the image receptor can be twisted to the right or left, or up or down, and it is therefore difficult for the image receptor and X-ray beam to be perpendicular. When the beam and receptor are not perpendicular the radiographers have to rely on their eyes and the judgement is difficult because the X-ray beam is invisible and travels in a straight line (Pope, 1999).

Consequently, perfect chest radiography, as in the x-ray department, is very difficult. If not done correctly the anatomical structures and chest tubes and lines' shadows can appear rotated, kyphotic and lordotic. This can cause misinterpretation of the position of the tubes and lines in the chest.

De Lacey et al (2008) stated that the appearance of lungs and mediastinal can be distorted by the patient's rotation or the direction of the X-ray beam. Therefore when the patient is rotated to the right, the right side appears blacker than the left. When the X-ray beam is decentered to the left side, the left side of the chest tissues appears blacker than the right.

However, the authors did not discuss the rotation issue related to the mobile chest radiography for patients in the ICU who are not able to co-operate. The possibility of a rotated position is higher in the ICU than for patients who are tested in the radiology department (Moskowitz, 2010). Another problem is that the authors fail to take into account the impact of rotation upon the appearance of chest tubes and lines, which is one of the main reasons for requesting chest radiography in the ICU.

As a result of the distortion of the appearance of the mediastinal the tubes and lines can seem misplaced and their location misinterpreted (Moskowitz, 2010). Therefore, if the tubes and lines were not in their typical position and were not detected by the chest radiography due to the rotation issue, the complications due to the malposition of the tubes could be serious.

A study of chest radiography in heart disease by Wilson (2002), stated that the size of the heart's shadow in chest radiography is impacted by patient rotation. So when the patient is rotated with the right shoulder forward the cardiac shadow is enlarged, whereas the reverse rotation reduces it. Wilson points out how rotation can affect the appearance of the chest lines which are placed close to the heart, such as CVC (superior vena cava located) and Swan-Ganz (left or right pulmonary artery located) lines.

Martensen(1996) stated that when the chest midcoronal plane is vertical the manubrium is projected at the level of the 4^{th} thoracic vertebra and about 2.5 cm of the lung apices are visualized above the clavicle, and therefore the heart and lungs are visualized in the chest radiography without foreshortening.

However, when the chest is tilted forward (kyphotic), the lungs and heart are foreshortened, the manubrium is demonstrated at the level of 5^{th} thoracic vertebra or lower and more than 2.5 cm of apices is visualized above the clavicles. Conversely, when the chest is titled backwards (lordotic), the lungs and heart are foreshortened, the manubrium is situated between the 1^{st} and 3^{rd} thoracic vertebrae, and less than 2.5 cm of apices is visualized above the clavicles.

Although Martensen (1999) has discussed the impact of kyphosis and lordosis on the visualization of the anatomical structures in chest radiography, he fails to demonstrate the precise degrees of chest angulation that lead to changes in the appearance of the anatomical structures.

No attempt was made to consider the positional factors (kyphosis and lordosis) with chest radiography in the ICU, where the possibility of kyphotic or lordotic patients is high and they are more likely to be uncooperative. In the ICU the ability to actually produce a standardized arrangement of position of a patient is difficult. Consequently, the appearance of the chest anatomical structures in mobile chest radiography is changed and the appearance of the chest life support devices is changed as well.

A study by Joseph et al (1978) about the hyper transradianthemithorax noted the importance of lateral decentring and the explanation for it's appearance due to rotation. This study indicated that 80% of the increase in unilateral film blackening on the chest radiograph resulting from rotation of patient is due to asymmetrical absorption of the x-ray beam. The occurrence of the hyper transradianthemithorax always on the side to which the patient is rotated.

A study by Hollman and Adams (1989) considered the influence of the lordotic projection on the interpretation of chest radiograph. This study compared 14 pairs of lordotic and standard chest radiographs taken within 24 hours of each other in the same time. The results found that there was poor visualisation of lung bases, elevation of diaphragm, loss of definition of the aortic knuckle and widening of the superior mediastinum.

Although Joseph et al (1978) and Hollman and Adams (1989) have paid attention on the role of rotation and lordotic projections in influencing the interpretation of chest radiograph, no attempt has been paid to the impact of them on the appearance of chest tubes and lines on mobile chest radiograph.

Therefore, perfect mobile chest radiography is very difficult and that can make the anatomical structures' shadows look rotated, kyphotic or lordotic. As a result, chest tubes and lines can seem misplaced and the location of the tubes and lines in the chest radiography can be misinterpreted (Moskowitz, 2010).

2.4 Evaluation of x-ray imaging technology

Traditionally, an X-ray of a body was captured by X-ray film. The film was placed inside a cassette, between two intensifier screens, which converted the received X-rays from the body to light (Dowsett et al., 2006). The intensity of light produced depended on the amount of X-rays were received (Fauber, 2009). The more X-ray was received, the more light was produced (Easton, 2009).

However, the intensity of light depended not just on the amount of X-rays received but on the thickness of the phosphor layer in the intensifier screen. Rare earth phosphor is also faster than calcium tungsten in absorption and conversion of the X-ray received (Fauber, 2009). Processing of the X-ray film by chemicals generates the film sheet, ready for interpretation (Carter and Vealé, 2008). However, only one copy is produced, which is a major disadvantage of conventional imaging (Dixon, 2008).

The variation of conventional film density between tissues – contrast factor – can be high or low due to the intensities of the X-ray received by the image receptors. High contrast (short-scale contrast) shows few densities with great differences between the individual densities; low contrast (long-scale contrast) shows a large number of densities with few differences between individual densities, which can reduce the appearance of some findings in the radiographs(Fauber, 2009) and which can also affect the quality of the diagnostic information. For example, in a chest X-ray film, the contrast between the darkest area, which is the lung, to the lightest area, which is bone (Moskowitz, 2010), in some cases causes tubes and lines to be missed due to the narrow dynamic range (Dowsett et al., 2006). Additionally, kilovoltage plays the main role of controlling the contrast on film and creating penetrating effects through the amount of the primary X-ray photons received by the radiographic film (Fauber, 2009).

Recent developments within computed radiography (CR) mean that there is no need to use film sheet, although both processes require use of a photostimulable image plate, which records a two-dimensional image. In computed radiography the photostimulable image plate absorbs the energy from the received X-ray beam and stores it on the computed radiography plate. When the photostimulable image plate is scanned by laser beam in the processing unit, the stored energy is released as light. This light is picked up by the photomultiplier tube and converted to electronic signals stored as a digital data figure (2-3).

Figure 2-3: The photomultiplier tube and converted to electronic signals stored as digital data

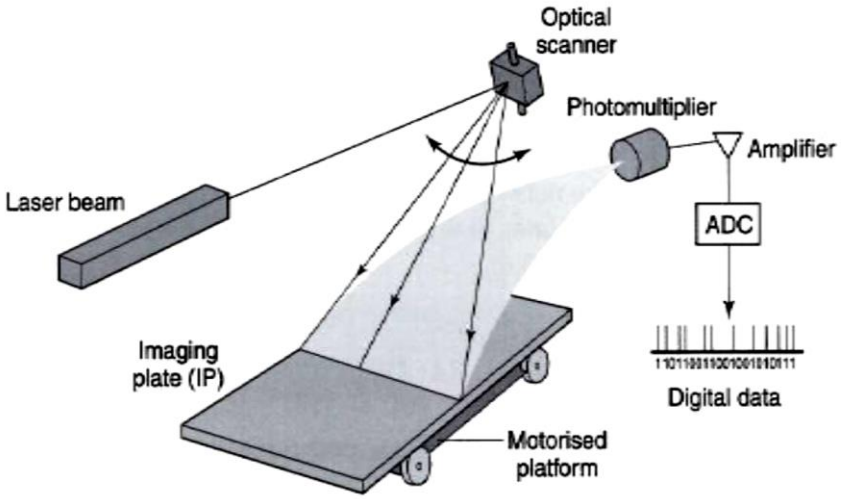

Source: (Easton, 2009)

However, with digital radiography (DR) there two ways of acquiring the image. The first is indirect and involves striking the X-rays with the scintillator phosphor (cesium iodide) to emit light, which is then converted to electrical pulses by the photodetector (amorphous silicon). The second, direct, way converts the X-ray directly to electronic pulse via a photoconductor (amorphous selenium) (Fauber, 2009).

The data can be viewed either as soft copy on monitor or hard copy on a sheet film (Dixon, 2008). The wide dynamic range of DR – 'the ratio between the X-ray attenuation of most radiolucent and the most radio-opaque paths through the patient to be included on the same image' (Dowsett et al., 2006) – has improved the visualisation of chest anatomical structures and passing through chest tubes and lines (Moskowitz, 2010).

Image receptors' responses in digital imaging are different when compared to conventional X-ray receptors (Fauber, 2009). The wide dynamic range of DR is due to image receptors being more receptive of the wide range of exposure intensities (low, medium and high) that can be detected and recorded and which create high-resolution images (Fauber, 2009). Therefore, DR's ability to detect features in greyscale in chest radiography, such as tubes and lines, is better than that of conventional radiography (Moskowitz, 2010).

2.5 Changes in work patterns due to developing of radiographic image acquisition

The acquisition and display of radiographic images are inseparably connected, which has limited the flexibility of conventional radiography recording systems (Macmahon and Vyborny, 1994). Acquisition of a chest image by producing an electronic image that can be displayed and manipulated on a computer (Carter and Vealé, 2008) has improved the representation of diagnostic data and offers reliable access to mobile chest radiographs needed in an intensive care unit (Moskowitz, 2010), where is difficult to reimage patients who are in critical situations(Henschke et al., 1997). Picture archiving and communication systems (PACS) make images available at any time for all clinicians through a network of computers (Carter and Vealé, 2008) and this may reduce costs, decrease the exposure of patients and staff to radiation and decrease workload. It also enables the storage of a large amount of images in a small space, which can also be later accessed for reference (Bansal, 2006).

Interpretation of radiological images has also changed; images can now be read through a work station (Pudas et al., 2005). A study by Eisenhuber et al. (2003) evaluated the need for routine mobile chest X-rays and positioning of different support and monitoring equipment, such as lines and tubes, and concluded that digital chest X-rays were considerably better quality than those created by the conventional system.

Digital technology enables superior structural contrast when suitable processing is utilized. Therefore, the depiction of monitoring equipment is increased on mobile digital chest radiographs, in contrast with the conventional system. This result is possibly clearer with soft copy, when alteration of window level and window width is accessible. Nevertheless, while improving mobile X-ray imaging, mobile chest radiography's consistent high quality of interpretation is still difficult to manage due to the effects of technical quality upon mobile chest X-rays.

Digital imaging has developed rapidly recently, as has the picture archiving and communication system (PACS), which provides a wide and dynamic range of recording systems to post process images by adjusting window level and allowing for image acquisition in real time (Bacher et al., 2006). Therefore, many issues associated with the conventional mobile radiograph have been solved.

Alternatively, the use of digital imaging and PACS by radiographers, clinicians and radiologists has meant that the technical quality of the radiographs has been affected as a result of this changing way of work (Larsson et al., 2007). This is because one person reviews the radiograph and makes a decision without consulting other experts face to face (Larsson et al., 2007). Clinicians' actions have been shown to be poorer as a result of less communication (Watkins et al., 2000).

Although many studies have been published about the development of digital imaging and its impact upon the workplace, chest image quality and radiation dose, no study has yet evaluated how the technical quality of the mobile chest radiography can impact the appearance of chest tubes and lines.

2.6 Image processing

The imaging process has a similar technique for all radiologic and imaging modalities. All modalities have stages, which are acquired, processed, archived and displayed for analysis. The difference between conventional film/screen radiography and digital radiography are the specifics of how these processes are achieved (Carlton and Adler, 2006).

2.6.1 The role of characteristic curve with film/screen in the image processing

The characteristic curve is a graphical representation of the relationship between the intensity of radiation exposure received by the film and the optical density resultant on the film (Jenkins, 1980). Some references refer to the characteristic curve as a sensitometric curve, or H & D curve, as it was first described by Hurter and Driffield in 1890 (Fauber, 2009).

The horizontal axis (x axis) is compressed into logarithmic scale because of the wide range of exposure possible, and the vertical density axis (y axis) is shown as a log scale Figure (2-4). Therefore, the curve is known as density log exposure or D log E (Carlton and Adler, 2006).

Figure 2-4: Characteristic curve

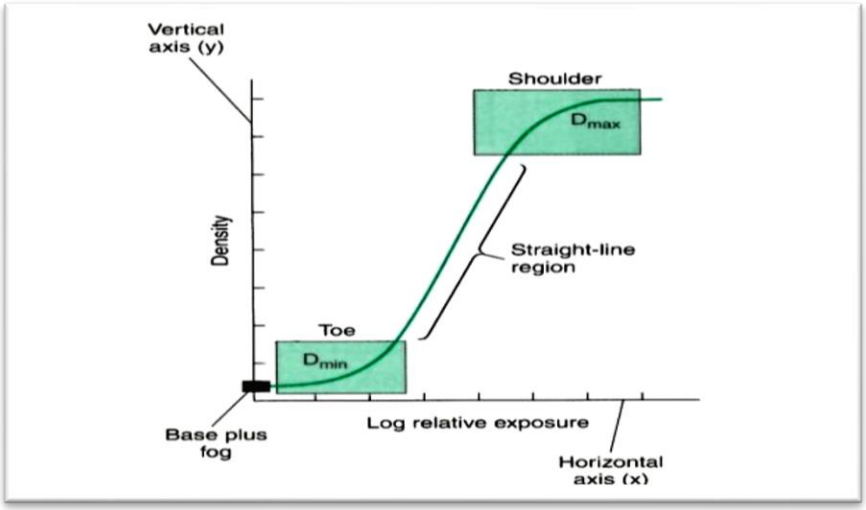

Source: (Fauber, 2009)

The important regions of the characteristic curve are the toe region, straight-line region and shoulder region. The toe region shows that the minimum amount of exposure produced a minimum amount of optical density. The lowest point in the toe region is known as D min, where the lowest changes in exposure intensity can produce little effect on the optical density (Fauber, 2009).

The straight-line region of the curve is that between the toe and shoulder, and it is usually fairly straight, due to the film reacting in a linear fashion to exposure range. This is the most useful range of densities produced (Fauber, 2009).

The shoulder region includes the highest point of the curve, where overexposure intensity no longer affects the optical densities. This point is known as D max. D max represents the state where practically all silver halides have a full complement of silver halide atoms or black metallic silver and cannot accept more. Additional exposure beyond D max will result in less density because silver atoms will be ionized again, reversing their charge and causing less specks on the X-ray film. This process is called reversal solarisation (Carlton and Adler, 2006).

Alternatively, toe and shoulder regions for chest radiographs are still useful areas because the chest contains a variety of densities, such as the air in the lung, which requires a low intensity in order to appear on the image, and bones, which require a high intensity. Therefore, the toe region can be useful to demonstrate that the shadow of air in the image here, and in the shoulder region, can demonstrate the shadow of the bone in the chest X-ray.

2.6.2 Digital image characteristics

Digital imaging possesses a number of unique attributes that distinguish it from conventional imaging. Although the design of the image receptor in digital imaging may differ widely, a latent image is still produced and is processed to form a manifest image (Carlton and Adler, 2006).

Digital image receptors can respond to a wider range of X-ray exposure than conventional film. The response of an image receptor in digital imaging is linear compared with radiographic film (i.e. the exposure latitude is very wide because a

single detector can be sensitive to a wide range of exposure – Figure (2-5). This also means that moderately underexposed or overexposed images will produce diagnostic information (Fauber, 2009).

Figure 2-5: The response of image receptor in digital imaging is linear compared with the radiographic film

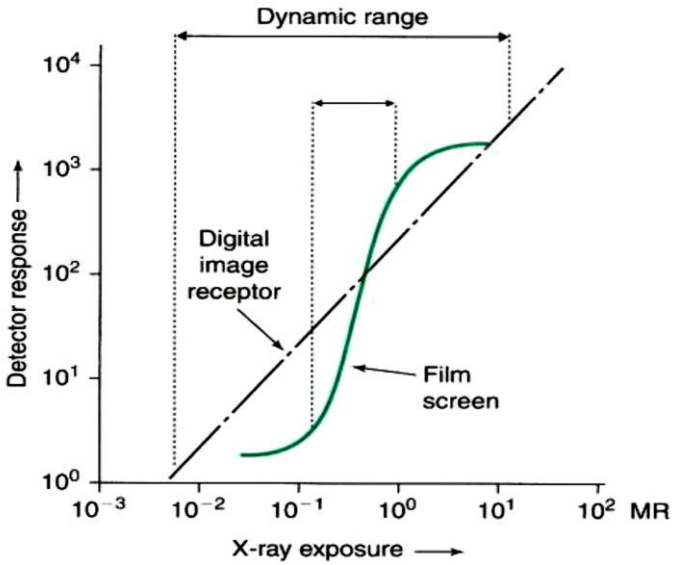

Source: (Fauber, 2009)

Consequently, digital images have a greater dynamic range of radiographic density/brightness (white to black scale) for anatomical areas of widely different attenuation (bone or soft tissues structures), which means that they can be better visualised (Carlton and Adler, 2006).

Digital images are composed by numerical data that can be easily manipulated by a computer. Unlike conventional radiography, which is made up of tiny deposits of dark metallic silver, a digital image is recorded as a matrix or a combination of rows and columns (array) of small elements called pixels. Each pixel is recorded as a single numerical value, which is represented as a single brightness level on display monitor. The location of the pixel within the image matrix corresponds to an area within the patient, or volume of tissue (Fauber, 2009).

Look-up tables (LUT) provide a variety of methods of changing the display of the digital image. Image densities and shades of grey can be manipulated to alter how the area of interest is visualised and thus alter the brightness and/or contrast of the image (Fauber, 2009).

Therefore, through visual comparison, pixel values of the original image can be changed in a processed image. If the image is not altered, the graph will show as a straight line. If the original image is altered, then the graph will no longer be in a straight line, but may resemble a characteristic curve for radiographic film Figure (2-6) (Fauber, 2009). In other words, an LUT is a histogram reference to correct the appearance of anatomical structures by appropriate brightness and contrast (Carter and Vealé, 2008).

Figure 2-6: The changes in pixel values from the original image to the processed image. The shape of the graph is similar to characteristic curve for radiographic film

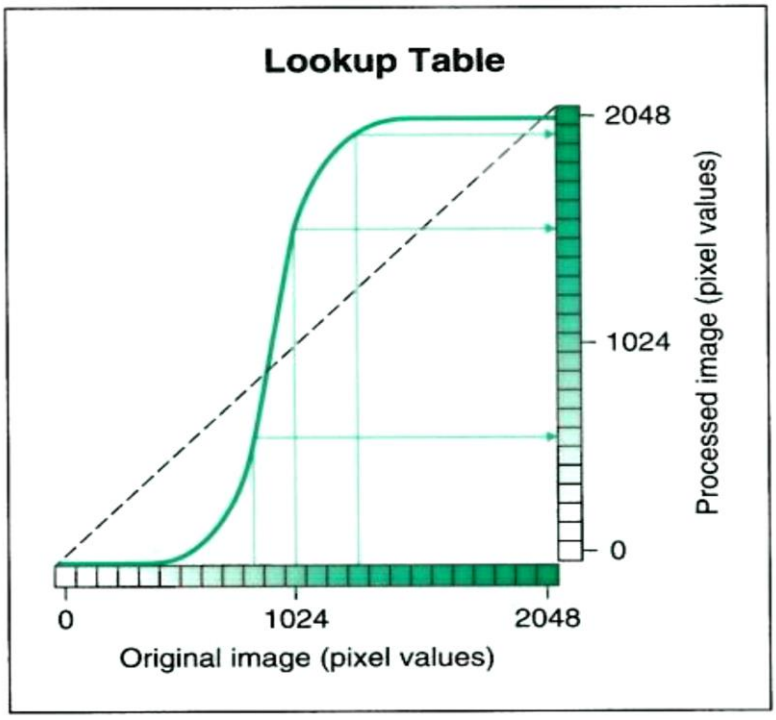

(Fauber, 2009)

2.6.3 Digital algorithms (filters)

Digital filtering of images utilises the computer to extract more diagnostic information. In images where the distinction between normal and abnormal tissue is subtle, accurate interpretation may become difficult to compare. For example, in the chest, the heart, lungs and blood vessels are so close together that contrast is critical to achieve accurate detail (Boiselle and White, 2007). Therefore, algorithms are used to reduce image noise and increase the contrast of structures of interest. Also, enhanced contrast edges can provide a clear image for human observer, reduce latitude and reduce the size of the image files (Bankman, 2009).

2.6.3.1 Low-pass filtering (smoothing)

Low-pass filtering is a postprocessing technique used to increase image contrast and decrease high-frequency noise. This process is often called image smoothing – removing the apparent graininess, due to image noise (Dowsett et al., 2006). This means that each pixel's frequency averages with surrounding pixel values to remove high-frequency noise (Carter and Vealé, 2008) Figure (2-7). However, this technique can blur small details or edges in the final image (Allisy-Roberts et al., 2008).

Figure 2-7: High frequencies rejected by a low-pass filter.

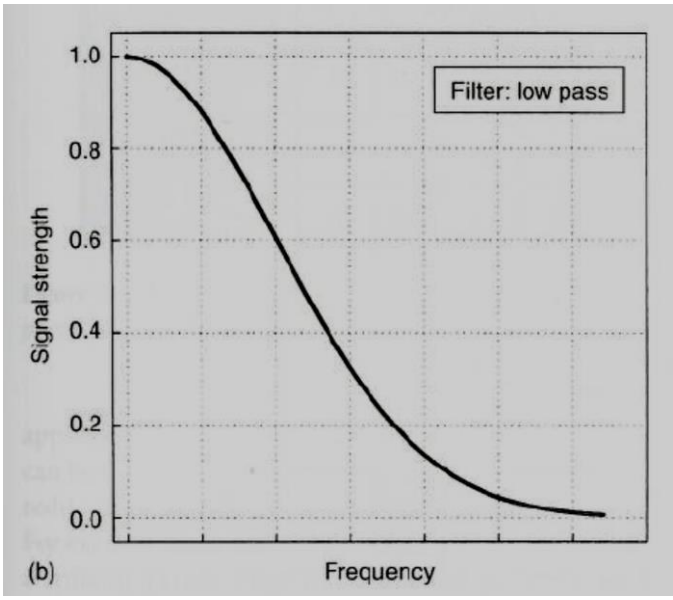

Source: (Dowsett et al., 2006)

2.6.3.2 Edge enhancement or high-pass filtering

Edge enhancement algorithms are postprocessing techniques used to refine data in an image and create better-enhanced contrast edges as a change in grey level. This helps the desired image's appearance to become easier to perceive and allows one to see details in the image that may not be immediately observable in the original (Bankman, 2009).

Edge enhancement or high-pass filtering adds a proportion of difference between the greyscale value of the pixel and that of it is neighbours. The effect is to exaggerate the contrast at the boundary between structures, thus making the structures more visible Figure (2-8). However, the image noise may be slightly increased due to applying edge enhancement techniques (Fauber, 2009).

Figure 2-8: Low frequencies rejected by high-pass filter.

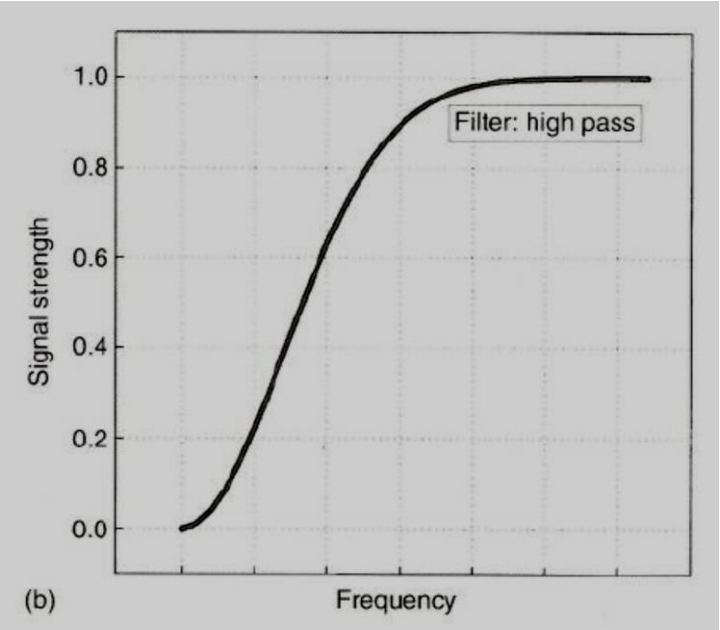

Source: (Dowsett et al., 2006)

For example, both Fuji and Agfa digital systems use edge-enhancement algorithms that emphasize high spatial frequencies for small objects (such as bony trabeculae) and low-spatial frequencies for large objects (such as the bowel and kidneys) (Carlton and Adler, 2006).

2.6.3.3 Histogram equalization

Histogram equalization is uniform distribution and linear cumulative plot. In other words, the histogram procedure is to spread out the displayed grey levels in peak areas selectively, compressing them in the valleys so that the same number of pixels in the display shows each possible brightness level (Russ and NetLibrary, 2007).

Histogram equalization is used to allow the area with low contrast to gain higher contrast by spreading out the most frequent intensity values and leaving greyscale to represent the pixel values which contain useful diagnostic information (i.e. covering all possible values in the greyscale Figure (2-9). The pixels holding

grey-level information in the middle of the histogram can be displayed by utilizing the full grey-level range (Dowsett et al., 2006).

Figure 2-9: Histogram B is the result after histogram equalization.

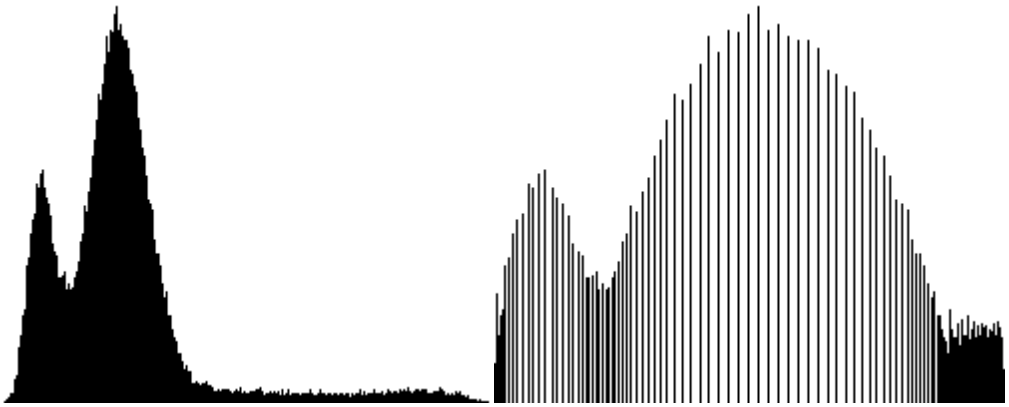

A B

Source: (Russ and NetLibrary, 2007)

2.6.3.4 Wavelet transform

Wavelet transform are used for image compression, feature extraction, removing noise and communication improvement (Dowsett et al., 2006) and belong to the general class of transform-based lossy compression techniques. These involve three steps: transformation, quantization and encoding (Erickson et al., 1998).

Transformation is a lossless step (original images can be restored by inverting the transform) in which an image is transformed from greyscale values in a spatial domain to coefficients in some other domain, such as reconstructing magnetic resonance images. No loss of information occurs in the transformation step. Quantization is the step where loss of information occurs. It attempts to preserve the more important coefficient, while the less important coefficients are roughly approximated to be compressed more efficiently, often as zero. It can simply be described as a converting floating point values to integer values. Finally, these quantized coefficients are compactly represented for efficient storage or transmission of the image (Erickson et al., 1998).

2.7 Algorithms experiment literature:

Generally with standard mobile chest radiography technique, the imaging parameters of chest radiography are set to produce the best average image, an image that will demonstrate a wide range of findings including pleural, pulmonary, mediastinal and other abnormalities (De Lacey et al., 2008).

However, because pulmonary disease is one of the most important abnormalities, and imaging parameters are usually optimised to visualise this condition, the technique used may mask the position of chest tubes and lines in the chest radiograph due to the possibility of their being obscured in the brighter regions such as the heart and mediastinum (Nodine et al., 1996).

In addition, it may be the position of the I.C.U patient is optimum (i.e. there is no rotation, kyphosis, or lordosis). In other words, there are no geometrical problems with image detail like shape distortion (foreshortening, elongation), which can lead to misrepresentations of the appearance of the anatomical structures and the chest tubes and lines around it in the chest radiograph (Carlton and Adler, 2006). However, malpositioning may further increase the difficulty of confidently determining whether tubes/lines are correctly positioned.

The visibility of tubes and lines in the chest radiography may be poor or not clearly defined due to the imaging procedure not being optimised for this purpose in the standard mobile chest radiography technique, which is manipulated to demonstrate general findings rather than focusing on visualising the appearance of chest tubes and lines (Foos et al., 2011).

Although information exists in the literature Bacher et al.(2006); De Boo et al.(2011) and Balassy et al.(2005) dedicated to the optimisation of the x-ray system for computed radiography of the chest, very little has been published on the optimisation of the CR system and the image processing algorithms (Moore et al., 2007).

Foos et al (2011) developed a new method to enhance the appearnce of the chest tubes and lines in the ICU chest radiographs while at the same time retaining the gray scale of the standard chest radiograph. This method has been adopted by Carestream to develop an algorithm specifically designed to optimize visualization of tubes/lines. An image with this algorithm applied can be automatically sent to the viewing station, accompanying the default image.

The method was designed for use as a companion view that delivers from the capture modalty to PACS, together with standard rendering. The method was not intended to replace standard modility processing, rather it was intended for use as a surrgate for window and level manipulations that might be required to identify tube and line location. The method was introduced to reduce the amount of time it takes to interpret the ICU chest radiograph and to seek a greater interpretation confidence.

2.8 Malpositioning of chest tubes/lines and discussion of Imaging geometry issues

The aim in producing a radiograph is to provide information so that an assessment can be made of some aspects of a patient's condition. The more complete this radiographic information, the better the radiographic diagnosis. However, while it is possible to provide much accessible information via radiographs, such as the shadow of the bones and the soft tissues, visually radiographs can be confusing for the observer in terms of seeing the examined object distorted (magnified or shortened or elongated) (Jenkins, 1980).

Magnification, which results from the geometry of the technique employed, can influence the radiographic image. Magnification is defined as the ratio of image size to the object size, where the image produced is larger than the object size (Jenkins, 1980).

Magnification (MF) = image size / object size

MF= SID/SOD

SID= source image distance.

SOD= source object distance.

SID means the distance from the radiation source to image receptor, SOD the distance from the radiation source to the object (Jenkins, 1980) Figure (2-10).

Figure 2-10: Source-to-object distance is the distance between the source of the X-ray and the object radiographed

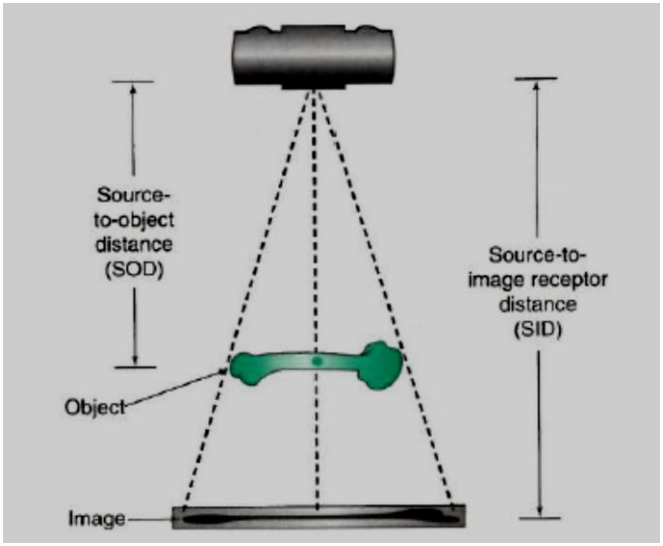

Source: (Fauber, 2009)

Therefore, when the SOD increases, the MF will decrease, and when the SID decreases the MF will increase Figure (2-11). Although the image is larger in size than the object, it is exactly the same shape. Hence, magnification has occurred. The object should be placed as close to the image receptor as possible and as large a SID as practicable used, for example in a posteroanterior chest radiography where SID is 180 cm (Meredith and Massey, 1977).

Figure 2-11: A long object-to-image receptor distance (OID) will create more magnification than a short OID. The image in A is larger than that in B because the object is further from the image receptor

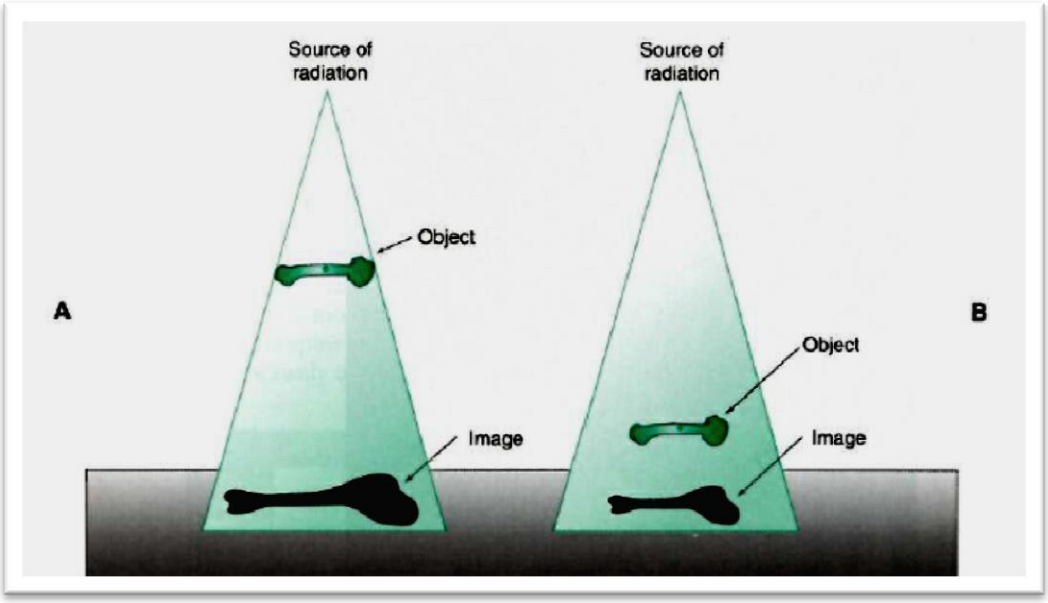

Source: (Fauber, 2009)

Distortion results from the radiographic misrepresentation of either the size (magnification) or shape of the anatomic part or structures being examined (Carlton and Adler, 2006). When the image is distorted, recoded detail (i.e. the degree of geometric accuracy of the structural lines which is actually recorded in the image) is also reduced (Fauber, 2009). Distortion of anatomical structures can exist in the image even when it cannot be seen due to poor visibility; in other words, when the image density and/or contrast are poor (Carlton and Adler, 2006).

Meredith and Massey (1977) mention that in some situations oblique rays, if the objects—here coins—are placed parallel to the image receptor and at the same distance from it, give equal shadows wherever placed (Meredith and Massey, 1977) Figure(2-12).

Figure 2-12:Three coins, placed parallel to the film and at the same distance from it, give equal circular shadows wherever placed

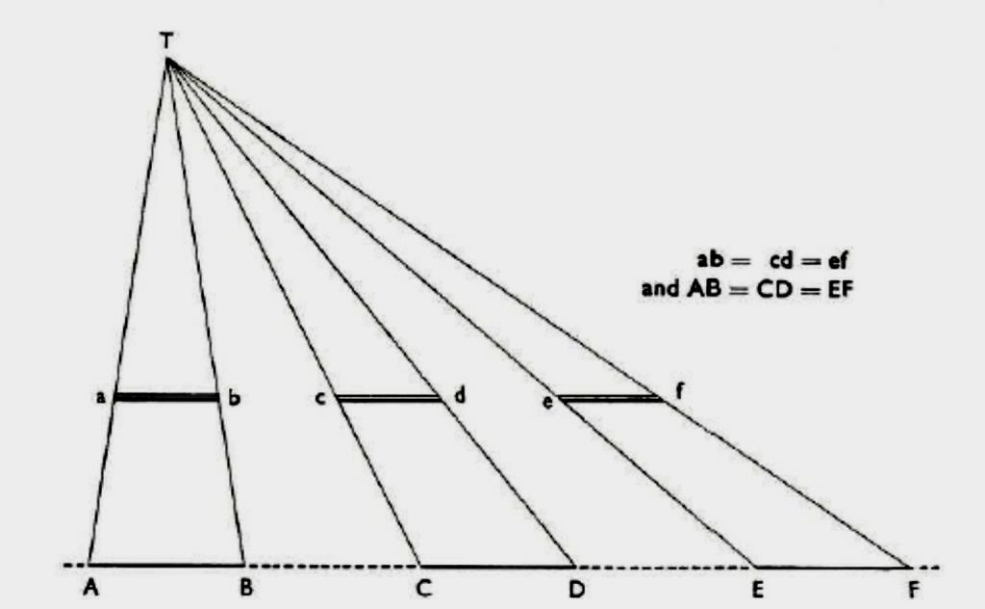

Source: (Meredith and Massey, 1977)

However, the shadows of anatomical structures in an image will not be equal (i.e. there will be distortion in shape) even if they are parallel to the image receptor and at the same level. This is because anatomical structures are three dimensional, not two dimensional like coins.

2.8.1 Factors affecting shape distortion

Shape distortion can appear in two different ways radiographically: as elongation or foreshortening. Elongation refers to an object that appears longer than the true image, while foreshortening refers to an object that appears shorter than the true image (Fauber, 2009). Elongation occurs when the tube and the image receptor are not parallel to each other. Foreshortening occurs only when the part – the object – is not parallel to the image receptor. Foreshortening depends on the angle of the object, so when the angle is large the foreshortening is great (Carlton and Adler, 2006) Figure (2-13).

Figure 2-13: In A the part is not parallel to image receptor; in B the image receptor is not parallel to the part

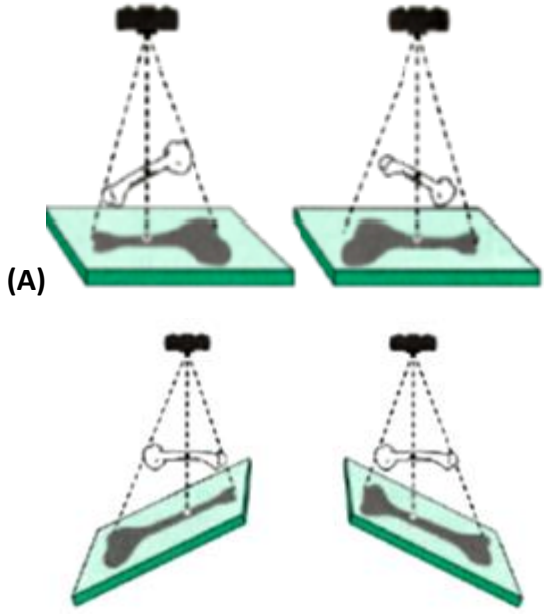

Source: (Fauber, 2009)

However, from Figure(2-13) it can be seen that differential magnification is also a key issue in shape distortion, where the nearest part of the bone to the source of the radiation is the largest appearance in the image and vice versa (Jenkins, 1980).

2.8.2 Geometrical factors that influence the chest radiography

Perfect patient position, optimum penetration, contrast and density can produce optimal chest radiography. However, because of patient condition and technical errors, such perfection is not obtained on every chest radiograph that is taken (McQuillen-Martensen, 1996). Although digital imaging overcomes the conventional radiography limitations in many respects, such as a narrow exposure latitude, consummation of time and film storage, accurate positioning of the patient for variety of projections remains a critical part of the imaging process (Carlton and Adler, 2006).

In the posteroanterior (PA) chest radiograph in Figure (2-14), the heart is situated anteriorly in relation to the image receptor distance (small OID) and the

SID is 180cm, which means that there is minimal divergence of the X-ray beam; therefore the magnification of the heart is limited (De Lacey et al., 2008). However, in the mobile anteroposterior (AP) chest radiograph in Figure (2-14), the heart is situated further from the image receptor (larger OID) than is the case with the PA chest radiograph and the SID is less than 180cm, therefore, the X-ray beam diverges at the margins of the heart, causing magnification Figure (2-14).

Figure 2-14: A – PA CXR 180cm and heart close to the cassette; B – on a mobile AP less than 180cm away from the cassette

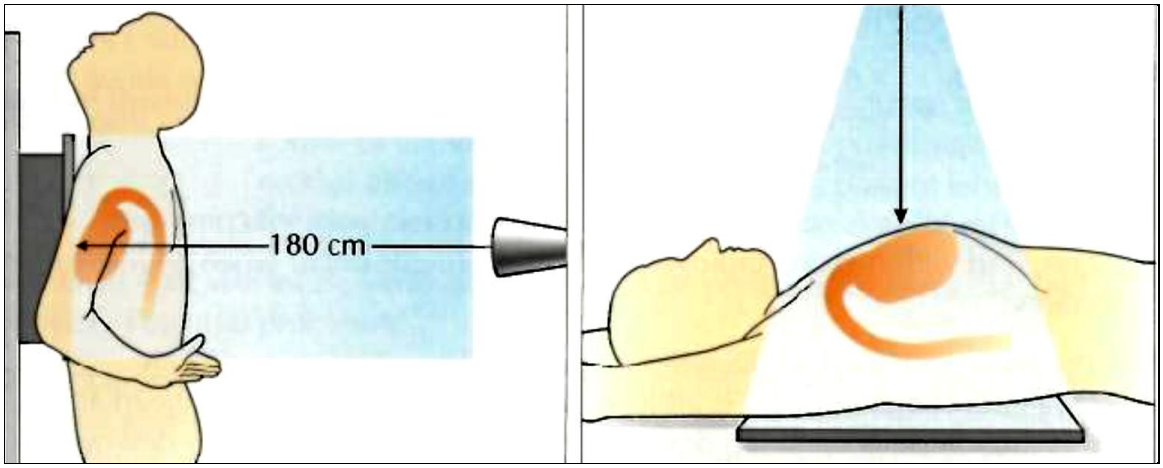

A **B**

Source: (De Lacey et al., 2008)

In a situation where a patient is in an intensive care unit (ICU) and connected with tubes and lines, if the patient's chest is tilted forward (kyphosis), the distance between the clavicles and the top of the lung apex is increased in mobile chest radiography Figure (2-16)compared with the normal position of the patient without tilt (Figure 2-15).

Figure 2-15: The normal chest position of the patient without tilt

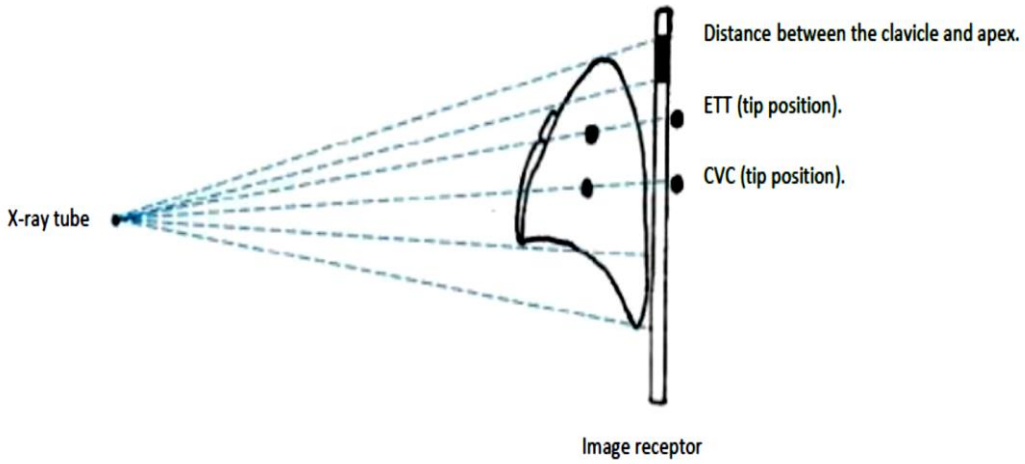

Figure 2-16: The patient's chest is tilted to forward (kyphosis)

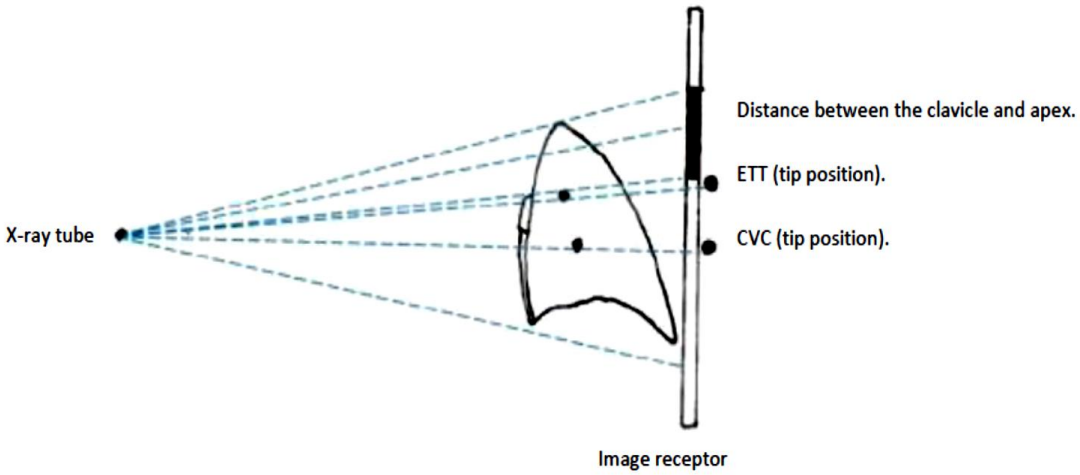

Alternatively, if the patient is tilted backward (lordosis), the distance between the clavicles and the top of the lung apex in mobile chest radiography is decreased Figure (2-17).

Figure 2-17: The patient's chest is tilted backward (lordosis)

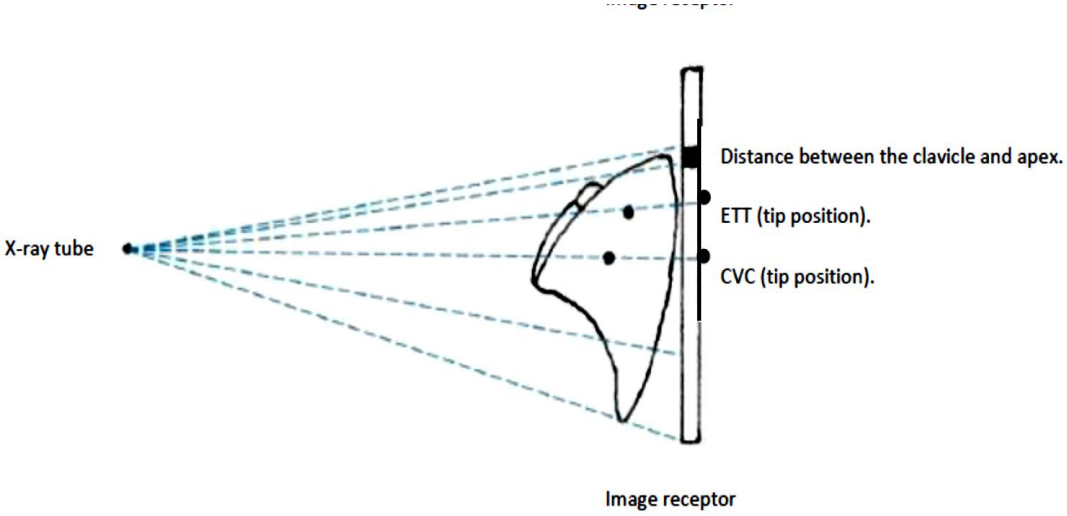

As a result, when changing the position of the patient forwards (kyphosis) and backwards (lordosis), the appearance of the position of the chest tubes and lines in the mobile chest radiography can be changed in relation to the change of the anatomical structures around it.

The geometrical issue of the foreshortening occurs when the part is not perpendicular to the image receptor. If a patient in an ICU is rotated to the left side during AP mobile chest radiography, the chest radiograph will be distorted. For example, the length of the left fourth rib will appear foreshortened (2-19) compared to the normal position of the chest Figure (2-18).

Figure 2-18: AP chest radiography without rotation

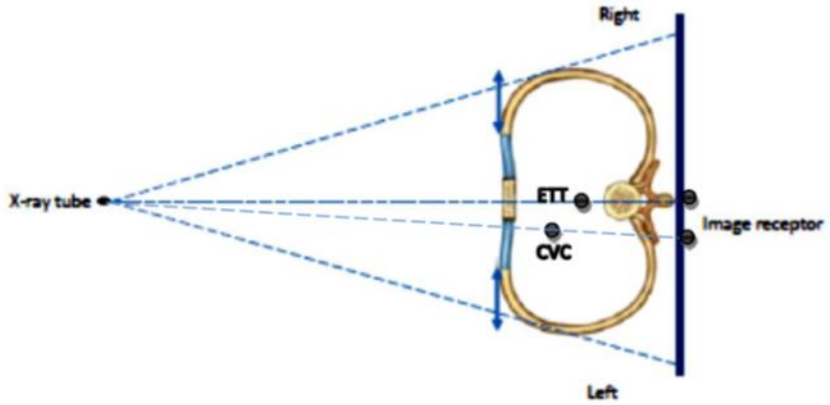

Figure 2-19: AP chest radiography rotated to the left

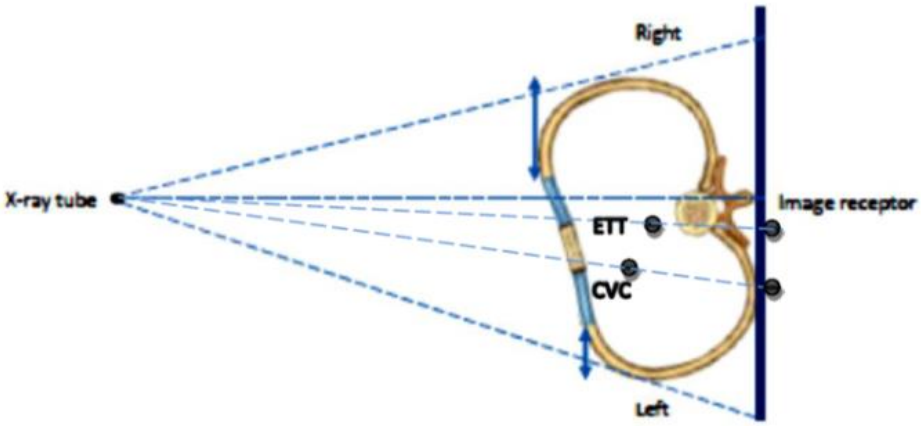

Alternatively, if the patient is rotated to the right during AP mobile chest radiography, the chest radiograph will be distorted so that the length of the right ribs will appear foreshortened when compared to the normal position of the chest Figure (2-20).

Figure 2-20: AP chest radiography rotated to the right side

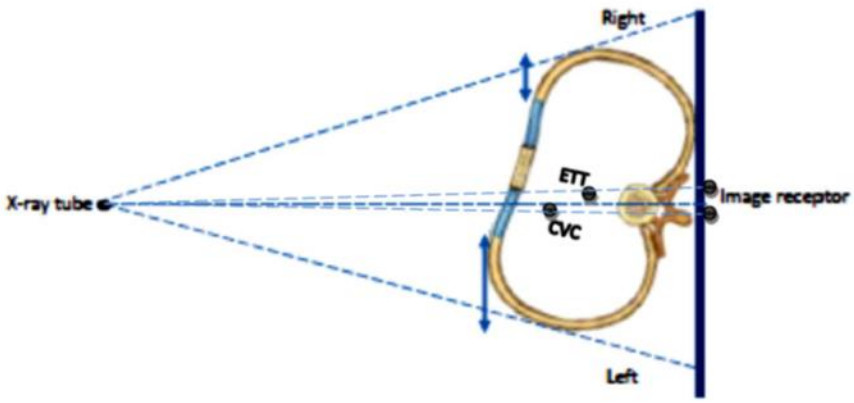

2.9 Justification for study

It can be seen from the literature review that there is gap in the study of ICU chest radiography technical quality and its impact on the appearance of chest tubes and lines. This means the appearance of the lines can be unreliable which makes clinical decision making difficult.

De Lacey et al(2008), Moskowitz(2010) and Briggs(2004) have addressed the fact that typical chest radiography should show the vertebral bodies just visible through the cardiac shadow and the medial ends of the clavicles should be equidistance on either side of the fourth thoracic vertebra spinous process to indicate no patient rotation.

The sixth or seventh anterior ribs should be visible and the diaphragm should lie on them. However, typical mobile chest radiographs for uncooperative patients in critical care, with life support devices connected through tubes and lines, are difficult to take, as it is very hard to put the patient in the correct position to take the X-ray. This typically results in poorer quality chest radiographs (Milne and Pistolesi, 1993). Therefore, the appearance of chest anatomical structures in mobile radiographs can be faulty (Moskowitz, 2010).

Although, many ICU chest X-ray readers can recognize the impacts of patient position (anterior posterior radiograph magnify the heart and mediastinum),on the image (vessels and heart can appear enlarged),and technical factors, such as the effects of changing the distance between the tube and the plate, it is still difficult to associate the changes of the apparent position of the anatomical structures and chest tubes and lines to precise changes in angulation resulting in rotation, kyphosis and lordosis.

Although malposition of chest tubes and lines incidence data is available in research, carried out in many countries, most research is focused on the incidence of the malposition and their complications, and little attempt has been made to examine the malpositioning of the chest tubes and lines due to technical qualities and their impact on the appearance of chest tubes and lines in ICU chest radiography.

Despite the many studies carried out on the technical considerations and limitations of mobile chest radiography in the ICU, little attention has been paid to the technical adequacy of the patient position, which can be rotated, kyphotic or lordotic, and how that can impact on the visualisation of the chest tubes and lines in chest radiography.

This study will consider how the technical quality of the intensive care unit chest radiography can impact upon the appearance of chest tubes and lines and how that appearance can impact on the decision making with regard to patients' clinical situations.

3 Chapter Three: Background literature

3.1 Background on X-ray history

Friday November 8th 1895 When Wilhelm Conrad Roentgen, a Professor and head of department of Physics at Julius-Maximillan University at Wurzburg in Germany (Bentley, 2005) ending his workday, he prepared his research apparatus (Crookes tube) to be conducted after he returns to his laboratory in the next day.

After Roentgen darkened the room he observed faint light emitted from material located several feet from his energized tube and the source was a piece of paper coated with barium platinocyanide, which was indicate that their interaction between the energy emitted from the Crookes tube and the material to produce the light or fluoresce (Fauber, 2009).

After that Roentgen demonstrated many experiments to detect the powerful of penetrating the X-ray through the paper, wood, tin and hand's of his wife with ring on one finger,(Glasser et al., 1933). This was the first X-ray that showed the bones of the hand on 22 December 1895 (Fauber, 2009). As the rays did not show the properties of the light he named them rays X-rays for such vagueness (Rowe, 2003). For this discovery Roentgen in 1901 was awarded Nobel Prize in physics(Haubrich, 2003).

In the years to come following properties of the new ray has been established, which were invisible, travels in straight lines, capable of blacking a photographic plate, absorbed in the matter and capable to produce biological reactions such as genetic mutation (Valkovic, 1996).

Hospitals acquired the X-ray equipment soon after the discovery of the X-ray by Roentgen, as doctors were using the X-ray to detect location of injuries and fractures (Lentle and Aldrich, 1997). However, taking chest X-ray was a lengthy process, for example in 1896 an X-ray of a girl took 30 minutes at St Thomas's in London. The image was made onto glass plate.

However, technology continued to evolve where a film was used in 1918 by Eastman for the first time and then became wide spread in 1923 (Thomas et al., 1995).

The discovering of the x-ray was a remarkable process in history and played a huge role in medical diagnosis. As it revealed the inner parts of the human body without need to cut into the flesh as observing surgical method.

3.1.1 Production of the X-ray

X-ray can be produced by two different processes, which are bremsstrahlung, the most interaction in the diagnostic energy range and characteristic X-ray production. Bremsstrahlung X-ray can be generated by interaction between the electrons and nuclear electric field, which by the positive charge of the nuclear the incident electrons direction will change and lose energy and some of the electrons kinetic energy will emitted as X-ray photons Figure (3-1)(Huda and Slone, 2003).

Figure 3-1: Production of bremsstrahlung radiation

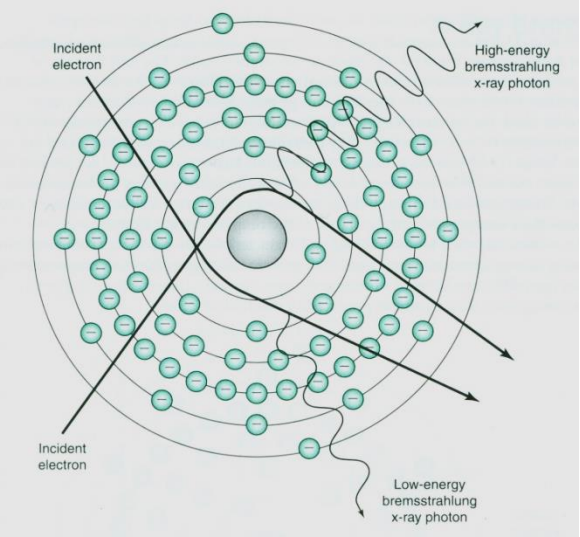

Source (Fauber, 2009)

Characteristic X-ray can be produced by the interaction between the incident electrons with inner shell electron as a result of this interact both of electrons ejected out the atom and the inner shell position will filled by the outer shell

electron and the energy difference between the inner and outer shell will emitted characteristic radiation Figure (3-2)(Huda and Slone, 2003).

Figure 3-2: Production of characteristic radiation

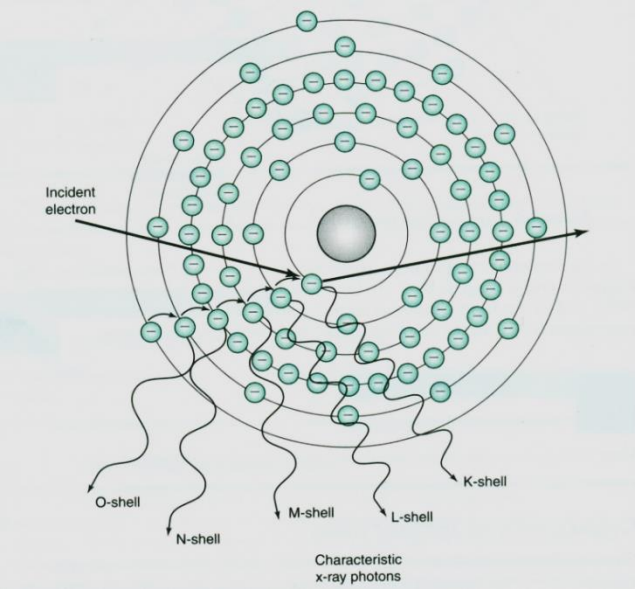

Source (Fauber, 2009)

X-ray generating requires quick moving flow of electrons from a cathode (negative electrode) by heating the filament to about 2000 ^{o}C. Generally filament of the cathode made from tungsten, which has high melting temperature (3410 ^{o}C), low vapour pressure and high atomic number (Easton, 2009). The flow of the electrons is stopped by anode (positive electrode). Anode stops the stream of the electrons coming from the cathode to produce the beam inside the x-ray tube (Carter et al., 1994).

The production of the X-ray is controlled by exposure factors, which are kilovoltage and milliampere-second. The kilovoltage determines the speed controlling of the electrons traveling from the cathode to the anode. A milliampere-second is the unit used to assess the tube current, which is the number of electrons traveling between the cathode and anode by the time in seconds (Fauber, 2009).

After exposing the matter an attenuation or reduction in the intensity of the primary x-ray photons beam will occur as it travels through the matter like the anatomical structures (Easton, 2009).

3.1.2 X-ray interactions

During the attenuation or decrease in the intensity of the x-ray photons as the X-ray primary beam penetrates the body, some photons are absorbed in the body so their energy will transfer to the body, some scattered with reducing in their energy and changing the primary beams direction and the rest of photons penetrates without reduction in their energy or direction (Dixon, 2008) however the extent of the attenuation in the medium depends on the atomic number of the medium and the primary x-ray photons energy received (Pope, 1999).

Radiographically there are two important attenuation processes, which are photoelectric effect and Compton scatter (Easton, 2009). Photoelectric effect can occur when x-ray photons interacting with electron in the inner shell of the atom. The incident photons' energy should be higher than the binding energy of the atoms' electron to eject an inner shell electron and lead to full the ejected electron hole by dropping electron from the upper level shell, the difference in the energy between the shells convert to energy photon emitted, which carried the same characteristic of the inner shell of the atom (Pope, 1999).

Compton Effect occurs when incoming x-ray photon with energy much greater than the binding energy interacts with an outer shell electron and that leads to loss of energy and a change in the direction of the x-ray photon, while Compton electron caries away the energy lost by the scattered photon (Huda and Slone, 2003). However, the interactions of the photoelectric and Compton effect cannot be separated during the attenuation process (Easton, 2009).

In radiographic imaging distinguishing between the anatomical structures shadows is the main purpose of the x-ray process (Pope, 1999). The image contrast resulting from differences in the X-ray absorption arising from the density differences and the variations in materials and the thickness of objects, which are the important parameters during the attenuation process in the human body (Moskowitz, 2010).

Because the appearance of the anatomical structures when the X-ray photons passing through it, depends on the differences in the body tissues absorption, therefore in the area where the density is low and the attenuation could be

neglected with X-ray beam totally transmitted the medium appearance like the air will be black. while in the area where the atomic number is high and the attenuation high as a result of absorbing the X-ray beam (photoelectric interactions), the appearance of the medium like bone will be white table 1 (Pope, 1999).

However, scattering process or scatter radiations (Compton interactions) from the primary X-ray beam will not provide any diagnostic information for the examined area rather it creates unwanted density on the X-ray film called fog contrast (Fauber, 2009). So this combination between the absorption and transmission of the primary X-ray photons beam produce the radiographic image that reflects the differential absorption of the tissue Table (3-1).

Table 3-1: X-ray attenuation

Medium	**Attenuation**	**Appearance on film**
Air	Negligible	Black
Fat	Small	Dark grey
Other soft tissues	Medium	Grey
Bone	High	White

Source: Pope(1999)

3.2 Chest anatomy

3.2.1 Introduction

This descriptive part will describe the chest radiographic anatomy structures and their radiological appearance. Because the chest cavity contains very important structures and many tubes and lines can pass through the chest for many purposes such as feeding, mechanical ventilation, medicine administering and monitoring atrial pressure (De Lacey et al., 2008). It is important to give a background about descriptive radiographic chest anatomy and illustrating the normal feature of the chest anatomical structures. Radiographic chest anatomy gives clear guidance to the proper position of the structures in chest radiography in order to be oriented with the abnormal findings in the heart, pleura, lungs, tracheal tree, oesophagus, thoracic lymph nodes, thoracic vertebrae and chest wall (Collins and Stern, 2008). From understanding the normal radiographic chest anatomy many pathological signs and symptoms can be detected and also chest tubes and lines can be placed in the proper position. However, the appearance of the anatomical chest structures and any pathological findings can be affected by the quality technique of the chest radiography. For example, the heart shadow size in the supine anterior posterior chest radiography appeared larger than the normal size due to gravity and the distance between the X-ray tube and the patient (Moskowitz, 2010).

3.2.2 The thoracic cage

There are three primary components of the thoracic cage, which are the ribs and costal cartilages, the sternum and the thoracic vertebrae (Moore and Dalley, 2006).

The ribs: there are three types of ribs; true ribs from first to seventh rib, these are attached directly to the sternum through their own costal cartilages. False ribs from eighth to tenth, their costal cartilages are joined to the rib just above them so their attachment to the sternum is indirect. Floating ribs from eleventh to twelfth; these ribs attach to vertebrae, but not to the sternum so they float on one end. The Radiological feature of the Upper ribs especially the first rib variation is common and the second rib is usually observed prominence(Ryan and McNicholas, 1994).

3.2.3 The Sternum

It has 3 parts: the manubrium, the body, and the xiphoid process. The manubrium is at the level of third and fourth vertebrae and articulating with the clavicle and costal cartilages . Sternal angle at the level of fourth and fifth thoracic vertebrae and articulating with second rib cartilage. A body which is located opposite fifth to ninth thoracic vertebrae articulates with five and one half costal cartilages and xiphoid process. Xiphoid process is the inferior part of the sternum (Snell, 2008).

in the posterior anterior view, only part of the body of sternum, manubrium and sternocalvicular articulation are defined. However, lateral view are helpful to define the cortical outlines and sternal angle (Lange and Walsh, 2007).

3.2.4 Thoracic vertebrae

There are twelve vertebrae most of them are typical and have characteristic features: Costal facets (flat spots for attachments) on the body of the vertebrae for articulation with the ribs (costovertebral articulation).Costal facets on the transverse processes for articulation with the tubercles of the ribs. Long spinous processes (Moore and Dalley, 2006).The radiological feature of the vertebrae within anterior posterior view of the chest radiography can be identified on well-exposed frontal view. On the lateral view, the superior and inferior articular processes can be identified (Lange and Walsh, 2007).

3.2.5 The trachea and bronchi

Trachea has cartilaginous horseshoe-shaped like rings from interior and lateral wall (Bourke and Burns, 2011). It begins at the level of C6 vertebra to the level of sternal angle at the level of fourth, fifth thoracic vertebra during inspiration process and at the level of sixth vertebra with expiration. The trachea about 15cm in length and diameter about 2cm (Ryan and McNicholas, 1994).

Main bronchi divided to right and left bronchus at the carina part. Carina lies at the level of T4/T5 and the level of sternal angle. It makes angle about 65%, the position of carina will move inferiorly to sixth thoracic vertebra with the inspiration process (Briggs, 2004).

The right main bronchus lies at approximately 25° to the median plane in the adult (Briggs, 2004). Their length about 2.5cm and 1.5cm wide (Ryan and McNicholas, 1994). The right bronchus divided into apical, posterior, anterior in the upper part and lateral, medial in the middle of the right lung; in the lower part of the right bronchus there is anterior, posterior, lateral medial basal bronchus. Left main bronchus lies at 40° to the median line. The left main bronchus length is about 5cm and 1.2cm in diameter. The left bronchus divided into upper part include apical posterior, anterior and lower part which include posterior, anterior, lateral and lingual part which include superior, inferior left bronchus.

The radiological appearance of the trachea and bronchi shows that the midline translucency with a slight tendency to the right in the lower part (Ryan and McNicholas, 1994).

In addition, the appearance of the left side is not isolated from the mediastinal shadows, and also in the feature of the trachea is usually seen smooth indentation on the trachea just over the bifurcation on the left side. On the plain films the bronchi give very little to the lung signs, but it might be the proximal bronchi seen if outlined by the lungs (Ryan and McNicholas, 1994).

3.2.6 Lungs

The lungs are divided into four surfaces, costal, apical, mediastinal and diaphragmatic surfaces (Ryan and McNicholas, 1994). The apex of the lungs lies above the level of anterior end of the first rib and grooved by subclavian artery and subclavian vein. The base of the lung have concave shape which rests on dome of the diaphragm, however the right side higher than the left (Bontrager and Lampignano, 2005).

The right lung divided into three lobes (upper, middle, lower) by fissures (oblique, horizontal). The oblique fissure begins posteriorly at the level of 5^{th} thoracic vertebra and passing antero-inferiorly in a spiral course to meet the inferior margin close to the 6^{th}costochondral junction. In the right lung the upper, middle lobes and lower lobe separated by the oblique fissure. The horizontal fissure extends form anterior margin at the level of 4^{th} costal cartilage and runs horizontally backwards to meet oblique fissure in the mid-axillary line. In the right lung the upper and middle lobes separated by the horizontal fissure. The left lung divided into two lobes (upper and lower) divide by oblique fissure (Briggs, 2004).The radiological appearance of the lungs seen black in the image because it contains air (De Lacey et al., 2008) and lungs fissures can be seen only if parallel to the source of the radiation (Ryan and McNicholas, 1994).

3.2.7 Pleura

A membrane covering the lung (i.e. the visceral pleura), mediastinum and thoracic cavity (i.e. the parietal pleura).Pleura divided into three parts mediastinal, apical, and diaphragmatic pleura according to their site (Ryan and McNicholas, 1994). The radiological feature of the pleura shadows can be seen only if at a tangent to the x-ray or if there is air or fat on each pleura side (Ryan and McNicholas, 1994).

3.2.8 Heart

Heart is pyramidal in shape with oblique position in the chest cavity. The heart is divided into four chambers left atrium, right atrium, left ventricle, right ventricle connected with blood vessels, which are the coronary arteries, superior vena cava, inferior vena cava, aorta, pulmonary artery, pulmonary vein (Ryan and McNicholas, 1994). The radiological feature for the heart as a soft tissue and counter appears grey on front and lateral chest radiography (De Lacey et al., 2008). The main parts which appear in the image are right atrium, right ventricle, left ventricle and aortic arch, ascending aorta and superior vena cava (Ryan and McNicholas, 1994).

3.2.9 Diaphragm

The diaphragm is the inferior border of the thoracic cavity, which is a dome shaped sheet. The radiological feature of the diaphragm in the posteroanterior view the right dome usually higher than the left dome by about 2 cm, where is the highest point of the right dome can reach the sixth intercostal space. However, the left dome can be higher than right dome in normal situation of swallowing gas in the colon (Ryan and McNicholas, 1994).

3.3 Chest tubes and lines

3.3.1 Central venous catheter

Figure 3-3: Central venous catheter

Source: Barlieindustry.com

The first use of the central venous catheter (CVC) or line Figure (3-3) in humans, for measuring right atrial pressure or cardiac output, was by Cournand and Ranges in 1941 (Hamilton and Bodenham, 2009). A CVC is used for both diagnostic and therapeutic purposes, but is commonly used diagnostically in critically ill patients to measure central venous pressure and blood draws (Collins and Stern, 2008). Therapeutically, the CVC is used to administer medicine, infuse fluids and administer nutrition (Kazerooni et al., 2004).

Although CVCs enable the administration of life-supporting medications and therapies, the presence of these catheters places patients at risk of catheter-related bloodstream infections or central line-associated bacteraemia (CLAB), which can be fatal (Moretti et al., 2005).

A CVC is typically inserted into the internal jugular, external jugular, subclavian vein or femoral vein, the latter avoiding risk of pneumothorax (Kazerooni et al., 2004). The preferred position of the tip is in the distal superior vena cava at the junction of the superior vena cava and the right atrium (De Lacey et al., 2008). The junction of the left and right brachiocephalic veins forms the superior vena cava, which lies to the right of midline at the level of the first intercostal space (Collins and Stern, 2008).

The tip of the catheter should be located in the superior vena cava Figure (3-4) or a brachiocephalic vein when medicine is delivered or blood drawn. For measuring central venous pressure, the typical placement of the tip should be in the superior vena cava, but not near to the valve within the brachiocephalic veins, as this can affect the measurements of pressure. In addition, to avoid atrial arrhythmias, it should not be placed too distally in the right atrium (Kazerooni et al., 2004).

There are many types of CVC, such as Hickman and Cutdown catheters, which are usually used in emergency situations when visualization of the peripheral vein is limited, and jugular and subclavian catheters, which are also used in emergency situations when the chest and arms only are accessible (Nentwich, 1990). The most regularly used version of the CVC is Hickman catheter, named after Dr Robert O. Hickman and developed in the 1970s. These have one, two or three lumens (are monoluminal, biluminal or triluminal), lumens being wide, thick-walled tubes, made from silicon to ensure flexibility (Kazerooni et al., 2004).

Figure 3-4: Chest radiograph for the CVC tip typical position.

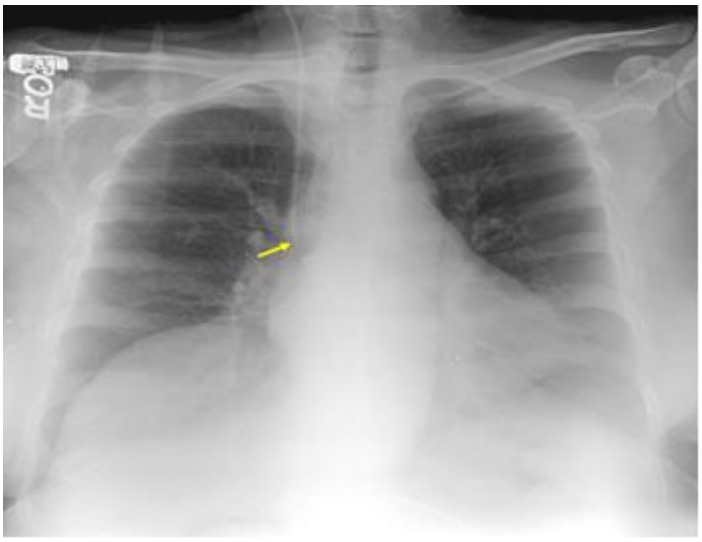

Source: http://webmm.ahrq.gov/case.aspx?caseID=292

3.3.2 Pulmonary artery catheter (Swan-Ganz)

Figure 3-5: Pulmonary artery catheter (SWAN- GANZ)

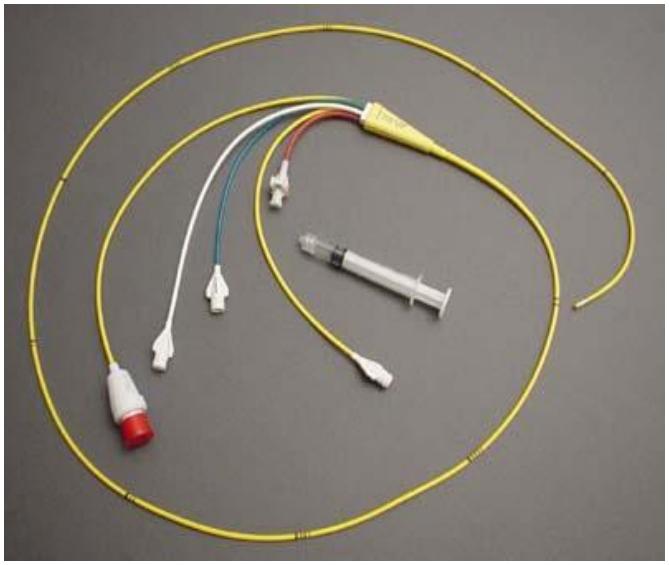

Source: healthsystem.virginia.edu.

This type of catheter is often called a Swan-Ganz Figure (3-5) in reference to cardiologists William Ganz, who placed a balloon at the end of a flexible catheter, to be inserted into an artery (allowing for quicker movement), and Jeremy Swan, who had added a thermistor to measure cardiac output in real time (Kazerooni et al., 2004).

The innovation of the pulmonary artery catheter greatly improved patient critical care, allowing physicians to measure many quantitative physiological parameters at the mobile (Marino et al., 2007). Beforehand, mobile evaluation of cardiovascular function was very basic and relied on indirect measurements such as listening to the sound of the heart via the stethoscope, using blood pressure apparatus, taking a patient's pulse or body temperature, or visually noting skin colour or oedema (Marino et al., 2007).

There are five types of pulmonary artery catheter, usage of which depends on the purpose. These are the standard pulmonary artery catheter (PAC), pacing PAC, continuous cardiac output PAC, continuous mixed venous O_2 PAC, and right ventricle ejection fraction PAC (Irwin and Rippe, 2010). This catheter's standard length is about 110cm, the tube's outside diameter being about 2.3mm. There are four lumens in the proximal end – the proximal port, port of the thermistor, port to the balloon and distal port (Irwin and Rippe, 2010)

A Swan-Ganz catheter is inserted through the internal jugular vein and subclavian veins (Marino et al., 2007), the most common place of insertion being through the right internal jugular vein (Kazerooni et al., 2004). The typical tip position is in right distal pulmonary artery, with no more than 2cm beyond the hilum centre (Aronchick and Miller, 1997) Figure (3-6).

The purpose of this catheter is to monitor pulmonary artery pressure, distinguish between cardiac and non-cardiac pulmonary oedema (De Lacey et al., 2008) and to assess the function of right and left ventricles and hemodynamic status (Irwin and Rippe, 2010).

Figure 3-6: Chest radiography for a pulmonary artery catheter.

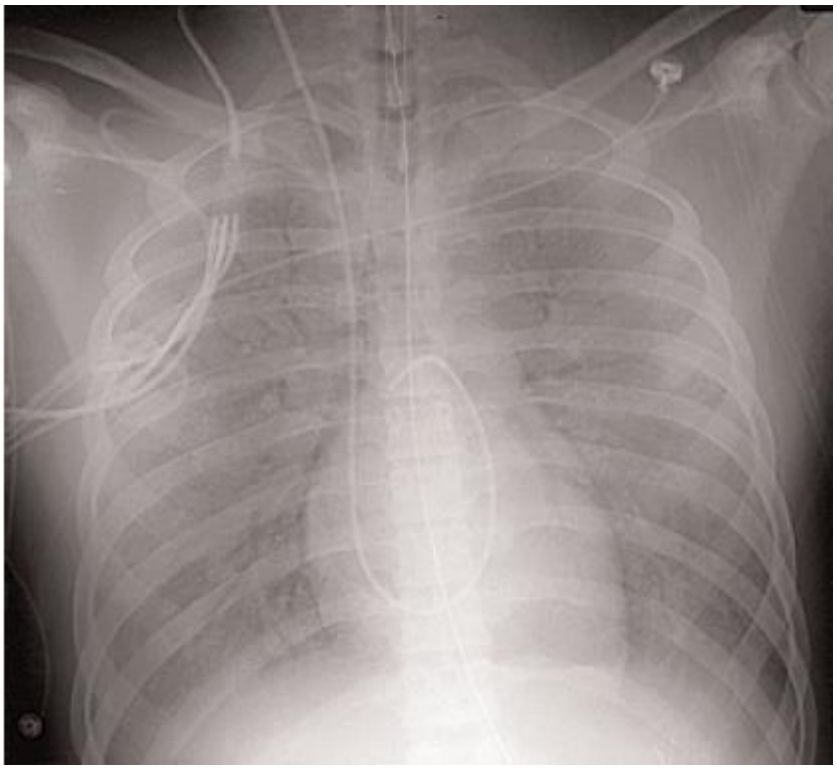

Source: Connolly(2001).

3.3.3 Nasogastric tube

Figure 3-7: Nasogastric tube.

Source: progressivemed.com

A nasogastric tube is a narrow tube passed through the nose to the stomach. It can used only for short or medium periods of time in order to avoid complications such as nasopharyngeal irritation, ulceration, sinusitis, serous otitis and pharyngitis (Javors and Wolf, 2003).

There are two types of nasogastric tube. The Levin tube is made from plastic or rubber, has a single lumen and measures 106.5 to 127cm in length. The second, the Salem sump, is made from pure plastic, has double lumens with radiopaque lines in order to monitor the tube position during and after insertion and measures about 122cm in length (Lippincott and Wilkins, 2009).

The ideal position for the tip of the nasogastric tube Figure (3-8) is about 10cm beyond the gastro-oesophageal junction (De Lacey et al., 2008). Its purposes are both diagnostic and therapeutic (assessing and treating upper gastrointestinal bleeding, gastric decompression/aspiration, performing gastric lavage, collecting gastric contents for analysis, providing nutrition and administering medicine) (Lippincott and Wilkins, 2009).

Figure 3-8: Chest radiography for appropriate position of nasogastric tube

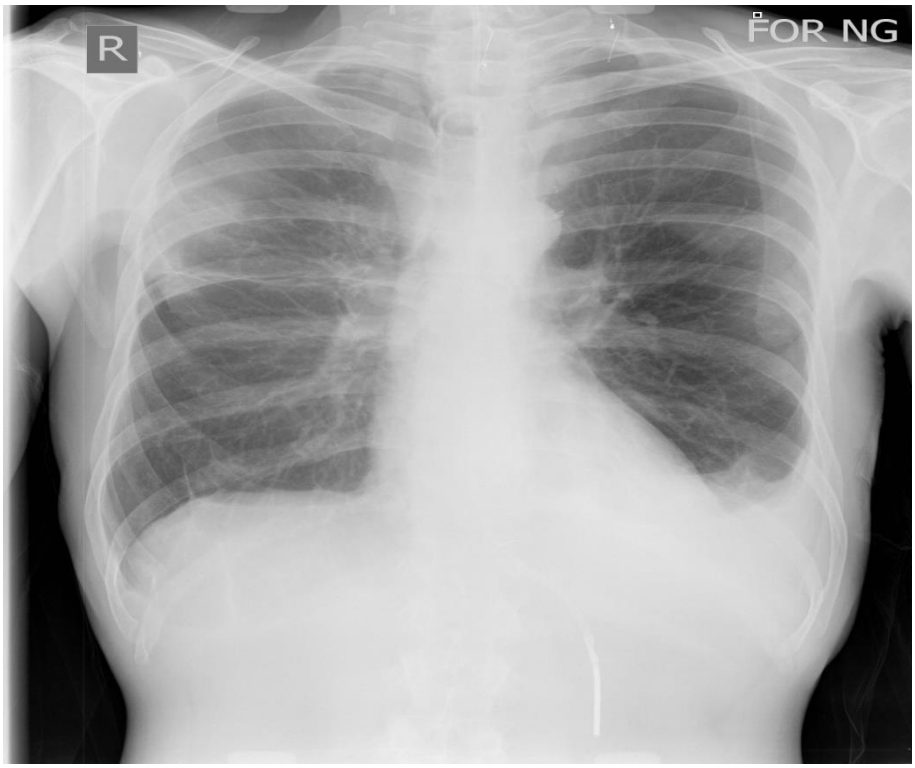

Source: Radiopaedia.org

3.3.4 Thoracostomy tube

Figure 3-9: Thoracostomy tube

Source: Endo.co.id

More commonly called a chest tube, a tube thoracostomy is usually inserted in the emergency department to remove blood (hemothorax), air (pneumothorax) or fluid (pleural empyema or effusion) from the pleural space or chest cavity (Mahadevan and Garmel, 2005). The chest tube is made from plastic and the length varies from 30 to 101cm (Mahadevan and Garmel, 2005).

The best location for the tip of the tube is in the lower part of the thorax, at the level of the fifth or sixth intercostal space Figure (3-10). However, this depends on the reason for insertion: posteriorly is the typical position for the drainage of pleural fluid while anterosuperiorly is ideal for removing air. For example, in the pneumothorax, the tube can be placed in the second intercostal space (Mahadevan and Garmel, 2005).

Figure 3-10: Chest radiography for the typical position of chest tube.

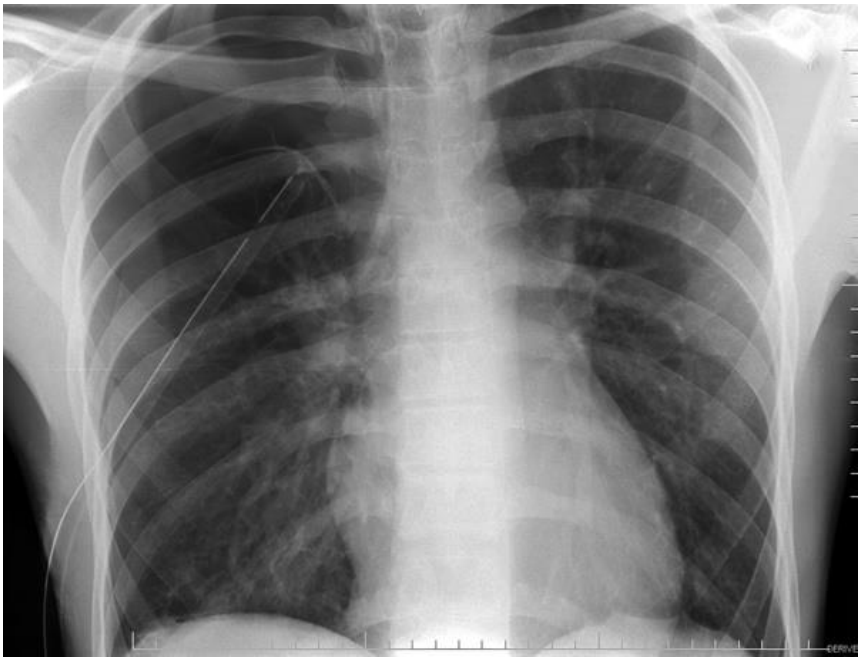

Source: CTSNET.org.

3.3.5 Endotracheal tube

Figure 3-11: Endotracheal tube

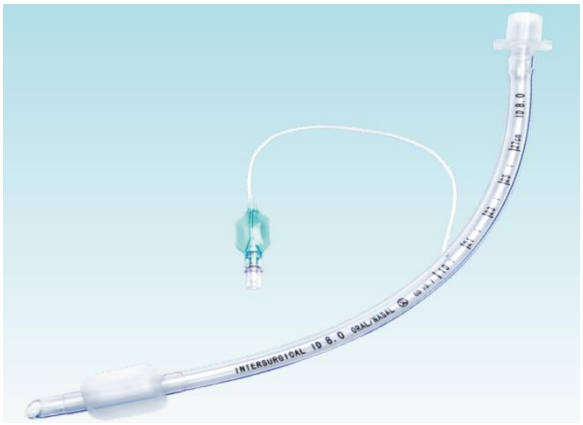

Source: Howequipmentworks.com.

Endotracheal tubes are today the most applied piece of emergency equipment in the medical field, especially during general anaesthesia. In addition, more than 80% of surgical operations from varying areas of specialism require the use of endotracheal tubes (Brandt, 1986). Anaesthetically, endotracheal tubes have been used for more than 1000 years, but a significant development in their usage was in 1869, when the first operation with endotracheal intubation was carried out by German surgeon FreidrichTrendelenburg (Brandt, 1986).

Various endotracheal tubes are used, such as cuffed and uncuffed, in a comprehensive range of sizes. An uncuffed endotracheal tubes (ETT) has a smooth tip, which aids traumatic intubations and reduces unnecessary trauma, a radiopaque line to assist in radiographic imaging and managing of the exact location of the tube, a Murphy eye near to the tip of the tube to reduce the risk of occlusion and to help maintain air flow, precise calibration to indicate the depth of the insertion, and a connector for reliable connection to all standard equipment (Hogan-med.com, 2008).

A cuffed ETT has a connector, soft tip, Murphy eye, radiopaque line, calibration and a valve to ensure continual cuff integrity (Hogan-med.com, 2008). Where the size of the ETT refers to the internal diameter, cuffed ETT sizes range from 4.5 to 10mm, uncuffed from 2 to 7mm (Howequipmentworks.com 2008). However, there are slight differences in ETT sizes due to there being different manufacturing companies, but in general for adult male and female patients the 7mm is the most used (Davidson and Treacher, 2002).

Traditionally, endotracheal tubes have been made from red rubber or latex for easy cleaning, sterilizing and reuse. Currently, however, ETTs are made from polyvinyl chloride – PVC – and more recently polyurethane. These are cheap to make, making reuse unnecessary (Moyle et al., 1998).

Insertion can be via the nose or the mouth. Oral insertion is the most common method in emergency cases, and this is easier if there is no cervical spine injury (Moyle et al., 1998). The best location for the tip of an endotracheal tube is about 5 to 7cm from the carina Figure (3-12).

ETTs can also move up or down, in relation to the flexing or extension and rotation of the neck. This allows for a 1.9cm downwards flexion, a 1.9cm upwards neck extension and a 0.7cm upwards neck rotation. Because of this, the tube should situated between the carina and vocal cords (De Lacey et al., 2008). The purpose of this tube is to support the ventilation process and to prevent disorders of gas exchange or obstruction in the airway (Aronchick and Miller, 1997).

Figure 3-12: Chest radiography for the endotracheal tube typical position

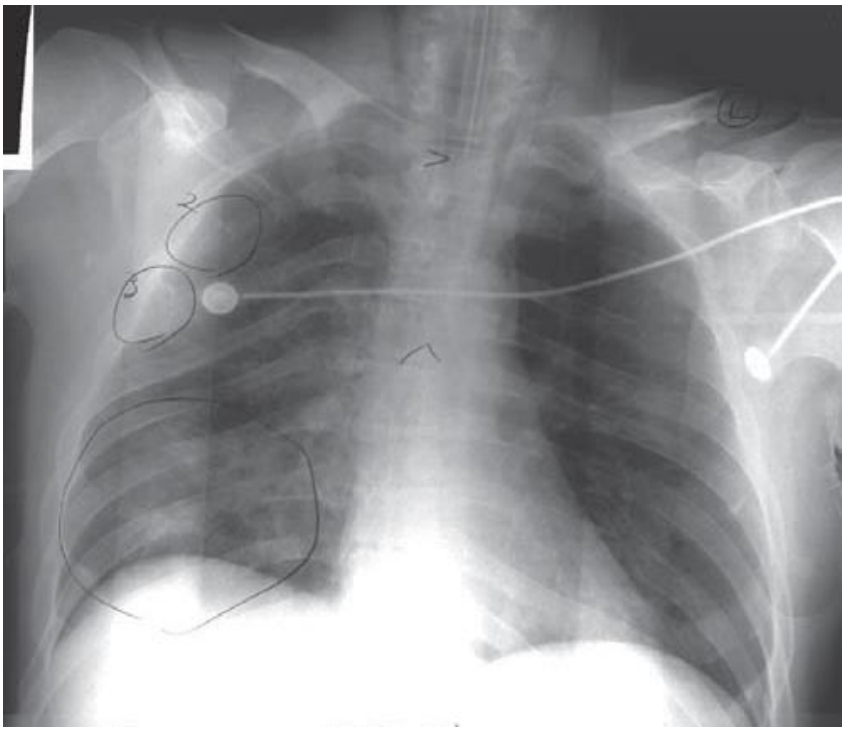

source : Hobbs(2007)

4 Chapter Four: An identification of degree of angulation (rotation, kyphosis and lordosis) and apparent of chest tube/line movement on chest phantom

4.1 Introduction

The purpose of conducting this experiment was to identify the measurements of rotation, kyphotic and lordotic degrees related to the chest anatomical structures, chest tubes and lines. Therefore, the experiment aimed to quantify degrees of angulation via anatomical structure indicators – rotation, kyphosis and lordosis – in order that by identifying measurements of anatomical symmetry it is possible to estimate the degree of angulation.

There are two aims. The first is to assess whether the degree of rotation and kyphosis/lordosis could be estimated from anatomical measurements from the phantom. The second is to identify apparent movement of tube/ line position with degree of rotation and kyphotic/lordotic angulation.

The data collected through the experiment answer the primary research question. They also serve to evaluate the acceptable level of the technical quality of ICU chest radiography and its impact on the appearance of chest tube and lines, and therefore the potential for these to appear malpositioned. For example, in ICU chest radiography based on measurements of anatomical indicators, the degree of angulation can be estimated.

4.2 Justification of chosen experimental approach

This experiment aimed to associate a very precise change of angulation with change in the apparent position of chest tubes and lines. In addition, it tried to find ways of using the appearance of normal anatomy in chest radiography to identify the degree of departure from the optimum position. However, it is difficult in real life, and in traditional clinical practice, to measure the precise degree of rotation, kyphosis and lordosis and their impacts on the appearance of anatomical structures

and chest tubes and lines. The experiment used a phantom chest with standard body morphology, which can affect the generalisability of measurements.

Consequently, using this experimental approach, we can control the precise degree of angulation and the changes of position in the anatomical structures and the appearance of chest tubes and lines and yield quantitative data, which can be analysed statistically (Altman, 1999). We can replicate the measurements to achieve precision in estimating the effects of rotation, kyphosis and lordosis on the appearance of tubes and lines.

4.3 Chest phantom measurements justification

Traditionally, in order to detect kyphosis and lordosis, the distance between the clavicles and lung apex is measured, and in order to detect rotation of a patient in chest radiography, the distance between the clavicles and the spinous process of thoracic vertebrae is measured De Lacey et al (2008). However, the distance between the clavicle and spinous process can be affected by the depth of the chest (i.e. the distance between the vertebral body at the back and the clavicles at the front of the chest). For example, if a patient has a small chest depth and is rotated (left or right) the distance between clavicles and spinous process, this distance will appear smaller than for a patient who has a large chest depth.

In this experiment, the rationale for choosing and measuring the fourth anterior rib length and the distance between clavicle and spinous process because both would be expected to be sensitive to rotation. It was though that this measure may be less influenced by patient size. For kyphosis and lordosis the rationale for choosing and measuring the fourth anterior rib angle and the distance between the clavicle and apex is expected to be sensitive to angulation due to changes in distortion of rib on the radiograph, which was explained in chapter 2.

Additionally, the anterior fourth rib was used because the projected position of the fourth anterior rib on the radiograph is approximately midway between the apex of lung and the diaphragm, and also because the fourth rib can be affected by rotating the upper and lower parts of the chest. Moreover, there are two ribs (left and right), so the ratio of ribs is more sensitive, which makes it easier to see and judge variation.

4.4 Materials and methods

4.4.1 Chest phantom experiment for assessing chest radiography rotation, kyphosis and lordosis

4.4.1.1 Introduction

This experiment was conducted in order to measure the change in apparent position of the tip of chest tubes and lines due to rotation, kyphosis and lordosis. The experiment attempted to understand the relationship between the change of the tip position and the degree of angulation by measuring the clavicle to apex distance and fourth anterior rib angle for lordosis and kyphosis, and the displacement of the midline between the clavicles and ratio of fourth anterior rib (left and right) length for rotation. The degree of angulation was measured in degree intervals of ± 2, 5, 7, 10, 15, 20, 25 for rotation, and for kyphosis and lordosis ± 2, 5, 7, 10, 15, 20, subsequently categorized as mild, moderate or severe in effect on visualisation of anatomical chest structures, tubes and lines.

4.4.1.2 Assessing the impact of rotation around sagittal axis of the chest phantom

For rotation element of the experiment, there were two distinct purposes:

1- The presence of rotation is identified by radiographers, subjectively by assessing whether the clavicle to spinous process distance and the rib lengths are symmetric. However, to date there has been no published study investigating the relationship between the degree of asymmetry and the amount (in degree) of rotation. This part of the experiment enables us to quantify this relationship.

2- To identify the influence of the angle of rotation on the apparent position of the tip of the central venous catheter.

A digital computed radiography (CR) X-ray machine in the experiment room of the School of Health Studies at the University of Bradford was used, with a ceiling-suspended CR (manufactured by WOLVERSON, ARCOMA, serial number 0170 CS, Fuji film image processor). Also used in the experiment was a chest phantom (PH1 multipurpose chest phantom, N1 "LUNGMAN" KYOTO KAGKU made in Japan) of approximately 45cm in height, 18 kg in weight and with a chest measurement of about 94cm. This was made from polyurethane for the soft tissue and vessels and epoxy resin and calcium carbonate for synthetic bones.

This chest phantom has been used in this experiment due to many reasons. The phantom is an accurate life-size anatomical model of a human torso. The thickness of the chest wall is based on measurement of clinical data. The soft tissue substitute material and synthetic bones have x-ray absorption rates very close to those of human tissues. The inner components consist of pulmonary vasculature, mediastinum and diaphragm block which allows insertion and detection of the radio-opaque ball. This phantom also is designed for interpretation training, not only to check the quality control of the radiographs. The "Duke" chest phantom (Made in USA) is only useful for the letter. The Alderson Lung/Chest phantom was not chosen because its structure consists of two parts which can lead to limitations in inserting the radio-opaque balls.

The chest phantom was placed in the digital CR room on a separate plate supported by a table Figure (4-1), which was located in front of the chest stand. The shape of the plate was circular and the plate was divided into two circular parts: a glass plate and a metal part under the glass plate. The metal part was marked with the degree of rotation (± 2, 5, 7, 10, 15, 20, 25); the circular glass plate was labelled by drawing two lines (vertical and horizontal) crossing at the centre point. The plate was put on the table, and between the table and the plate there was a lined sheet of paper (80x60cm) with the degree of angulation drawn on it in order to measure the angle of the phantom's rotation.

The chest phantom was in an erect position and was rotated to ± 2, 5,7,10,15,20,25 degrees. The degrees were determined by using a protractor to determine the zero-point angle on the sheet of paper, to be at the level ofmedian sagittal plane at the bottom of the chest phantom. The point on the sheet of paper was static and the point the chest phantom moved to reach each angle was measured (± 2, 5, 7, 10, 15, 20, 25).

Then, using a protractor, from the zero point in the chest phantom to ± 2 degrees, a diagonal line was drawn on the sheet of paper, which will be applied for all the degrees of rotation, exposing the phantom to X-rays at each degree, with left rotation and right rotation, to be oriented with the variation of the anatomical structures which will be projected towards the right or left side of the chest. For example, the aortic arch may appear enlarged due to rotation to the left on an anteroposterior chest radiograph (De Lacey et al., 2008).

Figure 4-1: Chest phantom over circular plate supported by table

4.4.1.2.1 Assessing rotation by measuring the clavicles equidistance

One of the important measurements used in assessing rotation in chest radiographs is the clavicles' equidistance to the spinous process of the thoracic vertebra (McQuillen-Martensen, 1996).

Measurement of the distance from the medial end of each clavicle to the spinous process of thoracic vertebral body (spinous process of T5) was achieved by drawing a diagonal line which attached the medial end border of the left clavicle

and the midpoint of the clavicle medial surface. This procedure was repeated for the right clavicle Figure (4-2). Afterwards, a vertical line at the level of T5 spinous process was drawn through the centre of the thoracic vertebral body (T5). A horizontal line was then drawn from the midpoint of the medial end of the left clavicle to the midpoint of the medial end of the right clavicle.

Then, in order to determine the midpoint of medial border in each clavicle through the diagonal line, the distance from the midpoint of the left clavicle medial border to the spinous process was measured and coded y. The distance from the midpoint of the right clavicle medial border to spinous process was coded x. Measurements were conducted with all degrees of rotation (± 2, 5, 7, 10, 15, 20, 25).

The reason for using this range of degrees of rotation in this experiment is that this would cover the maximum range encountered in practise. Then the degree of rotation can be associated with the ratio r =x/y.

The rationale for this ratio was related to different chest sizes of the chest between one person and another. This is dependent on human body morphology, that is differing body shapes, classified as sthenic, hyposthenic, asthenic and hypersthenic. Sthenic refers to a normal body shape and represents approximately 50% of the population; hyposthenic represents about 35% of the population and denotes a thin body shape; asthenic represents 10% of the population and denotes a long and narrow body shape; and hypersthenic represents 5% of the population who have a large and stocky body shape (Campeau and Phelps, 1993).

Figure 4-2: The measurements of the ratio of right and left clavicle distance from midline during rotation

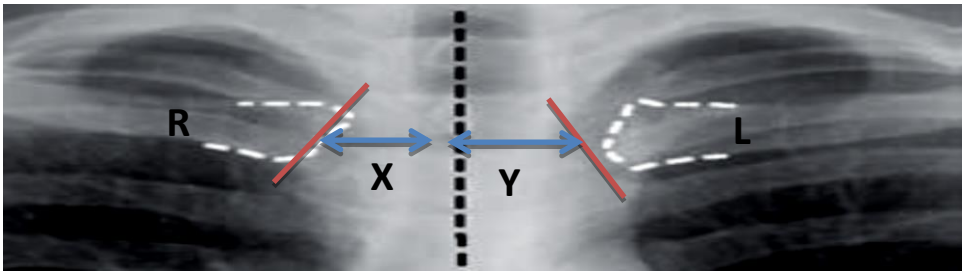

4.4.1.2.2 Assessing rotation by measuring the fourth anterior rib length

In order to measure the length of the fourth anterior rib, the process was to measure the thickness of each fourth rib from both ends (medial and lateral) (Figure 4-3). A line was then drawn from the midpoint of the lateral end to the midpoint of the medial end for each rib, the right (y) and the left (x). The measurements were recorded for all the degrees of rotation (± 2, 5, 7, 10, 15, 20, 25). Then the ratio of rotation was r =x/y.

Figure 4-3: The measurements of changing fourth rib length ratio related to the chest rotation.

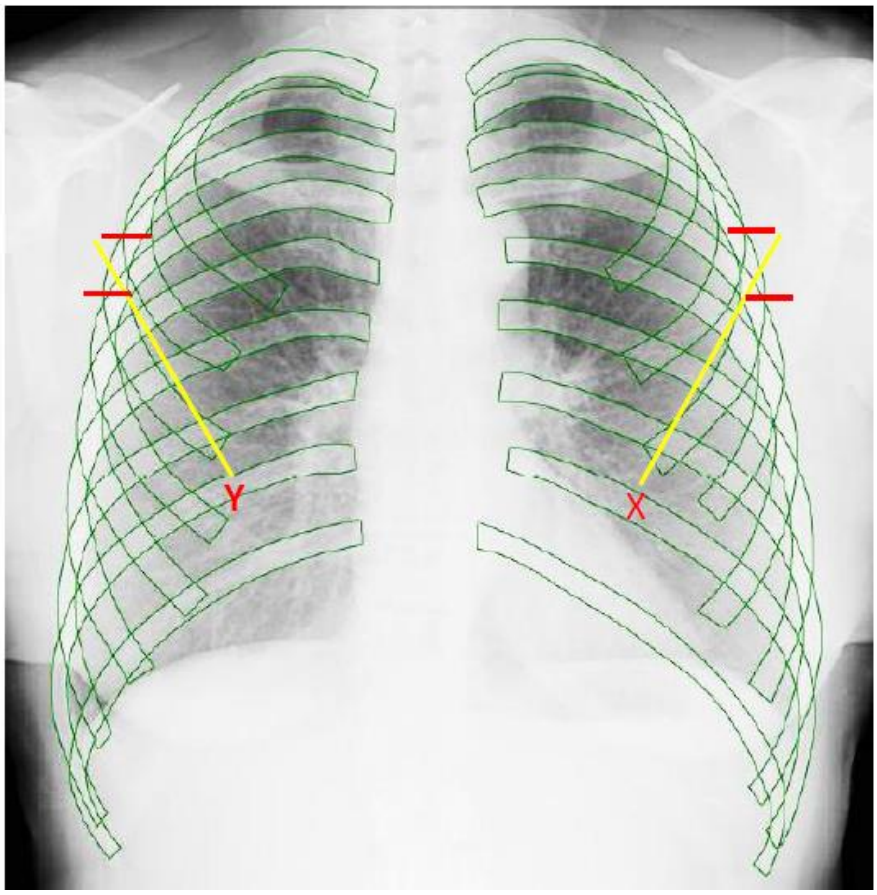

The measurements for both clavicles' equidistance and fourth rib length ratios was applied in the presence of a radio-opaque ball.

Method:

First, the chest phantom was placed erect with zero angle. The X-ray beam in the centre was placed between the manubrium and xiphoid and the distance between the X-ray tube and image receptor plate was set at about 100 cm. Second, an X-ray was taken to check the phantom was in the centre with no rotation. This was done by measuring the fourth anterior rib length and clavicles' equidistance to the spinous process (T5). Then the chest phantom was then rotated to 2 degrees right posterior oblique (RPO) and 2 degrees left posterior oblique (LPO). The reason for choosing 2 degrees in this experiment was to evaluate to what extent a slight rotation affected the visualisation of chest anatomical structures, tubes and lines.

The X-ray beam centre was centred between the manubrium and the xiphoid and the X-ray plate receptor put without the grid in holder, attached to the bucky standing table. The image receptor plate was placed in the landscape position. Then the chest phantom was exposed to the beam from the radiography X-ray machine. The distance between the radio-opaque metal ball and the chest wall for both sides (the right and left) was measured by drawing a vertical line at the inner chest wall side (for both the right and left), then drawing horizontal lines, one at the level of the lungs apex and the other at the level of the radio-opaque metal ball, which was at the level of the lower border of the third anterior rib. The same procedure was repeated for each subsequent angulation (5, 7, 10, 15, 20, 25).

The radio-opaque ball was located at the level of the carina, which is land mark for the position of tip of the CVC in the superior vena cava.

The reason why the distance from the radio-opaque ball (at the position of ETT) to chest wall during assessing the rotation was not measured, because it is position close to the sagittal plan and the change will be very little difference.

4.4.1.3 Assessing the impact of kyphosis and lordosis positions on the chest phantom

An experiment was conducted to identify the relationship between degree of angulation (caudally, cranially) and the distance between clavicles to apex and the fourth rib angle.

In this part of the experiment the endotracheal tube's typical position was the area of interest, because during kyphosis and lordosis movements the tip position of the endotracheal tube can shift upwards or downwards due to the angulation of the central ray related to the image receptor, with respect to the optimal position of endotracheal tube (Jenkins, 1980).

4.4.1.3.1 Assessing the impact of the kyphosis and lordosis positions on the chest phantom by measuring the distance between the clavicles and apex

Although measuring the distance between the clavicles and apex to evaluate the degree of kyphosis and lordosis was mentioned by McQuillen-Martensen (1996), they did not cite in which part of the clavicle the measurement should be taken or how this should be done. Therefore, in this experiment, a suitable measurement was described.

The distance between the clavicles and apex of the lungs was measured by drawing a horizontal line at the level of the upper medial end of the left clavicle and another horizontal line above the apex of the left lung at the highest point of the apex Figure (4-4).

Then a vertical line was drawn between the horizontal lines to identify the distance between them. The same procedure was applied for the right clavicle. The measurements were conducted over a range of angulations, from the likely minimum perceptible angulation to beyond the maximum angulation likely to be seen in clinical practice (± 2, 5, 7, 10, 15, 20 degrees).

Figure 4-4: The measurements of changing the distance between the clavicle and the apex of lung.

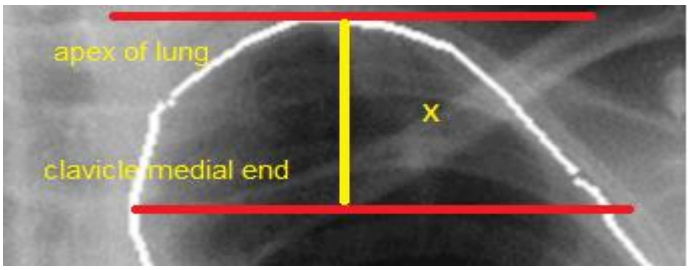

4.4.1.3.2 Assessing the impact of the kyphosis and lordosis positions on the chest phantom by measuring the fourth rib angle

Mehta (1972) described the rib vertebral angle, to differentiate between resolving and progressive infantile scoliosis. In this part of the experiment the fourth anterior rib angle was measured.

Measuring the fourth rib angle was achieved by drawing a line from the midpoint of the posterior end of the fourth rib to the point of intersection of the fourth rib and third rib on the exterior of the thoracic cavity Figure (4-5). Then, a line was drawn from the midpoint of the anterior end of the fourth rib to the point of intersection of the fourth rib and fifth rib on the exterior of the thoracic cavity. Next, a measure was taken of the angle subtended by intersection of these lines. The measurements revealed the degree of kyphosis and lordosis (± 2, 5, 7, 10, 15, 20).

Figure 4-5: The measurement of the fourth rib angle

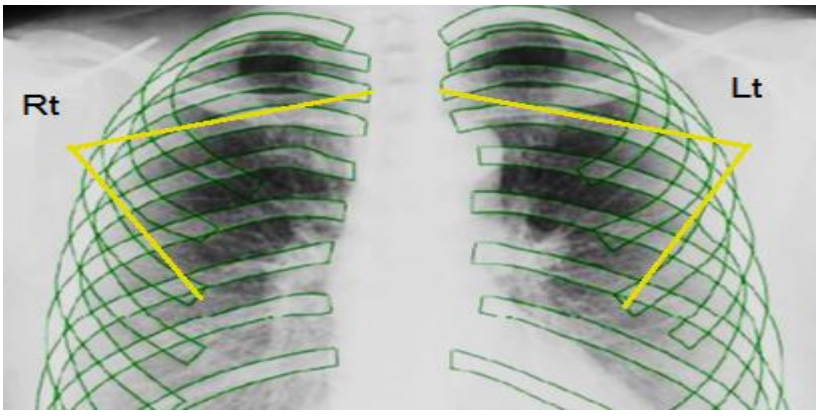

The measurements were applied in the presence of the radio-opaque ball. The chest phantom was placed in an erect position on a separate table opposite the bucky standing table and the distance between the X-ray tube and the image receptor plate was set at about 100 cm. The image receptor plate was placed in a holder attached to the bucky standing table. The radio-opaque ball was placed in the proper tip position of the endotracheal tube, which is in the mid-trachea, about 4–5 cm above the carina at the level of (T5, T6) (Moskowitz, 2010).

Method:

Firstly, the X-ray tube was tilted to zero angle and an X-ray taken to check that there was no kyphosis or lordosis in the chest phantom's position. Secondly, the X-ray tube was tilted to 2 degree cephalic and an X-ray taken, then 2 degree caudally and X-ray taken. The X-ray centre was midway between the sternal notch and xiphoid process, the diaphragm of the X-ray tube collimated appropriately, and the image receptor plate in landscape position. Then, to measure the radio-opaque ball position ratio, a horizontal line at the level of the radio-opaque ball was drawn parallel to the horizontal line at the level of the apex of the lung.

Next, measurements were taken of the clavicles to apex and the fourth rib angle, and the distance between the radio-opaque ball and the apex of the lung. The same procedure was repeated for each angle (5, 7, 10, 15, 20).

4.5 Statistical analysis

Stata Release 9.2 was used for all analyses. The data were collected to assess the relationship between the degree of angulation and the distance between the clavicles and spinous process, the fourth anterior rib length and the distance between the radio-opaque ball and the chest wall for rotation measurements. Also tested were the relationship between the degree of angulation and the distance between the clavicles and the apices of lungs, the fourth anterior rib angle and the distance between the radio opaque ball and the apices of lungs for kyphosis and lordosis angulation.

For rotation measurements the outcome measure were ratios of L/R clavicle to spinous process distances, fourth anterior rib lengths and radio-opaque ball to chest wall distances. The ratios were not a linear function of angle, but a logarithmic transform produced a reasonably linear fit.

Ratios are known to behave in this way since they vary between 0 and 1, if less than 1, and 1 and infinity if grater, i.e they are asymmetric about 1.

Linear regression analysis was applied to quantify the estimated change in the outcome measures per unit (degree) change in angulation.

For kyphotic/lordotic angulation the outcome measures were the mean distance of clavicle to apex of the lung and radio-opaque ball to apex distance and the mean fourth anterior rib angle, as previously described.

The outcome measures of kyphosis/lordosis angulation (distance measurements) were linearly related to angulation and therefore did not require transformation before undertaking the linear regression.

4.6 Results of chest phantom experiment

Chest phantom measurements were undertaken to associate very precise changes of angulation with changes in the apparent position of chest tubes and lines. Chest phantom measurements were also taken to identify precise changes in the appearances of normal anatomical indicators from the optimum position.

4.6.1 The measurements of rotation around the sagittal axis of the chest phantom

The measurements of chest phantom rotation have been collected for the degree of angulation (0 to 25 degree) Table (4-1).

Table 4-1: The measurements of chest phantom rotation

Angle	Clavicle–SP distance (mm)		Clavicle–SP ratio	Radio-opaque ball measurements distance (mm)		Radio-opaque ball ratio	Fourth rib length (mm)		Fourth rib length ratio
	R(y)	L(x)		R	L		R	L	
-25				101.18	166.50	1.64	46.16	118.46	2.56
-20				102.79	166.23	1.61	48.46	124.20	2.56
-15	43.09	4.36	9.9	106.54	167.84	1.57	53.20	113.92	2.14
-10	26.23	10.97	2.4	106.25	168.64	1.58	54.18	105.86	1.95
-7	31.85	13.65	2.3	106.80	168.64	1.57	58.78	96.48	1.64
-5	28.64	13.92	2.08	107.61	167.84	1.55	66.26	92.56	1.39
-2	21.41	19.54	1.09	110.55	167.57	1.51	70.33	86.33	1.22
0	23.82	22.49	1.06	111.89	166.23	1.48	77.50	81.23	1.04
2	21.68	25.97	1.19	111.62	165.69	1.48	81.93	73.50	1.12
5	15.79	27.84	1.76	111.09	164.36	1.47	88.41	69.73	1.28
7	14.99	32.39	2.16	112.16	163.55	1.45	91.95	68.52	1.35
10	13.38	40.15	3	112.43	159	1.41	96.09	61.61	1.56
15	9.64	45.24	4.69	113.23	157.40	1.39	106.43	53.89	2
20				114.57	153.38	1.33	113.55	47.39	2.43
25				116.17	149.63	1.28	116.60	39.44	3.03

Clavicle–SP distance: the distance between clavicle and spinous process.

Radio-opaque ball measurements distance: the distance between the radio-opaque ball and the chest wall.

The ratios for measurements for each (right and left rotation) measured for each, largest as numerator which changes according to the direction of rotation. For data analysis the ratios for right rotation were inverted so that all ratios were greater than one. This was done due to the symmetry of right/left rotation and so there were two estimates of the ratio for each angle.

The ratios were not linear function of angle, but natural log of ratios produced a reasonable linear fit.

Constant suppressed in the regression output (using noconstant option in the regression command) because we knew that for a perfectly symmetric image the ratios will both be 1 (i.e. the log rations will be zero). The unconstrained models (constant not forced to zero) have R^2 values for clavicle to spinous process and fourth anterior rib 0.89 and 0.94 respectively. The intercept values were both small, for clavicle to spinous process the intercept was not significant (p= 0.6) but for the fourth anterior rib length the intercept was significant (p=0.016). However, consideration of the constant of this part of experiment would indicate that the departure of the constant from zero is nevertheless due to experimental error.
Table (4-2) shows that there was a strong relationship between the angulation and the distance between the clavicles and spinous process and the fourth anterior rib length ratios where p value for all was ($p < 0.01$).

Table 4-2: Regression output of rotation measurements of clavicles and spinous process, and the log ratio of the fourth anterior rib length

Measurements	**Coefficient (CI) change per degree**	**P-value**
Clavicles to spinous process	0.119 (0.101-0.136)	< 0.01
Fourth anterior rib length	-0.045 (-0.049- -0.041)	< 0.01

The linear regression analysis illustrated that there was a strong relationship between the clavicle–midline spinous process ratios and the degree of angulation ($P < 0.01$). By increasing the ratio of the degree of angulation during the chest phantom rotation to left posterior oblique, the left clavicle–midline spinous process ratio gradually increased, while the right clavicle–midline spinous process ratio gradually decreased. When the chest phantom was rotated to right posterior oblique, the right clavicle–midline spinous process ratio gradually increased while the left clavicle–midline spinous process ratio gradually decreased.

The regression of the ratio of the fourth rib length was statistically significant ($P < 0.01$), where by rotating the chest phantom to the left posterior oblique, the ratio of the fourth rib was decreased by increasing the degree of angle.

When rotating the chest phantom to the right posterior oblique the fourth rib ratio was increased by decreasing the degree of angle.

a- For clavicle to spinous process, slope= 0.119 (95% conf. interval: 0.101, 0.136) this means that the log ratio increase by 0.119 units per degree of angulation (Table 4-2).

According to the results of statistics that showed the importance of linearity on the relationship between the ratios and the degree of angle rotation and depends on the general formula of straight line, which is $y = m.x + c$

Where in this experiment y= the ratio, m slope (coef), x angle value and c constant. Therefore, if a chest radiograph is taken and the clavicle to spine process ratio was 1.76 mm.

The general formula for linear regression model is $y = m.x + c$

In ratio (clavicle-spinous process) = 0.119 X angle

Therefore angle = $\ln(1.76) \div 0.119 = 4.75 \text{ degrees}$

b-For the fourth anterior rib length, slope= 0.045 (95%conf. interval: 0.041, 0.049) and this means the log ratio increase by 0.045 units per degree of angulation (Table 4-2).

Therefore, if chest radiograph has a ratio of fourth anterior rib lengths was 1.28 mm, the estimated degree of angulation will be:

Angle= $\ln(1.28) \div 0.045 = 5.5 \text{ degrees}$

Graph 4-1: Scatter plot between the ratios of clavicle–midline spinous process distance, fourth rib length and the degree of angle

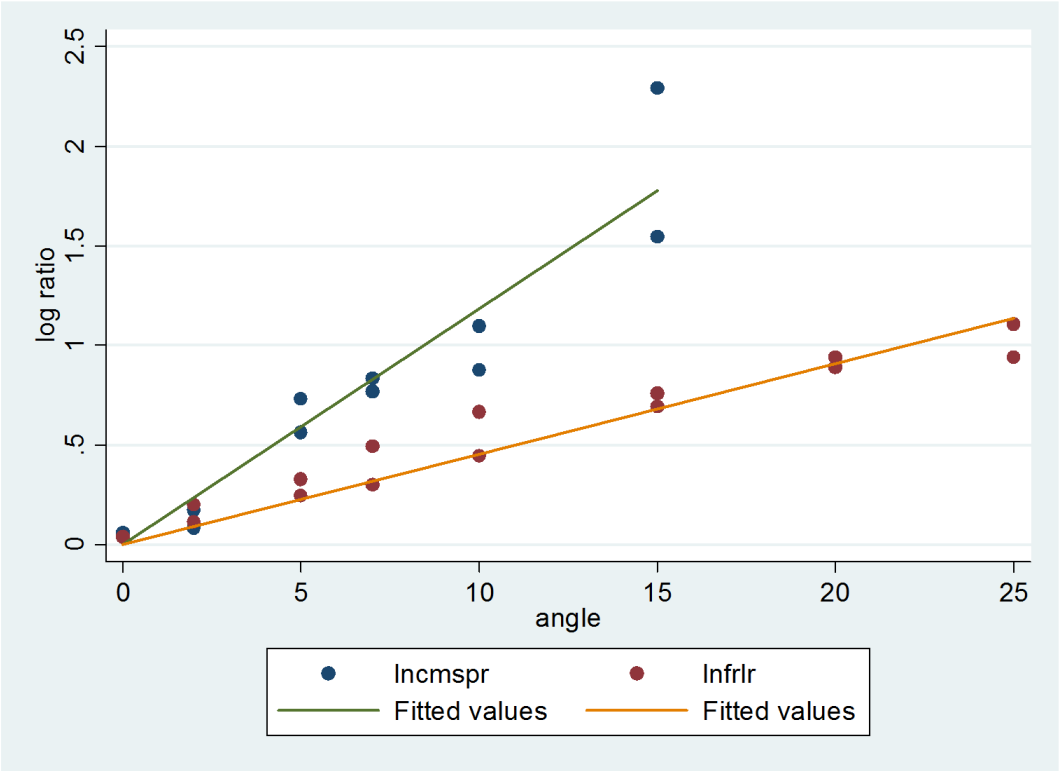

lncmspr*= natural logarithm of clavicle to midline spinous process ratio.*

lnfrlr*= natural logarithm of fourth rib length ratio*

-gradients of lines are the coefficient, given in table 4-2.

For the radio-opaque ball the measurements the ratios were modelled, rather than the log ratio, because in this instance the untransformed ratio produced a slightly better linear fit (R^2 = 0.96, v. R^2 = 0.95), probably due to the fact that the radio-opaque ball was offset from the midline so the ratios were always greater than 1 and over a narrow range of values (1.28 – 1.64).

In other words the slope line was not close to zero because the radio-opaque ball was offset from the midsagittal plane. The linear regression coefficient was negative (coef= -0.0071).

Linear regression analysis was applied to quantify the estimated change in the radio-opaque ball distance ratios per degree change in angle of rotation. The regression shows a strong relationship between the radio-opaque ball ratio and the degree of angle ($P < 0.01$). When rotating the chest phantom to left posterior

oblique, the radio-opaque ball ratio decreased by increasing the degree of angle. When rotating the chest phantom to the right posterior, the radio-opaque ball ratio increased by increasing the degree of angle.

Equation 4-2: Scatter plot between the ratios of the radio-opaque ball to chest wall distance and the degree of angle.

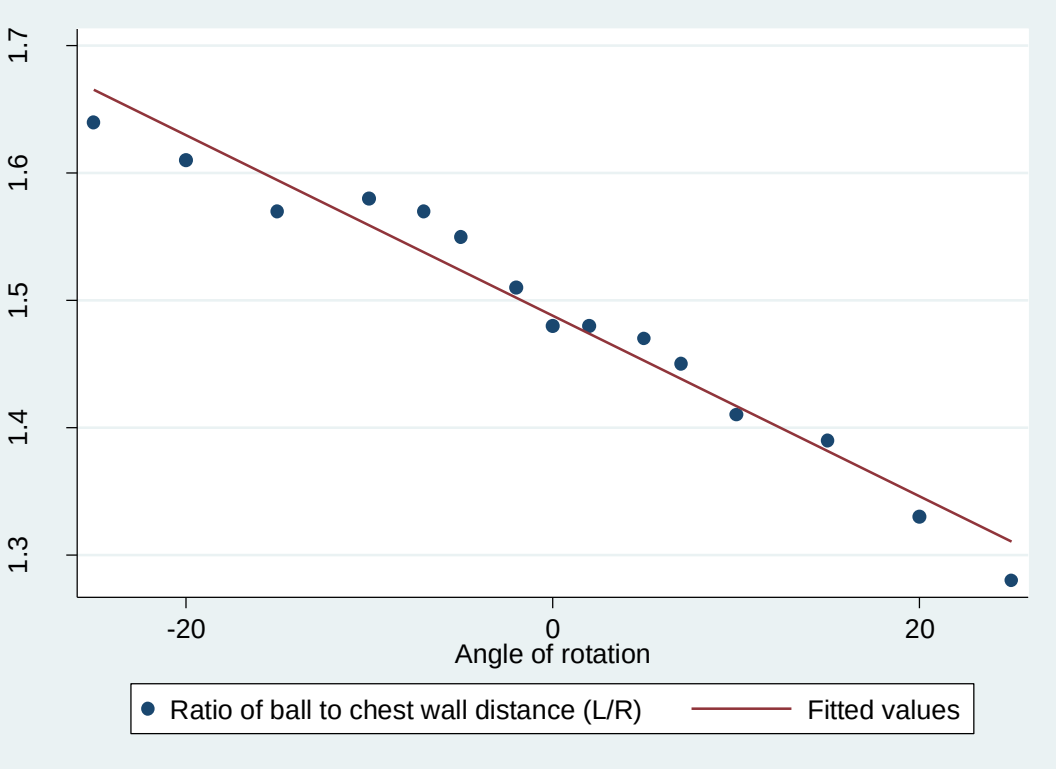

4.6.2 The measurements of kyphosis and lordosis on chest phantom

The measurements were collected for the degree of angulation where the X-ray tube had tilted cranially and caudally from (0 to 20 degrees) (4-3).

Table 4-3: The measurements of chest phantom with kyphosis and lordosis position

Angle	Clavicle–apex distance(mm)		Clavicle–apex mean (mm)	Radio-opaque ball measurements (mm)		Radio-opaque ball measurements mean (mm)	Fourth rib angle measurements (degrees)		Fourth rib angle mean (degrees)
	R	L		R	L		R(y)	L(x)	
-20	43.10	43.36	43.23	50.86	53.36	52.11	76	78	77
-15	31.32	33.19	32.25	49.25	51.66	50.455	71	72	71.5
-10	27.57	29.98	28.77	47.65	51.39	49.52	67	70	68.5
-7	27.30	24.89	26.09	48.45	49.52	48.985	63	67	65
-5	21.68	22.49	22.08	47.91	48.72	48.315	63	65	64
-2	19.43	19.83	19.63	46.08	47.31	46.695	59	63	61
0	20.63	20.14	20.38	48.56	48.08	48.32	58	58	58
2	16	17.53	16.76	45.23	47.06	46.145	56	54	55
5	15.70	14.36	15.03	45.39	45.10	45.245	53	54	53.5
7	12.21	12.07	12.14	43.94	44.51	44.225	47	50	48.5
10	8.14	9.06	8.6	43.90	44.21	44.055	44	46	45
15	4.37	4.07	4.22	42.03	42.03	42.03	40	39	39.5
20	1.60	1.39	1.49	40.87	41.73	41.3	36	30	33

Means of right and left values were calculated for all measurements, clavicles to apices, the fourth anterior rib angle and the radio-opaque ball. The radio-opaque ball was located 5–7 cm above the carina (endotracheal tube position).

Table (4-4) shows that there was a strong relationship between the angulation and the clavicles to apex, the fourth anterior rib angle and the radio-opaque ball where the p value for all was ($P < 0.01$).

Table 4-4: Regression output of kyphosis and lordosis measurements

Clavicles to apex	Regression coefficient = -0.99	P < 0.01
	Cons regression coefficient =19.28	P < 0.01
Fourth anterior rib angle	Regression coefficient = -1.105	P < 0.01
	Cons regression coefficient = 56.88	P < 0.01
Radio-opaque ball	Regression coefficient = -0.278	P < 0.01
	Cons regression coefficient = 46.72	P < 0.01

The regression coefficient was negative for all measurements: clavicles to apex (coef = -0.99), the fourth anterior rib angle (coef = -1.105) and the radio-opaque ball (coef = -0.278) graph (4-3).

The mean of the clavicles to apex, the fourth anterior rib angle and the radio-opaque ball slope (cons) had started at (cons = 19.28, 56.88 and 46.72) respectively. All means measurements were best fit with straight line where (P < 0.01).

Graph 4-3: Scatter plot between the clavicle–apex mean, radio-opaque ball mean, fourth rib angle mean and the degree of the X-ray tube angulations

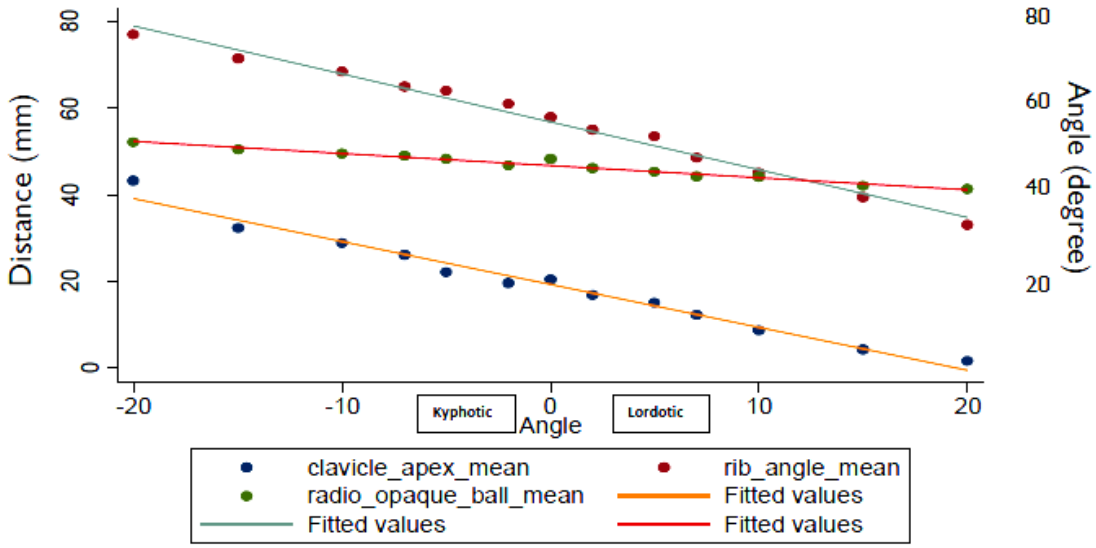

The regression outcome of the mean of the distance between clavicle to apex of lung, the mean of the distance between the radio-opaque ball and the apex of lung and the mean of the fourth rib angle with the degree of X-ray tube angulation illustrates that there is a strong relationship between these three measures ($P < 0.01$).

By increasing the degree of angulation during the X-ray tube rotation cranially (lordotic), the distance between clavicle–apex, the mean of the distance between the radio-opaque ball and the apex of lung, and the mean of the fourth rib angle has decreased. When the X-ray tube was rotated caudally (kyphotic), the mean of the distance between clavicle and apex, the mean of the distance between the radio-opaque ball and the apex of lung and the mean of the fourth rib angle increased.

Depends on the general formula of straight line, which is

$$y = m.x + c$$

Where in this experiment y= the mean, m slope (coef), x angle value and c constant.

Therefore, if a chest radiograph is taken and the clavicle to apex mean was 8.6 mm the estimated angle can be:

$$Estimated\ angle = \frac{constant - mean\ of\ measurement}{coef}$$

$$Estimated\ angle = \frac{19.28 - 8.6}{0.99} = 10.7°$$

4.7 Discussion

This study explored the effect of rotation, kyphosis and lordosis on the appearances of the chest radiograph. The position of the radio-opaque ball (located in central venous catheter position) relative to the heart wall and superior border of posterior seventh rib was relatively unchanged from 2– ≤10 degrees of rotation, which can be estimated as mild rotation. At >10- ≤15 degrees left posterior oblique, the radio-opaque ball (located in central venous catheter position) was moved nearer to the vertebral body and further away from the vertebral body at >10- ≤15 degrees right posterior oblique, which can be estimated as moderate rotation. At >15- ≤25 degrees left posterior oblique the position of the radio-oblique ball was superimposed over the heart shadow and spine and stayed on the edge of the heart shadow at >15- ≤25 degrees right posterior oblique, which can be estimated severe rotation Table (4-5).

Table 4-5: Categorization of the degree of rotation

Category	Angle	CSPR		ROBR		Fourth ARLR		Anatomical structures	
		LPO	RPO						
				LPO	RPO	LPO	RPO	LPO	RPO
Mild	2- ≤ 10	1.19 - 3	1.09-2.4	1.41-1.48	1.51-1.58	1.12-1.56	1.22-1.95	Superior border of posterior seventh rib	
Moderate	>10-≤15	3-4.69	2.4-9.9	1.39-1.41	1.57-1.58	1.56-2	1.95-2.14	Further away from the vertebral body	Moved nearer to the vertebral body
Severe	>15-25	superimposed		1.28-1.39	1.57-1.64	2-3.03	2.14-2.56	Stays on the edge of the heart shadow	Superimposed over the heart shadow

CSPR = the ratio of the distance between the clavicles and the spinous process

RPO = right posterior oblique

LPO = left posterior oblique

ROBR = radio-opaque ball ratio

Fourth ARLR = the ratio of fourth anterior rib length

At 2 to ≤5 cranial degrees and from 2 to ≤7 caudal degrees of kyphosis and lordosis the radio-opaque ball (located in endotracheal tube position) was at the level of the fourth posterior rib, which can be estimated as mild kyphosis and lordosis. The radio-opaque ball was above the level of the fourth posterior rib from >7 to ≤15 degree cranial and under the level of the fourth posterior rib from >10 to ≤15 degrees caudal, which can be estimated as moderate kyphosis and lordosis. At ≥20 degrees caudal the radio-opaque ball was at the level of the fifth posterior rib, while at ≥20 degrees cranial was at the level of the third posterior rib, which can be estimated as severe kyphosis and lordosis Table (4-6).

Table 4-6: Categorisation of the degree of kyphosis and lordosis

Lordosis (Carinaly)	**Category**	**Angle**	**Clavicle-apex**	**ROB**	**Fourth rib angle**	**Anatomical structures**
	Mild	2- ≤5	15.03-16.76	45.2-46.14	53.5-55	level of the fourth posterior rib
	Moderate	<7-≤15	4.22-12.14	42.03-44.22	39.5-48.5	above the level of the fourth posterior rib
	Severe	≥20	1.49	41.3	33	level of the third posterior rib
Kyphosis (Caudally)	**Category**	**Angle**	**Clavicle-apex**	**ROB**	**fourth rib angle**	**Anatomical structures**
	Mild	2-≤7	19.36-26.09	46.7-45	61-65	level of the fourth posterior rib
	Moderate	>10-≤15	28.7-32.25	49.5-50.4	68.5-71.5	under the level of the fourth posterior rib
	Severe	≥20	43.23	52.11	77	level of the fifth posterior rib

These findings further support with those of De Lacey et al (2008), Martensen (1996) and Moskowitz (2010), who found that rotation, kyphosis and lordosis can impact on the visualisation of chest anatomical structures, although none of them performed the measurements that were conducted in this experiment. They also did not consider the degree of acceptable limitations (mild, moderate or severe tilted patient) that can lead to rotated kyphotic or lordotic positions.

The measurements that we have identified therefore assist in our understanding of the role of technical quality of ICU/CCU chest radiography and their impact on the visualisation of anatomical structures, chest tubes and lines. Regression analysis revealed that the implications of these findings are that rotation and kyphosis/lordosis should be taken into account when reviewing ICU chest radiography.

4.8 Limitations of the experiment

One source of weakness in this study which could have affected the measurements of was that the phantom used in the experiment consisted of three parts (diaphragm, trachea and bronchus, main trunk include ribs and sternum). Thus, it was difficult to put the radio-opaque ball in the exact position of each tube/line. For example, the radio-opaque ball (CVC tip position) was put at the level of carina, because SVC was not available in chest phantom.

Therefore, the change in the appearance of radio-opaque ball in the chest phantom is not going to present how much changes in the practise because the SVC is not in the coronal plan as the carina but anteriorly displaced.

According to Schuster et al (2000) superior vena cava (SVC) located anteriorly to the carina at small sagittal distance between (range 1.5 to 4.1 cm), so the carina will appear superimposed to the tip of CVC when the x-ray beam was perpendicular to the carina.

However, in situation where the patient kyphotic or lordotic the central ray of the x-ray beam will not be perpendicular to the carina and as a result the position of the tip of CVC can be affected Figure (4-6).

Figure 4-6: The displacement of the apparent of CVC tip position during kyphotic and lordotic with regard to superior vena cava and the carina.

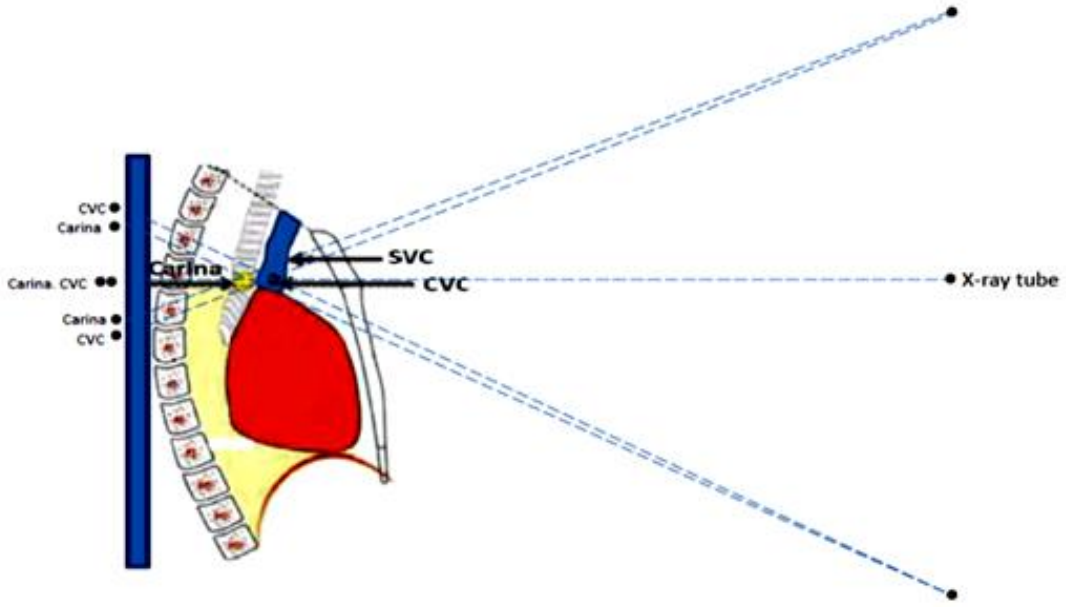

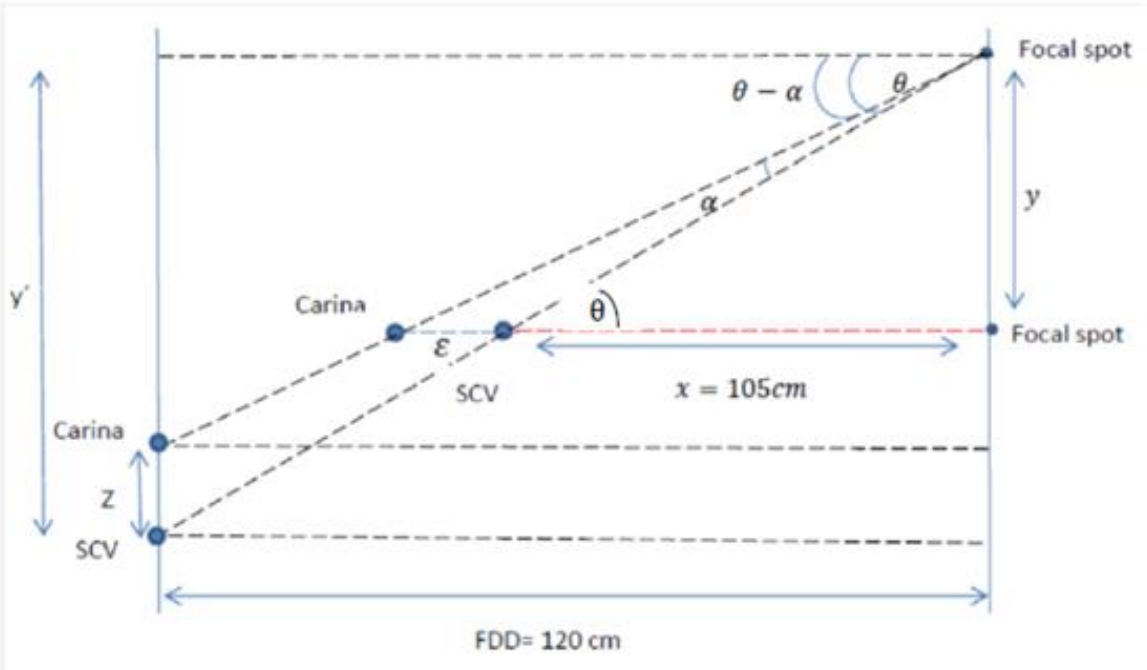

Therefore, theoretical work was done to estimate the displacement of the apparent of CVC tip position during kyphotic and lordotic with regard to superior vena cava (SVC) located anteriorly to the carina at small sagittal distance between (range 1.5 to 4.1 cm) Table (4-7).

Where FDD (the distance from the focal spot to the image receptor) = 120 cm

X (the distance from the focal spot to superior vena cava) = 105 cm (this taken from CT image).

ϵ (the distance between the SVC and carina) range = 1.5 – 4.1cm (Schuster et al., 2000).

$\theta = 0 - 20$ degree

y = the distance between the focal spot at 0 degree of angulation and the focal spot for each degree of angulation (2, 5, 7,10,15,20 degrees).

y' = the distance between the focal spot and the position of SVC on the image.

Z= the distance between the SVC and the carina regarding to the displacement of the apparent of CVC tip position during kyphotic and lordotic.

From (Figure 4-6):

$$\tan\theta = \frac{y}{x}$$

$$y = x\tan\theta$$

$$y = (x+\varepsilon)\tan(\theta - \alpha)$$

$(\theta - \propto) = \tan^{-1}\left(\frac{y}{x+\epsilon}\right)$

$\alpha = \theta - \tan^{-1}\left(\frac{y}{x+\varepsilon}\right)$

$$\frac{y'}{FDD} = \tan\theta$$

$\left(\frac{y'-z}{FDD}\right) = \tan(\theta - \alpha)$

$Z = y' - FDD\tan(\theta - \alpha)$

Z= FDD tan$\theta - FDDtan\ (\theta - \alpha)$)

Z= FDD (tan$\theta - tan\ (\theta - \alpha)$)

Therefore if $\theta = 20\ degree$

$y = x \tan\theta$ = 105 tan 20 = 105 X 0.36= 38.22

$\alpha = 20 - \tan^{-1}\left(\frac{38.22}{105+4.1}\right) = 0.7$

Z= FDD (tan$\theta - tan\ (\theta - \alpha)$)= 120 × 0.36 – tan (20 – 0.7)= 1.7cm

The same calculation was applied for each degree of angulation (kyphosis/lordosis) and for the range (1.5 – 4.1 cm) Table (4-7).

Table 4-7:Geometric modelling of the CVC tip position for kyphotic and lordotic angulation.

Angle		Z for ϵ =4.1 cm	Z for ϵ=1.5cm
Kyphotic	-20	-1.7	-0.48
	-15	-1.2	-0.47
	-10	-0.75	-0.26
	-7	-0.56	-0.22
	-5	-0.38	-0.15
	-2	-0.17	-0.07
	0	0	0
Lordotic	2	0.17	0.07
	5	0.38	0.15
	7	0.56	0.22
	10	0.75	0.26
	15	1.2	0.47
	20	1.7	0.48

Table (4-7) shows the displacement CVC tip position during kyphotic/lordotic angulation with regard to the distance between the carina and the SVC. This model shows that there was a small change in the apparent CVC tip position during kyphotic/lordotic angulation for small antero-posterior or displacement of CVC tip position from the carina.

However, for large antero-posterior or displacement of tip position from the carina, the apparent tip position can be displaced by more than 0.5cm for lordotic/kyphotic angles exceeding 5 degrees, and by 1 cm or more for angles exceeding 10 degrees.

5 Chapter Five: A comparison between two methods to estimate the degree of angulation for rotation, kyphosis and lordosis on 17 mobile chest radiographs

5.1 Method

Seventeen ICU/CCU mobile images have been collected to apply the measurements used in the chest phantom experiment. The ratios and means of the measurements (rotation, kyphosis and lordosis) have been calculated and then by using the straight line equation to estimate the angle, the degree of angulation has been calculated for each measure.

The methods used on the chest phantom were compared on the 17 mobile chest radiographs to estimate the degree of malpositioning (rotation, kyphosis and lordosis) in the 17 ICU/CUU chest radiographs and their assistance to measure the malpositioning in clinical practise to inform interpretation.

5.2 Statistical analysis

The data were collected to compare two methods applied to estimate the degree of angulation due to rotation, kyphosis and lordosis on mobile chest radiographs.

For rotation measurements, the differences between the estimated angles for ratios of the clavicles to spinous process and the estimated angles of the fourth anterior rib length. Also the estimated angle for the ratios of the distance between the chest wall and the tip of CVC. For kyphosis and lordosis the differences between the estimated angles for the mean of clavicle to the apex of lung and the estimated angles of the fourth anterior rib angle. Also the estimated angle of the mean of the distance between the tip of the ETT and the apex and the distance between the tip of CVC and the apex.

Statistical methods for assessing agreement between two methods of clinical measurements addressed by Bland and Altman (1986) has been applied on these measurements. This approach is based on graphical techniques and simple calculations.

5.3 Methods of estimation for the rotation

The ratios of the distance between the clavicle and the spine process and the fourth anterior rib length have been calculated Table (6-1). The estimation of the degree of angulation for each ratio has been calculated by using the straight line equation. The regression coefficient was calculated from phantom experiment.

$$y = m.x + c$$

For clavicle to spinous process ratios the equation is:

y= the ratio, m slope (coef = 0.119), x angle value, constant = 0

$$Estimated\ angle = \frac{\ln ratio}{0.119}$$

For the anterior fourth rib length ratios the equation is:

y= the ratio, m slope (coef = 0.045), x angle value and c constant = 0

$$Estimated\ angle = \frac{\ln ratio}{0.045}$$

Table 5-1: Methods of estimation for the rotation

image	clavicle-sp ratio	clavicle-sp estimated angle (degree)	fourth rib length ratio	fourth rib length estimated angle (degree)	CVC to chest wall ratio
1	1.4	2.8	2.4	19.4	1.7
2	1.8	4.9	1.2	4.05	1.2
3	1.5	3.4	1.3	5.8	1.3
4	10.7	19.9	1.03	0.65	NCVC
5	1.1	0.8	1.2	4.05	1.3
6	1.6	3.9	1.01	0.22	1.3
7	1.4	2.8	1.2	4.05	1.9
8	1.9	5.3	1.4	7.4	NCVC
9	1.4	2.8	1.5	9.01	2.1
10	2.3	6.9	1.6	10.4	1.2
11	1.3	2.2	1.4	7.4	NCVC
12	6.3	15.4	1.7	11.7	1.4
13	7.1	16.4	1.8	13.06	2.3
14	1.7	4.4	1.7	11.7	1.1
15	4.7	13	1.9	14.2	2.05
16	2.2	6.6	1.02	0.44	1.9
17	2.5	7.6	1.01	0.22	NCVC

NCVC= No Central Venous Catheter in this image.

5.3.1 Results of the estimated degree of angulation for rotation measurements.

Statistical methods have used for assessing agreement between two methods of clinical measurements addressed by Bland and Altman(1986). The first step is to plot the data to see the level of agreement between measurements Graph (5-1).

Graph 5-1: Scatter plot for clavicle-spinous process and fourth rib length angles

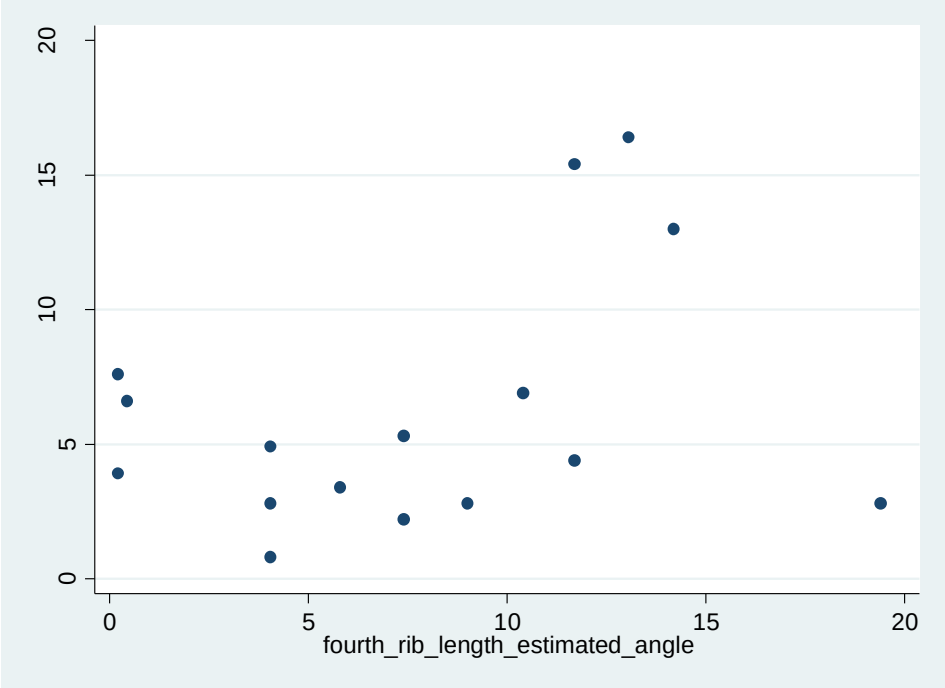

The second step is to calculate the correlation coefficient (r) between the two methods. For the data $r = 0.55 (p = 0.026)$ Table (5-2). Here (r)measures the strength of a relation between the two methods. So that means there is a moderate correlation between the two methods (clavicle-spinous process ratio and the fourth rib length ratio).

Table 5-2: Regression output of clavicle-spinous process and fourth rib length estimated angles.

Mean difference	-1.49
SD	5.92
r	0.55
P value	0.026

By plotting the results of the methods against the mean angles Graph (5-2) we can investigate how much data points (estimated angles for both methods) cluster near the line.

Graph 5-2: Scatter plot of the deference against mean for the estimated angles of clavicle-spinous process and the fourth rib length.

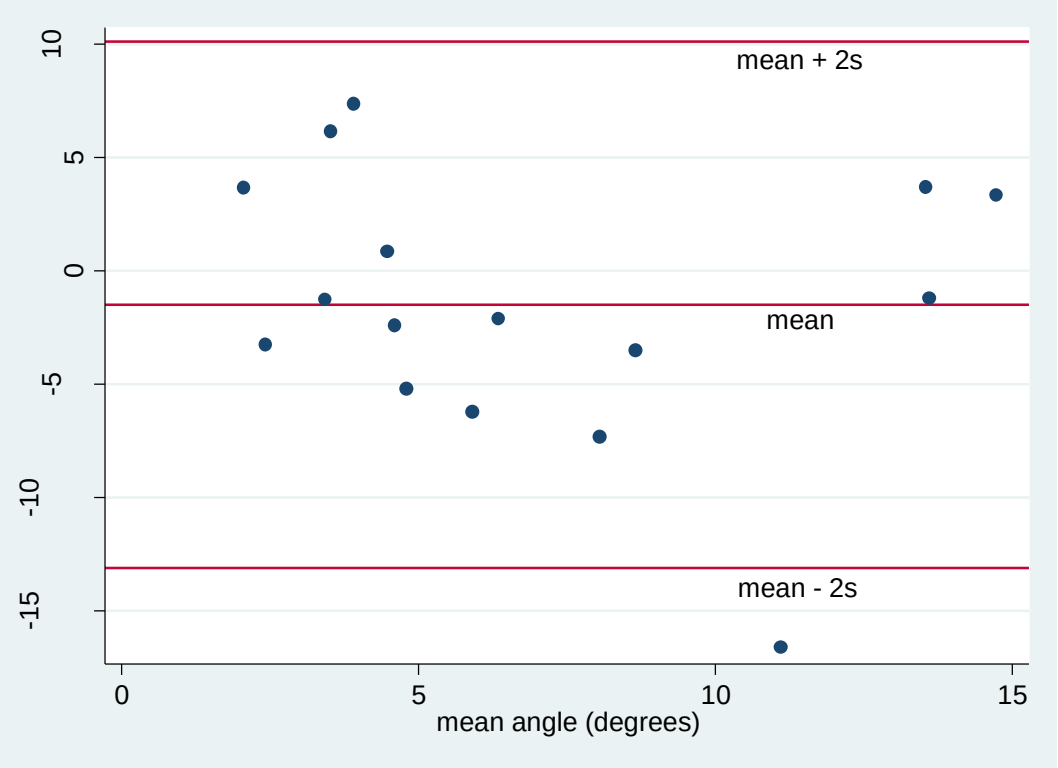

From the graph it can be seen that there is lack of agreement between the two methods (clavicle-spinous process and fourth rib length), where few data cluster to the line.

The bias is estimated by the mean difference = -1.49 and the standard deviation (SD = 5.92). the differences lie between $d - 2s \; and \; d + 2s$, where more precisely 95% of differences in estimates from the two measures lie between $d - 1.96s \; and \; d + 1.96s$ (Bland and Altman, 1986).

Upper limit = -1.49 + 1.96 X 5.92 = 10.11

Lower limit = -1.49 - 1.96 X 5.92 = - 13.09

The standard error and confidence interval of have been calculated to investigate the precision of estimated limits of agreement:

For the mean differences in estimated angles the standard error= √ S^2 /n = 5.92/ √16 = 1.48. For the confidence interval for bias is =

-1.49 + 1.96 X 1.48 = 1.41 degree

-1.49 - 1.96 X 1.48 = -4.4 degree

The standard error of limits = √3S^2 /n = 2.56 degree. Hence the 95% confidence interval = limit ± (2X2.56) =5.13 degree.

The 95% confidence interval for the lower limit of the agreement is

= -13.09 - 5.13 = -18.22 degree

= -13.09 + 5.13 = -7.96 degree

The 95% confidence interval for the upper limit of the agreement is

= 10.11 - 5.13 = 4.98 degree

= 10.11 + 5.13 = 15.24 degree

5.3.2 For the central venous catheter measurements of the 17 images

Prediction ratios have been calculated by taking the mean of angles of the clavicle to spinous process and fourth rib length. Also regression analysis was conducted and the coef was (- 0.00711, p= 0.01) and constant (1.49). The regression coefficient was calculated from phantom experiment.

Therefore by applying $y = m.x + c$

$$predected\ ratio = angle\ X - 0.00711 + 1.49$$

This equation has been applied on each mean of angle Table (5-3).

Table 5-3: The Equation applied on each mean of angle

image	clavicle-sp estimated angle (degree)	fourth rib length estimated angle (degree)	mean angle	CVC to chest wall ratio	Predicted ratio
1	2.8	19.4	11.1	1.7	1.41
2	4.9	4.05	4.5	1.2	1.45
3	3.4	5.8	4.6	1.3	1.45
4	19.9	0.65	10.3	NCVC	1.41
5	0.8	4.05	2.4	1.3	1.47
6	3.9	0.22	2.06	1.3	1.47
7	2.8	4.05	3.4	1.9	1.46
8	5.3	7.4	6.3	NCVC	1.44
9	2.8	9.01	5.9	2.1	1.44
10	6.9	10.4	8.6	1.2	1.42
11	2.2	7.4	4.8	NCVC	1.45
12	15.4	11.7	13.5	1.4	1.39
13	16.4	13.06	14.7	2.3	1.38
14	4.4	11.7	8.05	1.1	1.43
15	13	14.2	13.6	2.05	1.39
16	6.6	0.44	3.5	1.9	1.46
17	7.6	0.22	4	NCVC	1.46

NCVC= No Central Venous Catheter in this image.

A scatter diagram and a Pearson's product moment correlation were used to determine the relationship between the CVC to chest wall ratios and the estimated angle of rotation Graph (5-3).

Graph 5-3: Scatter plot of the CVC to chest wall ratios and the estimated angle of rotation.

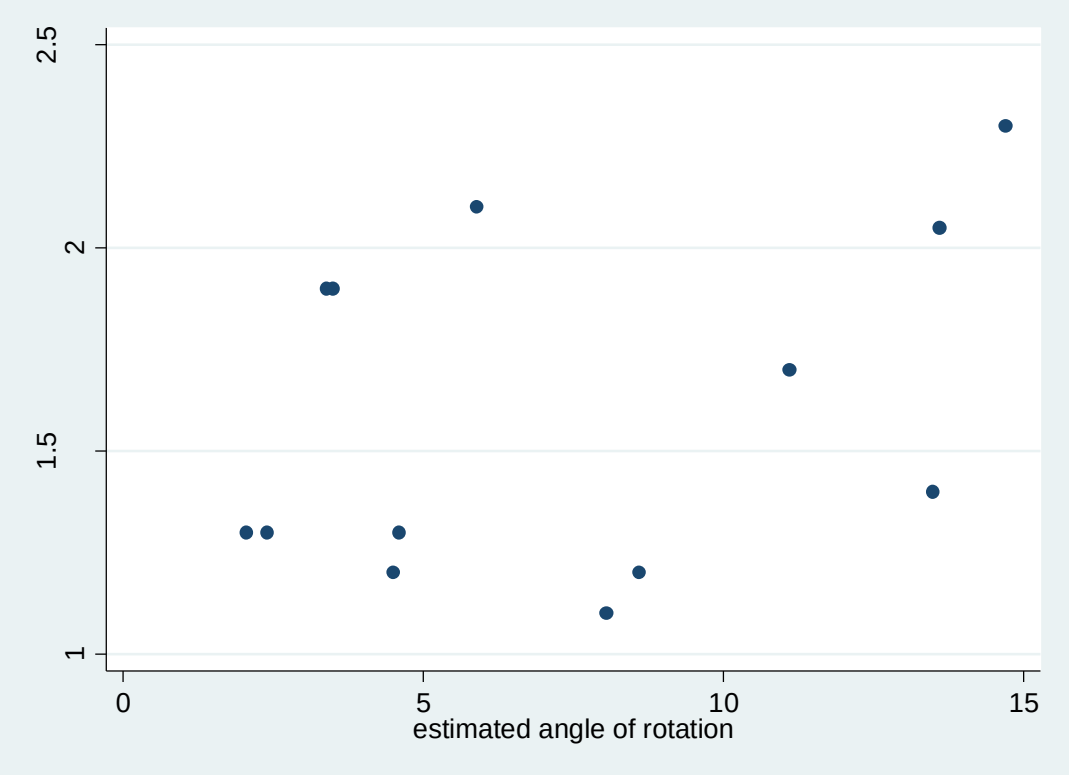

From the graph above it can be seen that there was a weak correlation between the ratio of the CVC to chest wall and estimated angle and also was not statistically significant (r = 0.36, p= 0.22).

A scatter plot and correlation has also used to determine the relationship between the CVC to chest wall ratios and the predicted ratios Graph (5-4).

Graph 5-4: Scatter plot of the CVC to chest wall ratios and the predicted ratios.

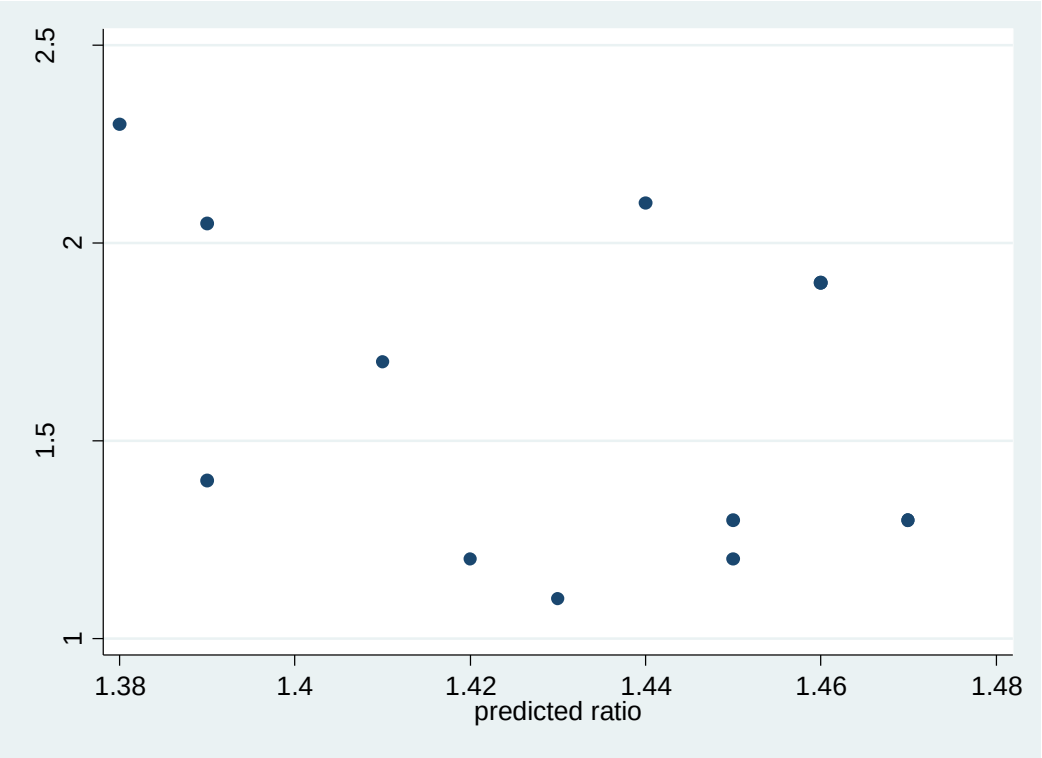

The graph above and the output of regression illustrates that there was a weak correlation between the ratios, the relation was not statistically significant (r = 0.37, p= 0.21).

5.4 Methods of estimation for kyphosis and lordosis

The mean of the distance between the clavicle and the apex and the fourth anterior rib angle have been calculated Table (5-4). The estimation of the degree of angulation for each mean has been calculated by using the straight line equation.

$$y = m.x + c$$

For clavicle to apex the equation is:

y= the mean, m slope (coef = -0.99), x angle value and c constant = 19.28

$$Estimated\ angle = \frac{constant - mean\ of\ measurement}{coef}$$

$$Estimated\ angle = \frac{19.28 - mean\ of\ measurement}{0.99}$$

For the anterior fourth rib angle the equation is:

y= the mean, m slope (coef = -1.105), x angle value and c constant = 56.88

$$Estimated\ angle = \frac{constant - mean\ of\ measurement}{coef}$$

$$Estimated\ angle = \frac{56.88 - mean\ of\ measurement}{1.105}$$

Table 5-4: Methods of estimation for kyphosis and lordosis

image	clavicle-apex mean	clavicle-apex estimated angle	4th rib angle mean	4th angle estimated angle	CVC-apex	ETT-apex mean
1	4.26	15	56	0.79	105.06	37.7
2	23.1	-3.8	70	-11.8	111.99	NETT
3	9.9	9.4	59.5	-2.3	129.41	NETT
4	45	-25.9	82.5	-23.1	NCVC	NETT
5	11.6	7.7	55.5	1.2	121.47	41.9
6	7.8	11.5	66.5	-8.7	102.42	NETT
7	10.5	8.8	45.5	10.2	120.94	NETT
8	20.5	-1.2	65	-7.3	NCVC	NETT
9	26.3	-7.09	58.5	-1.4	99.5	74.3
10	51.5	-32.5	85	-25.4	113.8	67.5
11	20.5	-1.2	64	-6.4	NCVC	NETT
12	34.88	-15.7	82.5	-23.1	122.92	NETT
13	25.4	-6.1	75	-16.3	90.51	NETT
14	36.2	-17.09	81.5	-22.2	118.03	NETT
15	9.9	9.4	63	-5.5	107.72	41.5
16	16.1	3.2	69.5	-11.4	107.71	NETT
17	25.9	-6.6	74	-15.4	NCVC	NETT

NETT= No Endotracheal Tube

NCVC= No Central Venous Catheter in this image.

5.4.1 Results of the estimated degree of angulation for kyphosis and lordosis measurements

The first step is to plot the data and draw the line of equality to see the degree of agreement between measurements Graphs (5-5).

Graph 5-5: Scatter plot for the degree of the angulation of clavicle- apex and fourth rib angle

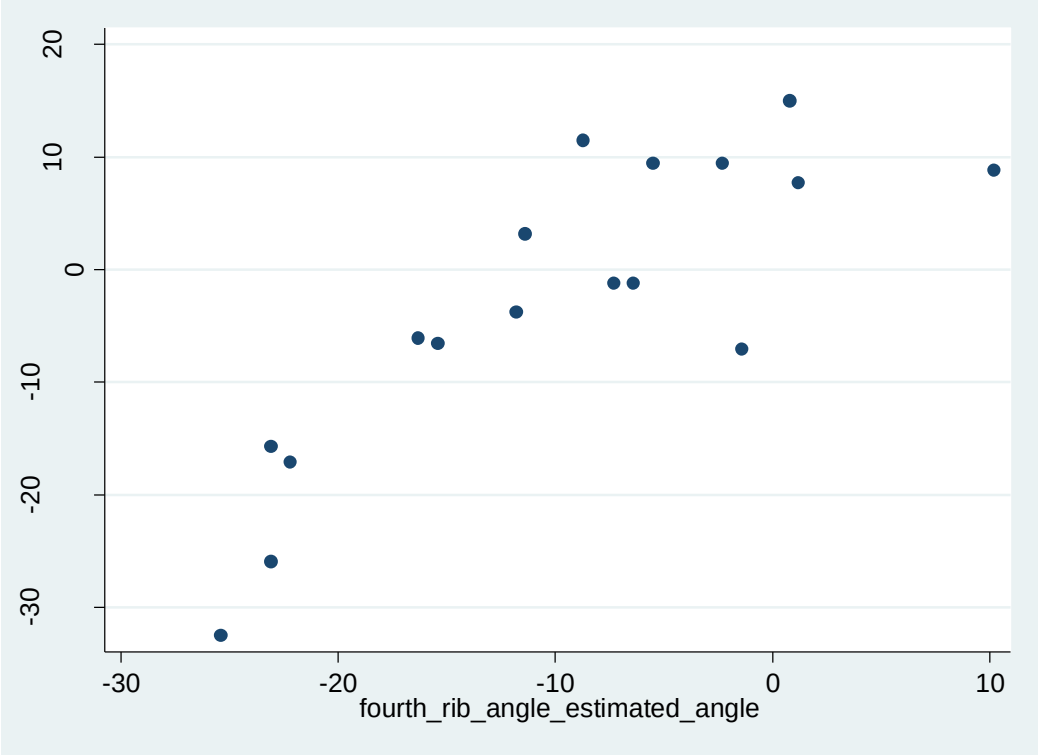

The second step is to calculate the correlation coefficient (r) between the two methods. For the data $(r = 0.84, p = 0.01)$ Table (5-5). Here (r)measures the strength of a relation between the two methods. So that means there is a fairly strong and statistically significant relation between the two methods (clavicle- apex mean and the fourth rib angle mean).

Table 5-5: Regression output of estimated angles of clavicle-apex and fourth rib angle.

Mean difference	6.82
SD	7.57
r	0.84
P value	0.01

By plotting the results of one method against those of the other Graph (5-6) to see how much data points (estimated angles for both methods) will cluster near the line.

Graph 5-6: Scatter plot of the difference against mean for the estimated angles of clavicle-apex and the fourth rib angle.

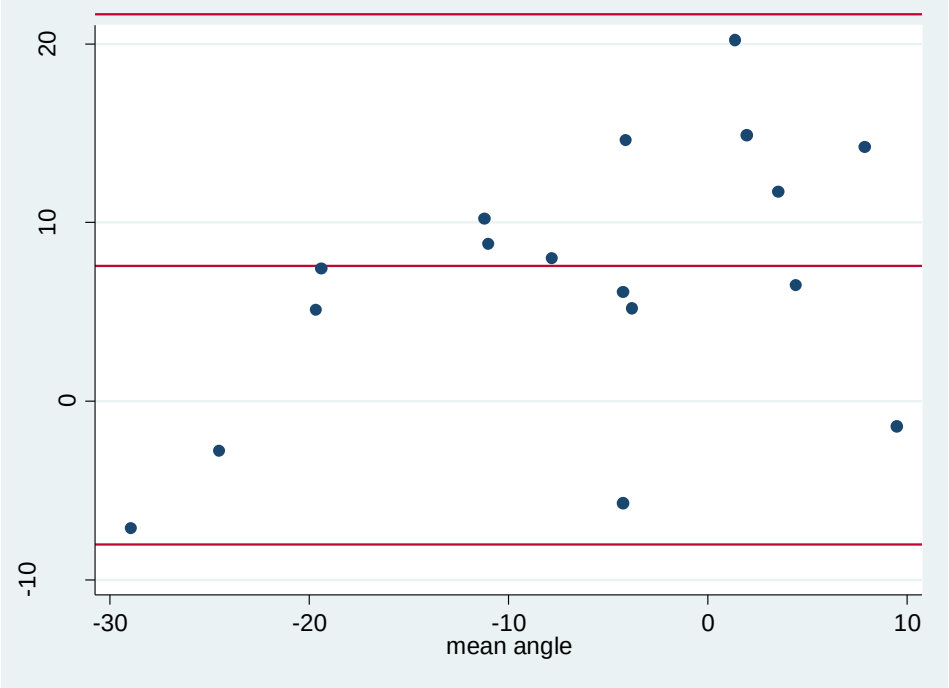

From the graph it can be seen that there is lack of agreement between the two methods (clavicle- apex and fourth rib angle), where few data cluster to the line.

By calculate the bias, estimated by the mean difference = 6.82 and the standard deviation (SD = 7.57). the differences lie between $d - 2s \; and \; d + 2s$, where more precisely 95% of differences in estimates from the two measures lie between $d - 1.96s \; and \; d + 1.96s$ (Bland and Altman, 1986).

Upper limit = 6.82 + 1.96 X 7.57 = 21.66

Lower limit = 6.82 - 1.96 X 7.57 = - 8.02

The standard error and confidence interval of have been calculated to investigate the precision of estimated limits of agreement:

For the mean differences in estimated angles the standard error= √ S^2 /n = 7.57/ √16 = 1.84. For the confidence interval is =

6.82 + 1.96 X 1.84 = 10.4 degree

6.82 - 1.96 X 1.84 = 3.2 degree

The standard error of limits = √3S^2 /n = √3X 7.57^2 / 17= 3.18 degree. Hence the 95% confidence interval = limit ± (2X2.3.18) = 6.36 degree.

The 95% confidence interval for the lower limit of the agreement is

= -8.02 – 6.36 = - 14.4 degree

= -8.02 + 6.36 = -1.66 degree

The 95% confidence interval for the upper limit of the agreement is

= 21.66 – 6.36 = 15.3 degree

= 21.66 + 6.36 = 28.02 degree

5.4.2 For the central venous catheter measurements of the 17 images

Scatter plot and regression analysis has been undertaken to illustrate the linear relationship between the CVC to apex and the mean of angle of the distance from the clavicle to apex and the fourth rib angle.

Graph 5-7: Scatter plot of the CVC to apex and the mean angle.

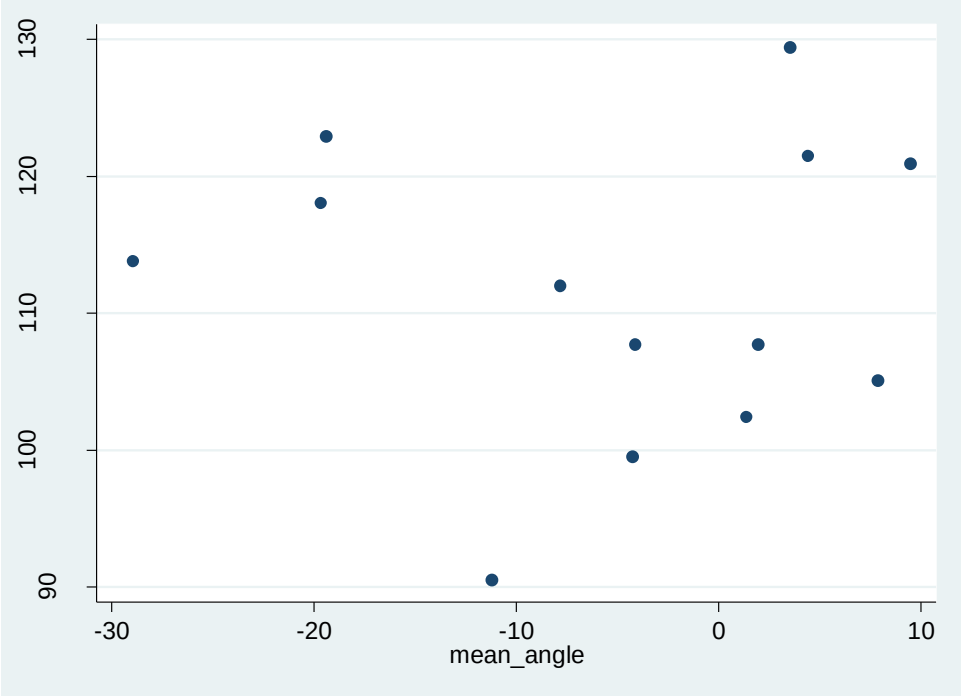

The graph and regression output show that there was a weak and also not statistically significant correlation between CVC to apex and the degree of angulation (r= 0.01, p= 0.96).

5.4.3 For the ETT measurements of the 17 images

Regression output shows that there was a moderate correlation Graph (5-8) between the degree of angulation and the method of measuring the changes of the position of ETT and the degree of angulation (kyphotic/lordotic), where (r= 0.7, p= 0.18).

Graph 5-8: Scatter plot of ETT to apex mean and the mean of angle.

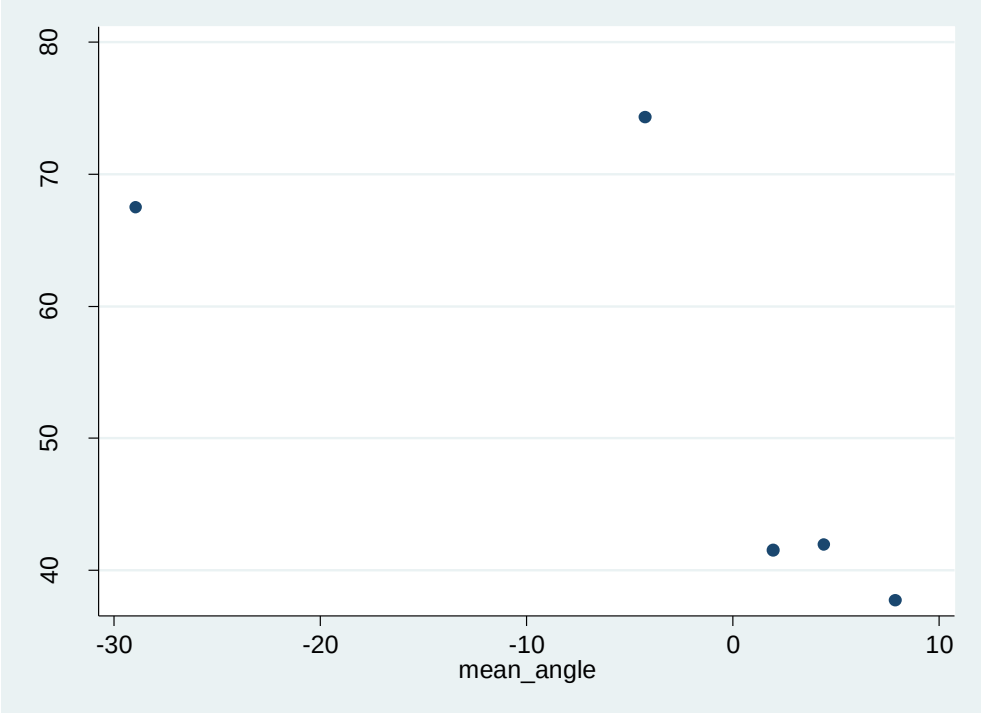

5.5 Discussion

5.5.1 Level of agreement between methods of estimating angle of rotation

For the clavicle to spinous process and the fourth rib length estimated angle, there was a statistically significant but moderate correlation(r= 0.55, p= 0.026) between the two methods used to assess the estimated degree of angulation. There was a small bias (approximately 1.5 degree), which was not statistically significant. However, there was a large uncertainty in the upper and the lower limits of agreement and the limits were themselves wide (greater than ± 10 degrees).

Therefore, it can be concluded that there is not close agreement between these methods of estimation for the degree of rotation. The methods of measuring (the distance between clavicle to spinous process and fourth rib length ratios) are not influenced in a very predictable way by the degree of rotation. The natural variation in the distance between clavicle to spinous process and fourth rib length between patients may be large enough to obscure any small systematic variation. Therefore, these measurements (distance between clavicle to spinous process and

fourth rib length) can only provide limited useful information to the image interpreter in estimating for the degree of rotation.

5.5.2 Influence of angle of rotation on measurement of CVC position

Predicted ratios were calculated from the phantom experiment where a linear relationship was found between the CVC to chest wall ratio (left/ right). For each of the 11 radiographs with CVC placement the mean angle of rotation was calculated from the clavicle to spinous process and the anterior fourth rib length ratio. The predicted ratio was calculated from the regression coefficient from the phantom experiment. These were the correlated with the measurements of the CVC to chest wall ratios ($r= 0.37$, $p= 0.21$).

The correlation was weak and not statistically significant. This suggests that the CVC to chest wall ratio is not influenced in a predictable way by the degree of rotation. In the phantom experiment, the ratio varied only slightly with angle of rotation (range: 1.57 at -15° rotation, to 1.39 at 15° rotation). The natural variation in the SVC to midline distance between patients may be large enough to obscure any small systematic variation. Therefore, this measure (CVC to chest wall ratio) is not likely to provide useful information to the image interpreter in deciding if the CVC is correctly placed.

5.5.3 Level of agreement between methods of estimating angle of kyphosis and lordosis

For the method of the estimated angles of clavicle to apex and the fourth rib angle, there was a strong correlation($r=0.84$, $p=0.01$) between the two methods used to assess the estimated degree of angulation. There was a moderate bias (approximately 6.82degree).The relation between the two methods was statistically significant (the 95% confidence interval limit was positive, 2.3° to 10.4°). Clavicle to apex distance estimates a more lordotic angle than the fourth rib angle. Limits were similar to those for rotation, but a large angular range covered by the data; hence the correlation is a little stronger.

In conclusion the agreement between the methods is still quite poor, due to the wide limits of agreement (upper limit= 21.66 degrees, lower limit= -8.02 degrees). Therefore, these measurements (clavicle to apex and the fourth rib angle) again produce limited useful information to the image interpreter in estimating the degree of kyphosis or lordosis.

5.5.4 Influence of angle of kyphosis/lordosis on measurement of CVC and ETT position

The methods of measuring the CVC to apex and the ETT to the apex were not well correlated to the mean angles (when the patients were kyphotic or lordotic), ($r= 0.01$, $p= 0.96$, $r= 0.7$, $p= 0.18$ respectively).

The natural variation in the SVC to midline distance and also the distance between the carina (as landmark for ETT position), between patients may be large enough to obscure any small systematic variation. Therefore, this measure (CVC, ETT to apex) is not likely to provide useful information to the image interpreter in deciding that the CVC and ETT are correctly placed.

6 Chapter Six: An observer study to compare the effect of a standard post-processing algorithm versus a greyscale inverted image on mobile chest radiographs and their impact on the visualisation of chest tubes and lines and the general findings in the chest radiograph

6.1 Rationale for study

the original intention was to evaluate a number of alternative image processing algorithms to identify which algorithm demonstrated the chest tube and line position most clearly (1- default, 2- chest line placement, 3 soft tissue, 4- bone details, 5- invert).

However, a technical problem did not anticipate the protocol has changed. The idea was that the images transferred from the CR Agfa system to the PACS were in DICOM format this was a universal standard, so any tools on the system can be useable on any image in this format. Unfortunately the images imported were from Agfa CR and the advanced imaging presets was only work on Fuji CR generated image, apart from the inverted tool.

During the chest phantom experiment to performing certain measurements tasks requiring visualisation of anatomical landmarks that were difficult to see, it was subjectively found that the landmarks appeared to be easier to identify on the inverted images. In addition, Foos et al (2011) as limitations of his study was not enable to examine this algorithm because the greyscale algorithm was available after finishing his study.

Therefore, this was the motivation for using several observers to evaluate both standard postprocessing algorithm and inverted algorithm, on the 17 ICU/CCU images collected.

6.2 Materials and method

Seventeen ICU and CCU mobile chest radiographs were captured from the Computed Radiography system (CR). All the ICU and CCU chest radiographs were selected from the database of the CR ICU images that have been retrospectively collected. All the ICU chest radiographs were for adult patients in critical care, who have at least two inserted tubes/lines.

There were three observers at the University of Bradford, who were specifically trained and experienced in chest image interpretation. The manipulation was applied in the postprocessing stage through the Picture Archiving and Communication Systems (PACS) at the University of Bradford.

The Picture Archiving and Communication System (PACS) at the University of Bradford was established in 2007 by Fujifilm Company. Fujifilm developed SYNAPSE to support diagnostic imaging with high quality images and provides of user-easy image processing features. Fujifilm has developed tools to automate presentation of diagnostic information through Reading protocols.

In this observer evaluation study 17 images were evaluated using each of two image presets: 1- standard 2- invert.

The image assessment template was completed by the observers and each mobile chest radiograph will be presented to the observers with the algorithms in different random order for each image. The assessment criteria was based on the European Guidelines on the Quality Criteria for Diagnostic Radiographic Images (Carmichael, 1996).

The Quality Criteria of the European Commission are divided to three parts: diagnostic requirement, criteria for radiation dose to the patient and example of good radiographic technique. This experiment is focused on the diagnostic requirements.

Questions were added to the European Guidelines on the Quality Criteria for Diagnostic Radiographic Images which relate to identification of the location of tubes and lines related to the surrounding anatomy.

The primary analysis will be to see if there are difference between the two algorithms / presets in conspicuity and accurate location of the tubes and lines. The standard CEC image quality criteria will also be compared as a secondary analysis.

In this context the method is not comparing their results against a known truth, but rather against each other.

The visibility of tubes and lines including the endotracheal tube (ETT), central venous catheter (CVC), chest tube drainage (CT), pulmonary artery catheter or Swan-Ganz (SG), and nasogastric tube (NG) will be evaluated by scoring on a 0 to 7 ordinal scale (Hamer et al., 2005).

Hamer et al (2005) used a seven point scale in which each of the 12 variables was assigned score subjectively by using the same seven-point ordinal scale: score 1, excellent (no limitations); score 2, good to excellent; score 3, good (minor limitations, full diagnostic information); score4, moderate to good; score 5, moderate (major limitations, limited diagnostic information); score 6, poor to moderate; and score 7, poor visualization (nondiagnostic).

There was four-point scale (0-3) for the observers to assess their confidence in whether the tube/line is positioned correctly, 0= definitely not, 1= probably not, 2= probably is and 3= definitely is (see appendix 2).

17 ICU/CCU chest radiographs were collected from the database of the ICU/CCU images, which involve at least two tubes/lines. Cases were selected to cover as wide a range of combinations as possible Table (6-1).

Table 6-1: Cases selected to cover as wide a range of combinations of tube-lines

Case	Accessing NO	Tube/line
1	Cr-9325	CVC & ETT
2	Cr-9326	CVC, ETT
3	Cr-9327	CVC, NG &ETT
4	Cr-9328	CT & NG
5	Cr-9330	CVC, ETT& NG
6	Cr-9331	CVC, ETT& NG
7	Cr-9332	CVC,NG
8	Cr-9333	CT & NG
9	Cr-9334	ETT & CVC
10	Cr-9335	ETT, NG & CVC
11	Cr-9336	NG
12	Cr-9337	NG, EET & CVC
13	Cr-9338	CVC, ETT& NG
14	Cr-9339	ETT & CVC
15	Cr-9340	CVC, NG &ETT
16	Cr-9341	CVC, CT, ETT& NG
17	Cr-9343	NG

CVC= Central venous catheter, ETT= Endotracheal tube, NG= Nasogastric tube, CT= Chest tube (drainage tube).

The templates were applied, independently, by each of the observers/raters to apply the two algorithms for each image.

Due to ethical issues the data is not being used for any purpose other than that for which it was intended (i.e. tube and line visualisation). Also the data was kept on CD's, with patients' identity data removed, stored in a lockable metal cabinet within a secure office environment. Moreover, the data records and data analysis materials were kept on the researcher's laptop with a password which was only known to the researcher and the supervisor.

The seventeen ICU/CCU mobile chest x-ray images were viewed in the PACS University of Bradford. Two algorithms were applied for each image by the observers, so each observer scored 34 images randomly distributed to avoid any bias. There are two possibilities to order the applied algorithms (1x2=2) evaluated to the observers. Each observer has a random order of the algorithms for each image Figure (6.1). The randomised sequences of algorithms were generated using the random number generator function (from a uniform distribution) in Stata version 12.

Figure 6-1: The flow chart shows the image processing and the process of scoring system by the observers.

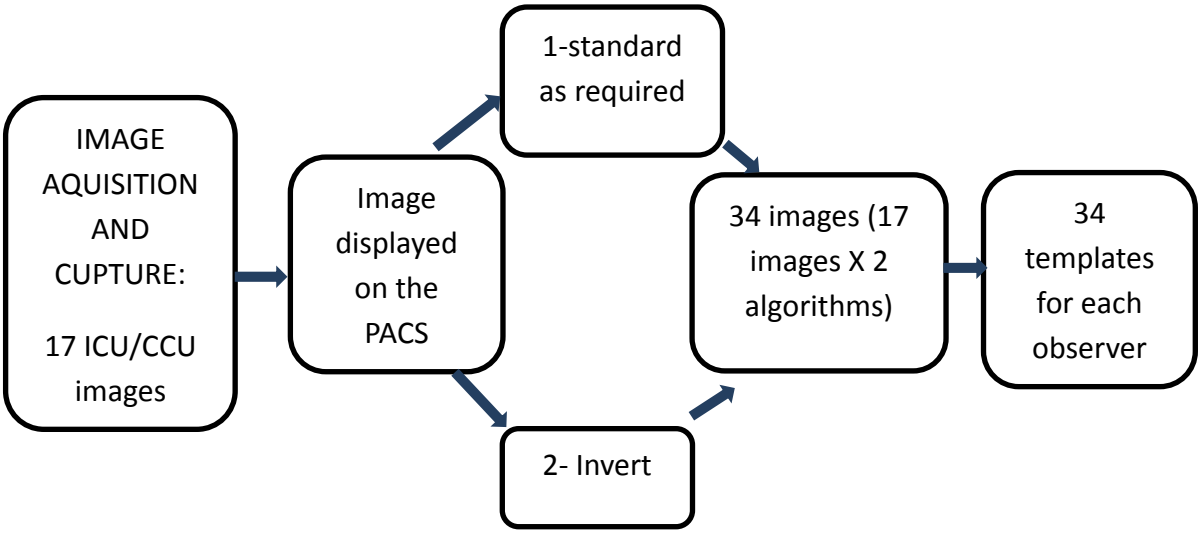

6.3 Statistical analysis

Comparison of the images was undertaken using a repeated measures regression model, to ascertain inter-rater variability. In this model the algorithm (s) used as a categorical predictor and the image as a random factor. This model used to evaluate the size of score for the all images for each algorithm and the variances between them. Kappa statics used to assess the degree of agreement between the observers (Viera and Garrett, 2005). Therefore, in this analysis Kappa was used to measure the reliability of scoring the data by the observers.

6.4 Justification for using an experimental approach

The experimental method has control over the variables and helps to establish cause and effect (Robson, 2002). Therefore, the algorithms will be controlled through the postprocessing stage to identify the optimum algorithm(s) that can be applied to enhance the visualization of chest tubes and lines in ICU chest radiography. Another advantage of the experiment is the ability to repeat the process of applying the algorithms to yield reliable and valid enhanced algorithms (Ramlaul, 2010).

6.5 Results of observer study

A total of 34 templates were collected from the observers, the template was designed to evaluate the CEC image Quality Criteria, and the identification of tube/line position, on a series of 17 ICU/CCU chest radiographs. The evaluation was performed on images using the default (standard) post-processing algorithm and on a greyscale inverted image.

The first set of analyses is repeated measures regression mixed model, with algorithm as categorical predictor and image as a random factor because the there are multiple readings for each image and the image quality can be expected to vary between images (see appendix 2)**.** After scoring the data by three observers with varying degrees of radiologic experience, the repeated measures regression model

output shows the score for the all images for each algorithm Table (6-2). However, question 13 was excluded because there were no data to analyse in all observations.

Table 6-2: Summary of algorithm comparison

Question	Mean score algorithm 1	Difference algorithm 2- algorithm 1	p- value
Q1 (Visualization of the retrocardiac lung and the mediastinum).	1.07	0	1.000
Q2(Visualization of the spine through the heart shadow).	1.9	0.11	0.56
Q3(Reproduction of the whole rib cage above the diaphragm).	4.2	-0.31	0.211
Q4 (Visually sharp reproduction of the vascular pattern in the whole lung, particularly the peripheral vessels).	3.9	-0.24	0.37
Q5 (Visually sharp reproduction of the trachea and proximal bronchi).	2.7	-1.33	0.01
Q6 (Visually sharp reproduction of the borders of the heart and aorta).	3.2	-0.33	0.19
Q7 (Visually sharp reproduction of the diaphragm and lateral costophrenic angles).	3.11	-0.18	0.38
Q8 (Small round details in the lung and retrocardiac areas, 0.7 mm, high contrast).	1.3	-0.5	0.24
Q9 (Small round details in the lung and retrocardiac areas 2 mm, low contrast).	1.09	-0.5	0.201
Q10 (Linear and reticular details to the lung periphery, 0.3 mm, high contrast).	2.2	-0.38	0.36
Q11 (Linear and reticular details to the lung periphery, 2 mm, low contrast).	1.9	-0.16	0.73
Q12 (identification CVC position).	5.4	0.05	0.68
Q14 (identification thoracostomy tube position).	4.6	0	1.00
Q15 (identification NG tube position).	4.3	0.23	0.29
Q16 (identification ETT position)	4.6	-0.35	0.18

From the table (6-2) the differences in the mean scores values of questions 1 to 16 for the algorithms 1 and 2 were not statistically significant, p value was over 0.05. In other words there is no statistically significant change in the quality of chest radiography related to the algorithms change (standard and inverse algorithm), where the most differences < 10%. However, only question 5 which about the visualisation of sharp reproduction of the trachea and proximal bronchi, the score approximately doubled for standard algorithm compared to inverse algorithm, there was statistically significant change in the quality of chest radiography related to change in algorithms (p = 0.01) and shows that algorithm 1 (standard) was better than algorithm 2 (inverse) to visualised a sharp reproduction of the trachea and proximal bronchi.

Also because we have a different type of scoring from question17 to question 21, therefore, descriptive analysis has been adopted to investigate the scoring size of the all observations (q17 to q21).

The set is descriptive analysis from question 17 to question 21 outputs

Analysis of question 18 (Sawn-Ganz catheter) was not involved because there was no data about it.

Table 6-3: Is CVC correctly positioned?

OBSERVER IF ALGORITHM =1				
OBSERVER				
Q17	1	2	3	Total
PROBABLY NO	3	0	0	3
PROBABLY IS	6	1	0	7
DEFINITELY IS	4	12	13	29
TOTAL	13	13	13	39
ALGORITHM =2				
OBSERVER				
Q17	1	2	3	Total
PROBABLY NO	3	0	0	3
PROBABLY IS	7	1	0	8
DEFINITELY IS	3	12	13	28
TOTAL	13	13	13	39

From the table (6-3) it can be seen that observer 1 was only sure that the CVC correctly positioned in just 4 observations mobile chest radiographs within the algorithm 1 (standard) and 3 observations within the algorithm 2 (inverse), while observer 2 and 3 in 12, 13 respectively mobile chest radiographs were CVC correctly positioned for both algorithms 1 and 2.

Table 6-4: Is thoracostomy tube correctly positioned?

OBSERVER IF ALGORITHM =1				
OBSERVER				
Q19	1	2	3	Total
PROBABLY IS	4	1	0	5
DEFINITELY IS	0	1	2	3
TOTAL	4	2	2	8
ALGORITHM =2				
OBSERVER				
Q19	1	2	3	Total
PROBABLY IS	4	1	0	5
DEFINITELY IS	0	1	2	3
TOTAL	4	2	2	8

From the table (6-4) it can be seen that observer 1 was not sure that thoracostomy tube correctly positioned in just 4 observations within the both algorithm 1 and 2, while observer 2 and 3 in in 1 and 2 observations respectively mobile chest radiographs were thoracostomy tube correctly positioned for both algorithms 1 and 2.

Table 6-5: Is NG tube correctly positioned?

OBSERVER IF ALGORITHM =1				
OBSERVER				
Q20	1	2	3	Total
PROBABLY NO	0	2	1	3
PROBABLY IS	4	5	3	12
DEFINITELY IS	9	9	11	29
TOTAL	13	16	15	44
ALGORITHM =2				
OBSERVER				
Q20	1	2	3	Total
PROBABLY NO	0	1	1	2
PROBABLY IS	4	4	3	11
DEFINITELY IS	9	9	11	29
TOTAL	13	14	15	42

From table (6-5) observer 1 and 2 were definitely sure 9 observations that the nasogastric tube correctly positioned for both the algorithms 1 and 2, while observe 3 was definitely sure 11 observations that the nasogastric tube correctly positioned for both the algorithms 1 and 2.

Table 6-6: Is ETT correctly positioned?

OBSERVER IF ALGORITHM =1				
OBSERVER				
Q21	1	2	3	Total
PROBABLY NO	2	0	0	2
PROBABLY IS	2	2	3	7
DEFINITELY IS	5	9	8	22
TOTAL	9	11	11	31
ALGORITHM =2				
OBSERVER				
Q21	1	2	3	Total
PROBABLY NO	2	0	0	2
PROBABLY IS	2	4	5	11
DEFINITELY IS	6	7	6	19
TOTAL	10	11	11	32

From table (6-6) observer 1 was definitely sure 5 observations that endotracheal tube correctly was positioned within algorithm 1, while observer 2 and 3 were definitely the position of the endotracheal tube correct 9 and 8 times respectively

within the algorithm 1. With algorithm 2, observer 1 and 3 were definitely sure that endotracheal tube correctly positioned in 6 observations, while observer 2 was definitely sure that endotracheal tube correctly positioned in 7 observations.

The third analysis is Kappa statistics (level of agreement)

After scoring by three observers, observer variation was assessed by using linear weighted kappa statistics to measure the degree of difference between observed agreement and that expected by chance (expected agreement). This difference is expressed as a score between (-1 and +1), where 1 is perfect agreement, 0 is what would be expected by chance. The following arbitrary standards for the strength of agreement were used: < 0 = less than chance agreement or poor, 0.01–0.2 = slight, 0.21–0.4 = fair, 0.41–0.60 = moderate, 0.61–0.80 = substantial, and 0.81–1 = almost complete(Viera and Garrett, 2005). The agreement and kappa statistics were used to also calculate p value in order to test whether the estimated Kappa is or not by chance (Viera and Garrett, 2005) Table (6-7) (see appendix 2).

Table 6-7: The output of Kappa statistics for the level of agreement between the observers for each question.

Question		Pair	Kappa	description	P- value
Q1	1	1,2	0.64	Substantial	0.01
	1	1,3	0.39	Fair	0.01
	1	2,3	0.41	Moderate	0.01
Q2	2	1,2	0.52	Moderate	0.01
	2	1,3	0.21	Fair	0.01
	2	2,3	0.37	Fair	0.01
Q3	3	1,2	0.10	Slight	0.12
	3	1,3	0.19	Slight	0.01
	3	2,3	0.02	Slight	0.32
Q4	4	1,2	0.29	Slight	0.01
	4	1,3	0.06	Slight	0.07
	4	2,3	0.03	Slight	0.15
Q5	5	1,2	0.25	Fair	0.01
	5	1,3	0.20	Fair	0.01
	5	2,3	0.40	Moderate	0.01
Q6	6	1,2	0.47	Moderate	0.01
	6	1,3	0.07	Slight	0.08
	6	2,3	0.17	Slight	0.01
Q7	7	1,2	0.36	Fair	0.01
	7	1,3	0.38	Fair	0.01
	7	2,3	0.57	Moderate	0.01
Q8	8	1,2	0.27	Fair	0.01
	8	1,3	0.00	Poor chance	
	8	2,3	0.00	Poor chance	
Q9	9	1,2	0.00	Poor chance	
	9	1,3	0.00	Poor chance	
	9	2,3	0.00	Poor chance	
Q10	10	1,2	0.15	Slight	0.02
	10	1,3	0.00	Poor chance	
	10	2,3	0.00	Poor chance	
Q11	11	1,2	0.001	Poor chance	0.41
	11	1,3	0.00	Poor chance	
	11	2,3	0.00	Poor chance	
Q12	12	1,2	0.33	Fair	0.01
	12	1,3	0.39	Fair	0.01
	12	2,3	0.26	Fair	0.01
Q14	14	1,2	0.11	Slight	0.25
	14	1,3	0.11	Slight	0.25
	14	2,3	0.42	Moderate	0.14
Q15	15	1,2	0.29	Fair	0.004
	15	1,3	0.23	Fair	0.01
	15	2,3	0.21	Fair	0.02
Q16	16	1,2	0.20	Fair	0.017
	16	1,3	0.13	Fair	0.02
	16	2,3	0.23	Fair	0.01
Q17	17	1,2	-0.03	Poor chance	0.77
	17	1,3	0.00	Poor chance	
	17	2,3	0.00	Poor chance	0.5
Q19	19	1,2	0.00	Poor chance	
	19	1,3	0.00	Poor chance	
	19	2,3	0.00	Poor chance	
Q20	20	1,2	0.47	Moderate	0.002
	20	1,3	0.54	Moderate	0.01
	20	2,3	0.33	Fair	0.012
Q21	21	1,2	0.38	Fair	<0.01
	21	1,3	0.53	Moderate	<0.01
	21	2,3	0.37	Fair	0.035

Table (6-7) shows that for question 1 (visualization of retrocardiac lung and mediastinum) that there was a substantial agreement between observer 1 and observer 2 (K= 0.64) and that was not by chance (p= 0.01), while the agreement between observer 1 and observer 3 fair (K= 0.39, P= 0.01) and between observer 2 and observer 3 was moderate (K= 0.41, P= 0.01).

For question 2 (visualization of the spine through the heart shadow) the level of agreement between observer 1 and observer 2 was moderate (K= 0.52, P= 0.01), between observer 1 and observer 3 and also between observer 2 and observer 3 it was fair (K= 0.21, 0.37 respectively, P= 0.01).

A slight level of agreement about visualising (Reproduction of the whole rib cage above the diaphragm) in question 3 between the observers 1, 2 – 1, 3 – 2, 3 (K= 0.1, 0.19, 0.02 respectively), the agreement was not by chance between observe 1 and observer 3 (p= 0.01), but between the observer 1 and observer 2 and also between observer 2 and observer 3 it was by chance (p= 0.12, 0.32 respectively).

A slight level of agreement about visualising a sharp reproduction of the vascular pattern in the whole lung, particularly the peripheral vessels in question 4 between the observers 1, 2 – 1, 3 – 2, 3 (K= 0.29, 0.06, 0.03 respectively), the agreement was not by chance between observe 1 and observer 2 (p= 0.01), but between the observer 1 and observer 3 and also between observer 2 and observer 3 it was by chance (p= 0.07, 0.15 respectively).

In question number 5 about (Visually sharp reproduction of the trachea and proximal bronchi) the level of agreement between observer 1 and observer 2 and also between observer 1 and observer 3 was fair (K= 0.25, 0.2 respectively, P= 0.01), but between observer 2 and observer 3 the level of agreement was moderate (K= 0.4, P= 0.01).

In question number 6 about (visually sharp reproduction of the borders of the heart and aorta) the level of agreement between observer 1 and observer 3 and also between observer 2 and observer 3 was a slight (K= 0.07, P= 0.08, K= 0.17, P=

0.01 respectively), but between observer 1 and observer 2 the level of agreement was moderate (K= 0.47, P= 0.01).

Fair agreement in question 7 (Visually sharp reproduction of the diaphragm and lateral costophrenic angles) between the observer 1 and the observer 2 and also between the observer 1 and the observer 3 (K= 0.36, 0.38 respectively, P= 0.01), however it was moderate between the observer 2 and the observer 3 (K= 0.57, p= 0.01).

The level of the agreement between the observers was generally poor for the image details questions (question 8, 9, 10 and 11), apart from the level of agreement in question 8 between observer 1 and observer 2 which was fair (K= 0.27, p= 0.01) and also in question 10 there was a slight agreement (K= 0.15, P= 0.02) between the observer 1 and observer 2.

The level of agreement about the identification of CVC in question 12 was fair between the observers (1, 2 – 1, 3 – 2, 3) (K= 0.33, 0.39, 0.26 respectively), however Kapa value shows that the agreement between the observer 1 and the observer 2 was by chance (P= 0.41).

In question 14 about the identification of the thoracostomy tube, although there was a slight agreement between the observer 1 and the observer 2 and also between the observer 1 and the observer 3 (K= 0.11, 0.11 respectively), it was by chance (P= 0.25, 0.25). Despite the moderate level of agreement between the observer 2 and the observer 3 (K= 0.42), again here it was by chance (P= 0.14).

Fair agreement about question 15 (the identification of the position of the NG tube) between the observer 1 and the observer 2, the observer 1 and the observer 3 and the observer 2 and the observer 3 (K= 0.29, 0.23, 0.21 respectively) (P= 0.01, 0.01, 0.02 respectively).

The level of agreement in question 16 about the identification of the position of the ETT was fair between the between the observer 1 and the observer 2, the observer and the observer 2 and the observer 3 (K= 0.20, 0.23 respectively) (P= 0.01, 0.01 respectively), between the observer 1 and the observer 3 there was a slight agreement (K= 0.13, P= 0.02).

The level of agreement in question 17 (the identification the correct position of CVC) was a poor between the observer 1 and the observer 2, the observer 1 and the observer 3 and the observer 2 and the observer 3 (K= - 0.03, 0.00, 0.00 respectively), but it was by chance between the observer 1 and the observer 2, and the observer 2 and the observer 3 (P= 0.77, 0.0.5 respectively).

The level of agreement in question 19 (the identification the correct position of the thoracostomy tube) was a poor between the observer 1 and the observer 2, the observer 1 and the observer 3 and the observer 2 and the observer 3 (K= - 0.00, 0.00, 0.00 respectively).

in the question 20 about the identification the correct position of the NG tube the level of agreement was moderate between the observer 1 and the observer 2, the observer 1 and the observer 3 (K= 0.47, 0.54 respectively), which was not by chance (P= 0.01, 0.01 respectively), but between the observer 2 and the observer 3 (K= 0.33, P= 0.01).

The agreement about the identification of the correct position of the ETT in question 21 was fair between the observer 1 and the observer 2 and between the observer 2 and the observer 3 (K= 0.38, 0.37 respectively) (P= 0.01, 0.03 respectively).

6.6 Discussion

In standard mobile chest radiography technique, the imaging parameters of chest radiography are set to produce the best average image, an image that will demonstrate a wide range of findings including pleural, pulmonary, mediastinal and other abnormalities (De Lacey et al., 2008). This technique used may mask the position of chest tubes and lines in the chest radiograph due to the possibility of their being obscured in the brighter regions such as the heart and mediastinum (Nodine et al., 1996).

In this study three observers participated to evaluate the CEC image Quality Criteria, and the identification of tube/line position, on a series of 17 ICU/CCU chest radiographs. The evaluation was performed on images using the default (standard) post-processing algorithm and on a greyscale inverted image.

The analysis of 34 templates (17 images, 2 algorithms) were collected from the observers, the analysis shows that there was little difference between the two algorithms (standard and inverse algorithm) in relation to visualisation of the retrocardiac lung and the mediastinum, the spine through the heart shadow, reproduction of the whole rib cage above the diaphragm, sharp reproduction of the vascular pattern in the whole lung, particularly the peripheral vessels, sharp reproduction of the borders of the heart and aorta, sharp reproduction of the diaphragm and lateral costophrenic angles, small round details in the lung and retrocardiac areas, linear and reticular details to the lung periphery, identification CVC position, identification thoracostomy tube position, identification NG tube position and identification ETT position.

However, the standard algorithm was better for visualising a sharp reproduction of the trachea and proximal bronchi than the inverted algorithm.

This means that the interpreters can use the both algorithms in clinical practice although they used to read the chest radiograph as standard algorithm. Therefore, the inverted algorithm can be an alternative to interpret the chest radiographs for the criteria above apart from the visualisation of sharp reproduction of the trachea and proximal bronchi, where the standard was better than the inverted as the results illustrated.

In terms of visualising the CVC correctly positioned the result shows that the observer 2 and 3 were strongly agree that the CVC correctly positioned in both algorithms. Although observer 1 was confident in 4 observations of 13 observations, it can be suggested that both algorithms can be used to confirm the correct position of CVC.

Thoracostomy tube the three observers were not confident to confirm it is correct position as the result shows, this suggest that there may be other reasons.

The NG tube was confirmed by the three observers as definitely in the correct position in 29 of 44 observations in standard algorithm and 29 of 42 observations in inverted algorithm. It can be seen that almost both algorithms can be adopted in the clinical practice to indicate the correct position. A possible explanation for this might be that NG tube clearly seen beyond the diaphragm in both algorithms so the observers can suggest that the tube was in a correct position. However, in some images radiographs were cut from down so the tip of NG tube was not apparent and as a result it is difficult to confirm the correct position of NG tube.

Regarding to confirm the correct position of the ETT from both algorithms (standard and inverted), the result shows approximately no difference between them (standard and inverted), where definitely indicated by the three observers in 22 of 31 observations (standard algorithm), 19 of 32 observations (inverted algorithm). So it can be suggested using the inverted algorithm in clinical practice as alternative algorithm for the standard algorithm.

In this study the level of agreement between the observers was tested by using linear weighted Kappa. In terms of the visualization of retrocardiac lung and mediastinum and visualization of the spine through the heart shadow, the Kappa arranged between (K= 0.21 to 0.64), which means from fair to substantial agreement between observers.

Compare scores for the standard and inverted algorithms result shows no significant different between the two algorithms in relation to visualise the retrocardiac lung and mediastinum and visualization of the spine through the heart shadow. Therefore it can be suggested that both algorithms can be used in clinical practice to visualise the retrocardiac lung and mediastinum and visualization of the spine through the heart shadow.

The level of agreement between the observers for visualising reproduction of the whole rib cage above the diaphragm and visualising a sharp reproduction of the vascular pattern in the whole lung, particularly the peripheral vessels was a slight; however the agreement was by chance for the majority of comparisons between the observers. There is inconsistency between the observers and that can explain the slight level of agreement.

Fair to moderate (K= 0.2 to 0.47) agreement between the observers about visualisation of sharp reproduction of the trachea and proximal bronchi, the agreement was not by chance (p= 0.01). However, the repeated measure analysis indicated that the standard was better than the inverted.

The range of agreement was between slight to moderate (K= 0.07 to 0.57) for visualising the sharp reproduction of the borders of the heart and aorta, and the sharp reproduction of the diaphragm and lateral costophrenic angles. In order to avoid misinterpretation one algorithm was preferred by the observers due to it is commonality in practise.

There was very poor agreement between the observers about the image details, the reason for that might be no answer from the observers in the template sheet or because it would need some measurements and that can take time so the observers roughly scored them.

In terms of indicating the CVC the agreement between the observers was fair, which means both algorithms (standard and inverted) were good to visualise the CVC. However, edge enhancement algorithm was also suggested by Jennings et al (1992) to detect the cardiovascular devices.

For thoracostomy tube there was a slight chance of agreement between the observers apart from between the observer 2 and observer 3 which was moderate but all of level of agreement was by chance (> 0.05), this is might because the position of thoracostomy tube, which may be located posteriorly for the drainage of pleural fluid or anterosuperior for removing air and that could have confused the observers. Therefore both algorithms are suggested in this study to use them in the clinical practices.

According to the results the level of agreement between the observers was fair for identifying the NG tube and the ETT. Because both of tubes made from plastic so their visibility can be the same on the chest radiograph.

In terms of confirming the correct position of the CVC the level of agreement between observer 1, 2 and 1, 3 was poor. The agreement between 2, 3 was high but very little variation in responses from comparing scores 12/12 and 13/13 assessed as correct position. Therefore chance agreement is also extremely high. The justification for that addressed by Viera and Garrett(2005) who stated that the level of agreement may not be reliable for rare observations due such a rare finding.

It was poor agreement between the observers in relation to the correct position of thoracostomy tube and this is due to very few answers in the template sheet or the observers were confident to detect the correct position of thoracostomy tube.

Some misinterpretation of presence of thoracostomy tube, all observers said definitely or probably in the correct position, observer 1 said all were probably in the correct position.

The level of agreement between the observers was fair to moderate and statistically significant in relation to localize the correct position of NG tube. The observers were also confident from the scoring size result so it can be suggested that the inverted algorithm can be alternative to the standard algorithm for detecting the correct position of NG tube.

Nodine et al (1996) found that edge enhancement algorithm was not the appropriate for visualising the ETT. In this study the level of agreement between the observers was fair and significant and ETT was detected by both algorithms. Therefore, the current study suggested using both algorithms to visualise the ETT in clinical practice.

6.7 Limitations of study

There were several limitations in this study, first because the evaluation was only on two algorithms (standard and inverse algorithm) and the original intention was to evaluate a number of alternative image processing algorithms (1- default, 2- chest line placement, 3 soft tissue, 4- bone details, 5- invert). Therefore, it might be one of these algorithms performances better to visualise tubes/ lines and other quality criteria. Second the sample size was quite small (17 cases) but the effect size were almost all <10% suggesting no evidence of large effect, except the visualisation of sharp reproduction of the trachea and proximal bronchi. In addition, all observers were experienced radiographers.

7 Chapter seven

7.1 Conclusion

Mobile chest radiography remains one of the simplest tests used in the intensive care unit (I.C.U). Usually there is at least one chest radiography per day to assess the cardiopulmonary condition of a patient in the I.C.U, and to detect the appropriate position of tubes and lines as well as monitor devices (Miller, 1997). Because the patients usually have many serious and complicated medical issues many devices, tubes, lines have to be connected to patients to constantly monitor them. However, it is difficult to transport the patient to the radiology department (Miller, 1997). Therefore, other imaging modalities such as computed tomography (CT), ultrasound (US), magnetic resonance imaging (MRI) and nuclear medicine are limited in their use for examining the patients in the intensive care unit.

Furthermore, one of the most frequent issues recognized radiographically with the patients in the intensive care unit is that chest tubes and lines are malpositioned (Aronchick and Miller, 1997) which might be related to technical quality. This can affect the appearance of the tubes and lines in mobile chest radiography (Foos et al., 2011). Difficult positioning of uncooperative patients in critical care can lead to rotation of the patient (De Lacey et al., 2008) and that can produce distortion in the cardiac shadow and other anatomical structures such as ribs, clavicles, trachea shadow (Moskowitz, 2010). Kyphotic, lordotic patients in the intensive care unit can lead to overlapping in the radiographic image (Leroux et al., 2002) therefore, the anatomical features of the chest structures will change in the radiographic image.

Another issue with standard mobile chest radiography technique, where the imaging parameters of chest radiography are set to produce the best average image, is that an image will demonstrate a wide range of findings including pleural, pulmonary, mediastinal and other abnormalities (De Lacey et al., 2008).

However, because pulmonary disease is one of the most frequently occurring abnormalities, imaging parameters have to be optimised to visualise this condition. But the technique used may mask the position of chest tubes and lines in the chest radiograph due to the possibility of their being obscured in the brighter regions such as the heart and mediastinum (Nodine et al., 1996).

Therefore, in this study a first stage of chest experiment was conducted to identify the measurements of rotation, kyphotic and lordotic degrees. The experiment tries to associate a precise degree of angulation and the changes of position in the anatomical structures and the appearance of chest tubes and lines. The data collected from the experiment have been used to support the third stage; to evaluate how useful these measurements are on 17 real ICU/ CCU chest radiographs.

The second stage was conducted to provide an appropriate algorithm(s) for visualizing chest tubes and lines in ICU chest radiography. The impact of the standard and the inverse algorithms upon decision making was also examined.

In terms of the methods used in the chest phantom experiment, the study found that the methods were used to estimate the degree of rotation; kyphosis and lordosis by measuring the clavicle to apex distance and fourth anterior rib angle for lordosis and kyphosis, and the displacement of the midline between the clavicles and ratio of fourth anterior rib (left and right) length for rotation. Although the linear relationships of the measurements conducted show the large effect upon the anatomical structures appearance due to the rotation, kyphosis and lordosis, it was almost horizontal for radio-opaque balls (CVC, ETT) and it does not have a particular large effect upon the changes of radio-opaque ball position.

In chapter 6, the study shows that there was a little difference between the two algorithms (standard and inverse) in relation to the evaluation of the CEC criteria. Also the identification of chest tubes and lines apart from the visualisation of sharp reproduction of the trachea and proximal bronchi, which was a significant change

in the quality of chest radiography by using the standard algorithm than the inverted algorithm.

However, it might useful to use the inverse algorithm in clinical practice if it is difficult to identify the chest tubes and lines with the standard algorithm. This may be enhanced significantly by using the special algorithm designed for identifying chest tubes and lines.

It needs to be mentioned that the kappa output of the study is not commendable in terms of research findings, since CVC Kappa result shows poor agreement between observer 2 and observer 3. However, the Kappa results are at times misleading, which is confirmed by the rare study done by Vier and Garett (2005). In their study they argued that in cases of rare observations, Kappa may not be reliable and discrepancy may occur between reality and kappa output. This study also confirms Vier and Garett s(2005) findings, since the result in table (5-3) shows that the findings of observer 2 and observer 3 is almost identical (score of 12 and 13), while the Kappa result shows poor agreement.

In relation to the comparison between the two methods to estimate the degree of angulation for rotation, kyphosis and lordosis on 17 mobile chest radiographs and also the apparent position of the CVC and the ETT the methods are not likely to provide useful information to the image interpreter in deciding estimation for the degree of rotation, kyphosis and lordosis. Therefore, these methods were not useful to use in clinical practice.

7.2 Suggestions for further work

The dissertation has investigated how the technical quality of the intensive care unit chest radiography can impact upon the appearance of chest tubes and lines and how that appearance can impact on the decision making with regard to patients' clinical situations. The methods used in the chest phantom experiment to measure the changes of the feature of the symmetry of some chest anatomical structures were not applicable on the 17 ICU/CCU mobile chest radiographs and the study found that there is a variation in the patients' chest size and also between the measurements (clavicle-spinous process, clavicle-apex, fourth anterior rib length and angle).

The algorithms used in the study (standard and inverse), show there are little differences between them in relation to the CEC criteria and the identification of the chest tubes and lines apart from visualising sharp reproduction of the trachea and proximal bronchi where the standard algorithm was better than the inverse one.

Therefore suggestions for further research include:

- There are little changes in the CVC tip position in relation to the changes in the degree of angulation (rotation, kyphosis and lordosis) so it would be better if the measurements were conducted on the relative anatomical structures not far from the position of CVC.
- Although theoretical work has been done to model CVC tip position during kyphotic and lordotic angle with regard to superior vena cava (SVC) location, more work is needed to model CVC tip position in rotation angle.
- In future investigations it might be possible to use a different chest phantom which enables insertion of each tube and line in their exact position.
- Inter-observer variation of chest phantom measurement should be repeated and tested by other researchers.

- further work is required to evaluate a number of alternative image processing algorithms to identify which algorithm can demonstrate the chest tube and line position most clearly (1- default, 2- chest line placement, 3 soft tissue, 4- bone details, 5- invert).
- Involved experienced people such as radiologists or cardiologists who are experienced in interpretation of chest radiographs to evaluate the efficiency of the algorithms on the ICU/CCU chest radiographs.

References

Allisy-Roberts, P. J., Farr, R. F. and Williams, J. (2008) *Farr's physics for medical imaging.* 2nd ed. London: Saunders.

Altman, D. G. (1999) *Practical Statistics for Medical Research.* CRC P.

Aronchick, J. M. and Miller, J. W. T. (1997) Tubes and lines in the intensive care setting. *Seminars in Roentgenology,* 32 (2)**,** 102-116.

Bacher, K., Smeets, P., Vereecken, L., De Hauwere, A., Duyck, P., De Man, R., Verstraete, K. and Thierens, H. (2006) Image quality and radiation dose on digital chest imaging: comparison of amorphous silicon and amorphous selenium flat-panel systems. *AJR Am J Roentgenol,* 187 (3)**,** 630-7.

Bakker, G. and Clark, L. (1988) *Explanation : an introduction to the philosophy of science.* Mountain View: Mayfield.

Balassy, C., Prokop, M., Weber, M., Sailer, J., Herold, C. J. and Schaefer-Prokop, C. (2005) Flat-panel display (LCD) versus high-resolution gray-scale display (CRT) for chest radiography: an observer preference study. *AJR. American Journal Of Roentgenology,* 184 (3)**,** 752-756.

Bankier, A. A., Mallek, R., Wiesmayr, M. N., Fleischmann, D., Kranz, A., Kontrus, M., Knapp, S. and Winkelbauer, F. W. (1997) Azygos arch cannulation by central venous catheters: Radiographic detection of malposition and subsequent complications. *Journal of Thoracic Imaging,* 12 (1)**,** 64-69.

Bankman, I. N. (2009) *Handbook of medical image processing and analysis.* 2nd ed. (Academic Press series in biomedical engineering) Amsterdam ; Boston: Elsevier/Academic Press. Available from http://www.knovel.com.ezproxy.brad.ac.uk/knovel2/Toc.jsp?BookID=2778

Bansal, G. J. (2006) Digital radiography. A comparison with modern conventional imaging. *Postgraduate Medical Journal,* 82 (969)**,** 425-428.

Bentley, H. B. (2005) Early days of radiography. *Radiography,* 11 (1)**,** 45-50.

Bland, J. M. and Altman, D. G. (1986) Statistical methods for assessing agreement between two methods of clinical measurement. *Lancet,* 1 (8476)**,** 307-310.

Boiselle, P. M. and White, C. S. (2007) *New techniques in cardiothoracic imaging.* New York ; London: Informa Healthcare.

Bontrager, K. L. and Lampignano, J. P. (2005) *Textbook of radiographic positioning and related anatomy.* 6th ed. St. Louis: Elsevier/Mosby.

Bourke, S. J. and Burns, G. P. (2011) *Lecture notes : respiratory medicine.* 8th ed. Malden, MA. ; Oxford: Wiley.

Brandt, L. (1986) [The history of endotracheal anesthesia, with special regard to the development of the endotracheal tube]. *Anaesthesist,* 35 (9)**,** 523-30.

Briggs, G. (2004) *McGraw-Hill's pocket guide to chest X-rays.* New York ; London: McGraw-Hill.

Brunel, W., Coleman, D. L., Schwartz, D. E., Peper, E. and Cohen, N. H. (1989) Assessment of routine chest roentgenograms and the physical examination to confirm endotracheal tube position. *Chest,* 96 (5)**,** 1043-1045.

Campeau, F. E. and Phelps, J. (1993) *Limited radiography.* New York: Delmar.

Carlton, R. R. and Adler, A. M. (2006) *Principles of radiographic imaging : an art and a science.* 4th ed*.* Albany, USA: Delmar.

Carmichael, J. H. E. (1996) *European guidelines on quality criteria for diagnostic radiographic images.* European Commission.

Carter, C. E. and Vealé, B. L. (2008) *Digital radiography and PACS.* St. Louis, Mo. ; London: Mosby Elsevier.

Carter, P., Paterson, A. and Chesney, D. N. (1994) *Chesneys' equipment for student radiographers.* 4th. ed*.* Oxford: Blackwell Scientific.

Chahine-Malus, N., Stewart, T., Lapinsky, S. E., Marras, T., Dancey, D., Leung, R. and Mehta, S. (2001) Utility of routine chest radiographs in a medical-surgical intensive care unit: a quality assurance survey. *Critical Care,* 5 (5)**,** 271-275.

Chan, L., Reilly, K. M., Henderson, C., Kahn, F. and Salluzzo, R. F. (1997) Complication rates of tube thoracostomy. *The American Journal Of Emergency Medicine,* 15 (4)**,** 368-370.

Collins, J. and Stern, E. J. (2008) *Chest radiology : the essentials.* 2nd ed*.* Philadelphia: Lippincott Williams & Wilkins.

Comte, A. and Lenzer, G. (1998) *Auguste Comte and positivism : the essential writings.* (History of ideas series) New Brunswick, N.J.; London: Transaction Publishers.

Connolly, M. A. (2001) Black, white, and shades of gray: common abnormalities in chest radiographs. *AACN Clinical Issues,* 12 (2)**,** 259-269.

CTSNET.org (2011) thoracoscopic management of spontaneous pneumothorax [image] available from: http://www.ctsnet.org/sections/clinicalresources/thoracic/expert_tech-34.html [accessed 6th November 2011].

Davidson, A. C. and Treacher, D. T. (2002) *Respiratory critical care.* London: Arnold.

De Boo, D. W., Weber, M., Deurloo, E. E., Streekstra, G. J., Freling, N. J., Dongelmans, D. A. and Schaefer-Prokop, C. M. (2011) Computed radiography versus mobile direct radiography for bedside chest radiographs: impact of dose on image quality and reader agreement. *Clinical Radiology,* 66 (9)**,** 826-832.

De Lacey, G., Morley, S. and Berman, L. F. (2008) *The chest X-ray : a survival guide.* Philadelphia, Pa. ; Edinburgh: Saunders Elsevier.

Dixon, A.-M. (2008) *Fundamentals of diagnostic imaging : an introduction for nurses and allied health care professionals.* Exeter ;: Reflect Press.

Dowsett, D. J., Kenny, P. A. and Johnston, R. E. (2006) *The physics of diagnostic imaging.* 2nd ed. London: Hodder Arnold.

Easton, S. (2009) *An introduction to radiography.* Edinburgh ; New York: Churchill Livingstone Elsevier.

Eisenhuber, E., Schaefer-Prokop, C. M., Prosch, H. and Schima, W. (2012) Bedside Chest Radiography. *Respiratory Care,* 57 (3)**,** 427-443.

Eisenhuber, E., Stadler, A., Prokop, M., Fuchsjager, M., Weber, M. and Schaefer-Prokop, C. (2003) Detection of monitoring materials on bedside chest radiographs with the most recent generation of storage phosphor plates: Dose increase does not improve detection performance. *Radiology,* 227 (1)**,** 216-221.

Endo.co.id (2011) thoracic drainage catheter chest tube [image] Available from: http://endo.co.id/romsons-thoracic-drainage-catheters.html[accessed 9th November 2011].

Erickson, B. J., Manduca, A., Palisson, P., Persons, K. R., Earnest, F., Savcenko, V. and Hangiandreou, N. J. (1998) Wavelet compression of medical images. *Radiology,* 206 (3)**,** 599-607.

Fauber, T. L. (2009) *Radiographic imaging and exposure.* 3rd ed. Edinburgh: Mosby.

Foos, D. H., Yankelevitz, D. F., Wang, X., Berlin, D., Zappetti, D., Cham, M., Sanders, A., Parker, K. N. and Henschke, C. I. (2011) Improved visualization of tubes and lines in portable intensive care unit radiographs: a study comparing a new approach to the standard approach. *Clinical Imaging,* 35 (5)**,** 346-352.

Gifford, F. (2011) *Philosophy of medicine.* Oxford: North Holland.

Glasser, O., Boveri, M. and Tucker, J. (1933) *Wilhelm Conrad Röntgen and the early history of the Roentgen rays.* London: Bale & Danielsson.

Greenhalgh, T. (2001) *How to read a paper : the basics of evidence based medicine.* 2nd ed. London: BMJ.

Greetham, B. (2006) *Philosophy.* (Palgrave foundations) Basingstoke ; New York: Palgrave Macmillan.

Hamer, O. W., Sirlin, C. B., Strotzer, M., Borisch, I., Zorger, N., Feuerbach, S. and Völk, M. (2005) Chest radiography with a flat-panel detector: image quality with dose reduction after copper filtration. *Radiology,* 237 (2)**,** 691-700.

Hamilton, H. and Bodenham, A. (2009) *Central venous catheters.* Hoboken, NJ: John Wiley & Sons.

Haubrich, W. S. (2003) Röntgen of roentgenology. *Gastroenterology,* 125 (5)**,** 1300-1300.

Haygood, T. M., Brennan, P. C., Ryan, J., Yamal, J.-M., Liles, L., O'Sullivan, P., Costelloe, C. M., Fitzgerald, N. E. and Murphy, W. A., Jr. (2011) Central venous line placement in the superior vena cava and the azygos vein: differentiation on posteroanterior chest radiographs. *AJR. American Journal Of Roentgenology,* 196 (4)**,** 783-787.

Hegde, H. V. and Raghavendra Rao, P. (2010) A near miss; malpositioned nasogastric tube in the left bronchus of a spontaneously breathing critically-ill patient. *Current Anaesthesia & Critical Care,* 21 (2)**,** 94-96.

Henschke, C. I., Yankelevitz, D. F., Wand, A., Davis, S. D. and Shiau, M. (1997) Chest radiography in the ICU. *Clin Imaging,* 21 (2)**,** 90-103.

Hobbs, D. L. (2007) Chest radiography for radiologic technologists. *Radiol Technol,* 78 (6)**,** 494-516; quiz 517-9.

Hogan-med.com (2008) Endotracheal tube [online] Available from: http://www.hongan-med.com/ [accessed 4th July 2011].

Hollman, A. S. and Adams, F. G. (1989) The influence of the lordotic projection on the interpretation of the chest radiograph. *Clinical Radiology,* 40 (4)**,** 360-364.

Huda, W. and Slone, R. M. (2003) *Review of radiologic physics.* 2nd ed. Philadelphia: Lippincott Williams & Wilkins.

Howequipmentworks.com (2008) tracheal tube [online] Available from: http://www.equipmentexplained.com [accessed 6th June 2011].

Howequipmentworks.com (2008) tracheal tube [image] Available from: http://www.equipmentexplained.co [accessed 3rd July 2011].

Irwin, R. S. and Rippe, J. M. (2010) *Manual of intensive care medicine.* 5th ed. ed. Philadelphia: Wolters Kluwer Health/Lippincott Williams & Wilkins.

Jarvie, I. C., Milford, K. and Miller, D. (2006) *Karl Popper : a centenary assessment.* Aldershot: Ashgate.

Javors, B. R. and Wolf, E. L. (2003) *Radiology of the postoperative GI tract.* New York: Springer.

Jenkins, D. b. (1980) *Radiographic photography and imaging processes.* Lancaster: M.T.P. Press.

Jennings, P., Padley, S. P. and Hansell, D. M. (1992) Portable chest radiography in intensive care: a comparison of computed and conventional radiography. *Br J Radiol,* 65 (778)**,** 852-6.

Joseph, A. E. A., de Lacey, G. J., Bryant, T. H. E., Stoker, D. J. and Ayr, G. (1978) The hypertransradiant hemithorax: The importance of lateral decentring, and

the explanation for its appearance due to rotation. *Clinical Radiology,* 29 (2)**,** 125-131.

Kawati, R. and Rubertsson, S. (2005) Malpositioning of fine bore feeding tube: A serious complication. *Acta Anaesthesiologica Scandinavica,* 49 (1)**,** 58-61.

Kazerooni, E. A., Gross, B. H. and Ovid Technologies, I. (2004) *Cardiopulmonary imaging [electronic resource].* (The core curriculum) Philadelphia: Lippincott Williams & Wilkins.

Kearney, T. J. and Shabot, M. M. (1995) Pulmonary artery rupture associated with the Swan-Ganz catheter. *CHEST,* 108 (5)**,** 1349-1352.

L'E and McSwiney, M. (2007) Fatal cardiac tamponade as a result of a peripherally inserted central venous catheter: a case report and review of the literature. *BJA: The British Journal of Anaesthesia,* 99 (3)**,** 384-388.

Ladyman, J. (2002) *Understanding philosophy of science.* London: Routledge.

Lange, S. and Walsh, G. F. (2007) *Radiology of chest diseases.* 3rd , fully rev. and expanded ed*.* Stuttgart, New York: Thieme.

Larsson, W., Aspelin, P., Bergquist, M., Hillergård, K., Jacobsson, B., Lindsköld, L., Wallberg, J. and Lundberg, N. (2007) The effects of PACS on radiographer's work practice. *Radiography,* 13 (3)**,** 235-240.

Lentle, B. and Aldrich, J. (1997) Radiological sciences, past and present. *Lancet,* 350 (9073)**,** 280-5.

Leroux, M. A., Zabjek, K., Simard, G. and Rivard, C. H. (2002) Estimated kyphosis and lordosis changes at follow-up in patients with idiopathic scoliosis. *Journal of Pediatric Orthopaedics,* 22 (1)**,** 73-79.

Lippincott, W. and Wilkins (2009) *Lippincott's nursing procedures.* 5th ed*.* Philadelphia ; London: Wolters Kluwer / Lippincott Williams & Wilkins.

Macmahon, H. and Vyborny, C. (1994) TECHNICAL ADVANCES IN CHEST RADIOGRAPHY. *American Journal of Roentgenology,* 163 (5)**,** 1049-1059.

Mahadevan, S. V. and Garmel, G. M. (2005) *An introduction to clinical emergency medicine : [guide for practitioners in the emergency department].* Cambridge ; New York: Cambridge University Press.

Marik, P. E. and Janower, M. L. (1997) The impact of routine chest radiography on ICU management decisions: an observational study. *American Journal of Critical Care,* 6 (2)**,** 95-98.

Marino, P. L., Sutin, K. M. and Ovid Technologies, I. (2007) *The ICU book [electronic resource].* 3rd ed*.* (LWW Doody's all reviewed collection.) Philadelphia: Lippincott Williams & Wilkins.

Marwede, D. and Fielding, M. (2005) The epistemological-ontological divide in clinical radiology. *Stud Health Technol Inform,* 116**,** 749-54.

Mattu, A. (2010) *Avoiding common errors in the emergency department.* (Avoiding common errors series) Philadelphia, Pa. ; London: Wolters Kluwer Health/Lippincott Williams & Wilkins.

McQuillen-Martensen, K. (1996) *Radiographic critique.* Philadelphia; London: Saunders.

Mehta, A. C., Chua, A. P., Gleeson, F. and Meziane, M. (2010) The debate on CXR utilization and interpretation is only just beginning: a Pro/Con debate. *Respirology,* 15 (8)**,** 1152-6.

Mehta, M. H. (1972) The rib-vertebra angle in the early diagnosis between resolving and progressive infantile scoliosis. *J Bone Joint Surg Br,* 54 (2)**,** 230-43.

Meredith, W. J. and Massey, J. B. (1977) *Fundamental physics of radiology.* 3rd ed*.* Bristol: J. Wright.

Miller, S. W. T. (1997) The radiologist in the intensive care unit. *Seminars in Roentgenology,* 32 (2)**,** 86-88.

Milne, E. N. C. and Pistolesi, M. (1993) *Reading the chest radiograph : a physiologic approach.* St. Louis ; London: Mosby-Year Book.

Moore, C. S., Liney, G. P., Beavis, A. W. and Saunderson, J. R. (2007) A method to optimize the processing algorithm of a computed radiography system for chest radiography. *The British Journal Of Radiology,* 80 (957)**,** 724-730.

Moore, K. L. and Dalley, A. F. (2006) *Clinically oriented anatomy.* 5th ed*.* Philadelphia, PA ; London: Lippincott Williams & Wilkins.

Moretti, E. W., Ofstead, C. L., Kristy, R. M. and Wetzler, H. P. (2005) Impact of central venous catheter type and methods on catheter-related colonization and bacteraemia. *Journal of Hospital Infection,* 61 (2)**,** 139-145.

Moskowitz, H. (2010) *ICU chest radiology : principles and case studies.* Hoboken, N.J.: Wiley-Blackwell.

Moyle, J. T. B., Davey, A. and Ward, C. S. (1998) *Ward's anaesthetic equipment.* 4th ed*.* London: W. B. Saunders.

Nentwich, P. F. (1990) *Intravenous therapy : a comprehensive application of intravenous therapy and medication administration.* (The Jones and Bartlett series in nursing) Boston: Jones and Bartlett.

Nodine, C. F., Liu, H., Miller Jr, W. T. and Kundel, H. L. (1996) Observer performance in the localization of tubes and catheters on digital chest images: The role of expertise and image enhancement. *Academic Radiology,* 3 (10)**,** 834-841.

O'Hear, A. (1980) *Karl Popper.* (The arguments of the philosophers) London (etc.)): Routledge and Kegan Paul.

Pope, J. A. (1999) *Medical physics : imaging.* (Heinemann advanced science) Oxford: Heinemann.

Popper, K. R. (1963) *Conjectures and refutations : the growth of scientific knowledge.* London: Routledge & Kegan Paul.

Porté, F., Basit, R. and Howlett, D. (2009) Imaging in the intensive care unit. *Surgery (Oxford),* 27 (11)**,** 496-499.

Pudas, T., Korsoff, L., Kallio, T., Uhari, M. and Alanen, A. (2005) Influence of film digitization on radiological interpretation. *British Journal of Radiology,* 78 (935)**,** 993-996.

Ramlaul, A. (2010) *Medical imaging and radiotherapy research : skills and strategies.* Edinburgh: Churchill Livingstone.

Robson, C. (2002) *Real world research : a resource for social scientists and practitioner-researchers.* 2nd ed. Oxford: Blackwell.

Rowe, R. C. (2003) Röntgen rays revealed. *Drug Discovery Today,* 8 (2)**,** 60-61.

Rubinowitz, A. N., Siegel, M. D. and Tocino, I. (2007) Thoracic Imaging in the ICU. *Critical Care Clinics,* 23 (3)**,** 539-573.

Russ, J. C. and NetLibrary, I. (2007) *The image processing handbook [electronic resource].* 5th ed. Boca Raton: CRC/Taylor and Francis.

Russell, B. (1927) *An outline of philosophy.* London: Allen & Unwin.

Ryan, S. P. and McNicholas, M. M. J. (1994) *Anatomy for diagnostic imaging.* London: W.B. Saunders.

Sarvazyan, A. P., Lizzi, F. L. and Wells, P. N. T. (1991) A new philosophy of medical imaging. *Medical Hypotheses,* 36 (4)**,** 327-335.

Savoca, C. J., Gamsu, G. and Rohlfing, B. M. (1978) Chest radiography in intensive care units. *West J Med,* 129 (6)**,** 469-74.

Schuster, M., Nave, H., Piepenbrock, S., Pabst, R. and Panning, B. (2000) The carina as a landmark in central venous catheter placement. *Br J Anaesth,* 85 (2)**,** 192-4.

Snell, R. S. (2008) *Clinical anatomy by regions.* 8th ed. Philadelphia ; London: Lippincott Williams & Wilkins.

Strotzer, M., Völk, M., Fründ, R., Hamer, O., Zorger, N. and Feuerbach, S. (2002) Routine chest radiography using a flat-panel detector: image quality at standard detector dose and 33% dose reduction. *AJR. American Journal Of Roentgenology,* 178 (1)**,** 169-171.

Tarrac, S. E. (2009) A Systematic Approach to Chest X-Ray Interpretation in the Perianesthesia Unit. *Journal of PeriAnesthesia Nursing,* 24 (1)**,** 41-49.

Thomas, A., Isherwood, I., Wells, P. N. T. and Röntgen Centenary, C. (1995) *The Invisible Light : 100 years of medical radiology.* Oxford: Blackwell Science Ltd.

Tocino, I. (1996) Chest imaging in the intensive care unit. *European Journal of Radiology,* 23 (1)**,** 46-57.

Tolsma, M., Kröner, A., van den Hombergh, C. L., Rosseel, P. M., Rijpstra, T. A., Dijkstra, H. A., Bentala, M., Schultz, M. J. and van der Meer, N. J. (2011) The clinical value of routine chest radiographs in the first 24 hours after cardiac surgery. *Anesth Analg,* 112 (1)**,** 139-42.

Vahid, B., Kotiah, S. and Marik, P. (2007) Malposition of central venous catheter in left superior intercostal vein in a patient with superior vena cava syndrome. *Radiography,* 13 (4)**,** 307-309.

Valkovic, V. (1996) First centenary of Röntgen's discovery of X-rays. *Nuclear Instruments and Methods in Physics Research Section B: Beam Interactions with Materials and Atoms,* 109-110**,** 1-8.

Viera, A. J. and Garrett, J. M. (2005) Understanding interobserver agreement: the kappa statistic. *Family Medicine,* 37 (5)**,** 360-363.

Wallace T, M., Sr. (1997) The chest radiograph in the intensive care unit. *Seminars in Roentgenology,* 32 (2)**,** 89-101.

Watkins, J., Weatherburn, G. and Bryan, S. (2000) The impact of a picture archiving and communication system (PACS) upon an intensive care unit. *European Journal of Radiology,* 34 (1)**,** 3-8.

Webb, W. R. and LaBerge, J. M. (1984a) Radiographic recognition of chest tube malposition in the major fissure. *Chest,* 85 (1)**,** 81-83.

Webb, W. R. and LaBerge, J. M. (1984b) Radiographic recognition of chest tube malposition in the major fissure. *Chest,* 85 (1)**,** 81-3.

Wilson, A. G. (2002) The Chest Radiograph in Heart Disease. *Medicine,* 30 (3)**,** 18-26.

Wulff, H. R., Pedersen, S. A. and Rosenberg, R. (1986) *Philosophy of medicine : an introduction.* Oxford: Blackwell Scientific.

Yilmazlar, A., Bilgin, H., Korfali, G., Eren, A. and Ozkan, U. (1997) Complications of 1303 central venous cannulations. *J R Soc Med,* 90 (6)**,** 319-21.

Zaman, M. H., Mitra, P., Bondi, E., Gintautas, J. and Abadir, A. R. (1990) A rare malposition of the central venous catheter. *Chest,* 98 (3)**,** 768-770.

Appendices

Appendix 1: glossary

AP

Anterior Posterior

CCU

Coronary Care Unit

CEC

Commission of the European Communities

CR

Computed Radiography

CT

Chest Tube (thoracostomy tube)

CT

Computed Tomography

CVC

Central Venous Catheter

CXR

Chest X-ray

D log E

Density log Exposure

DR

Digital Radiography

ED

Emergency Department

ETT

Endotracheal Tube

Fourth ARLR

The ratio of fourth anterior rib length

H & D Curve

Hurter and Driffield Curve

ICU

Intensive Care Unit

IW

Inpatient Ward

LnCMSPR

Natural logarithm of clavicle to midline spinous process ratio

LnFRLR

Natural logarithm of fourth rib length ratio

LPO

Left Posterior Oblique

LUT

Look-up Table

MF

Magnification Factor

MRI

Magnetic Resonance Imaging

NG

Nasogastric Tube

PA

Posterior Anterior

PAC

Pulmonary Artery Catheter

PACS

Picture Archiving and Communication System

OID

Object Image Distance

OR

Operating Room

RPO

Right Posterior Oblique

ROBR

Radio-opaque ball ratio

SG

Swan-Ganz Catheter

SID

Source Image Distance

SOD

Source Object Distance

SVC

Superior Vena Cava

US

Ultra Sound

Appendix 2 Chest phantom experiment

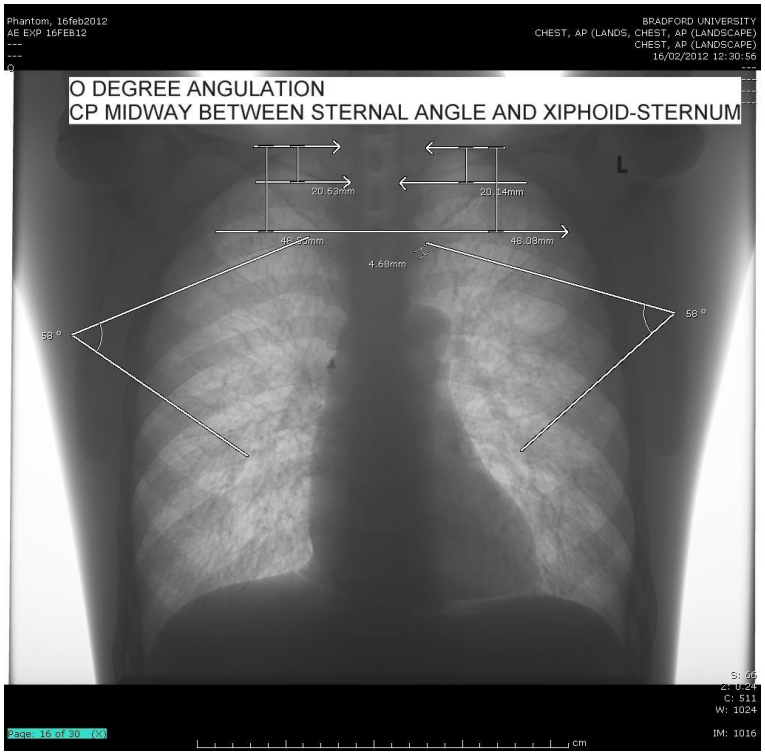

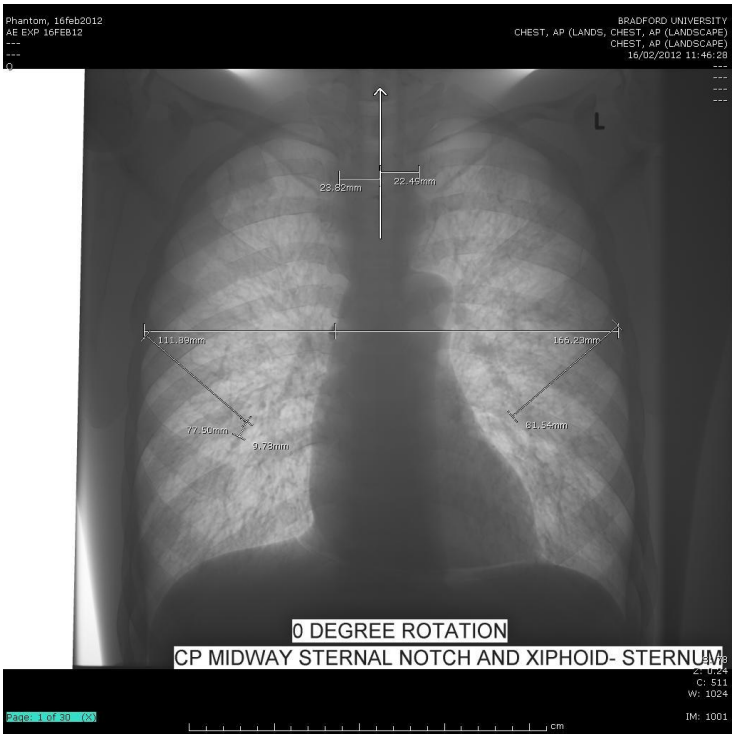

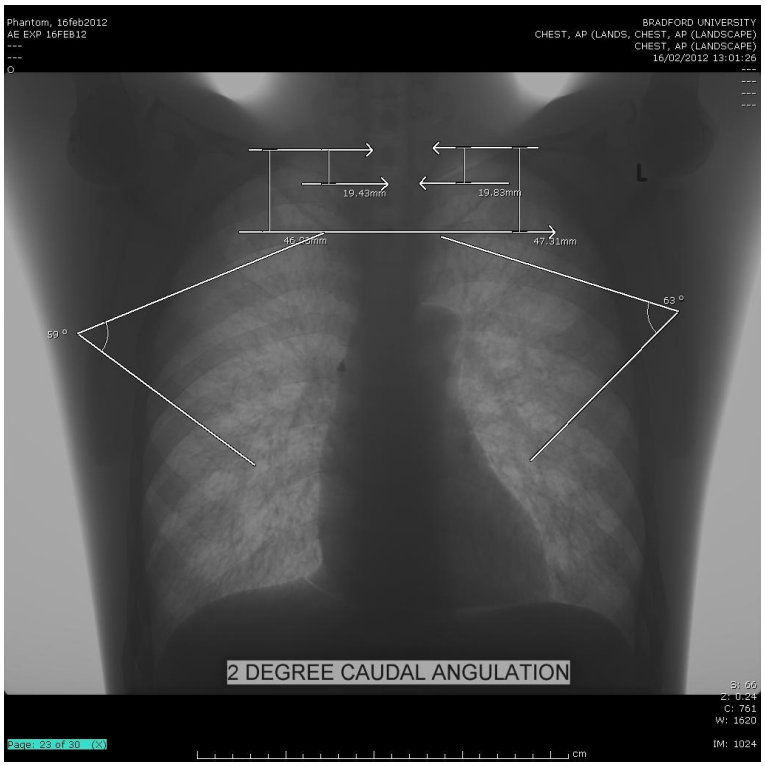
Phantom, 16feb2012
AE EXP 16FEB12
BRADFORD UNIVERSITY
CHEST, AP (LANDS, CHEST, AP (LANDSCAPE)
CHEST, AP (LANDSCAPE)
16/02/2012 13:01:26
19.43mm
19.83mm
47.91mm
63 °
59 °
2 DEGREE CAUDAL ANGULATION
C: 761
W: 1620
IM: 1024
cm

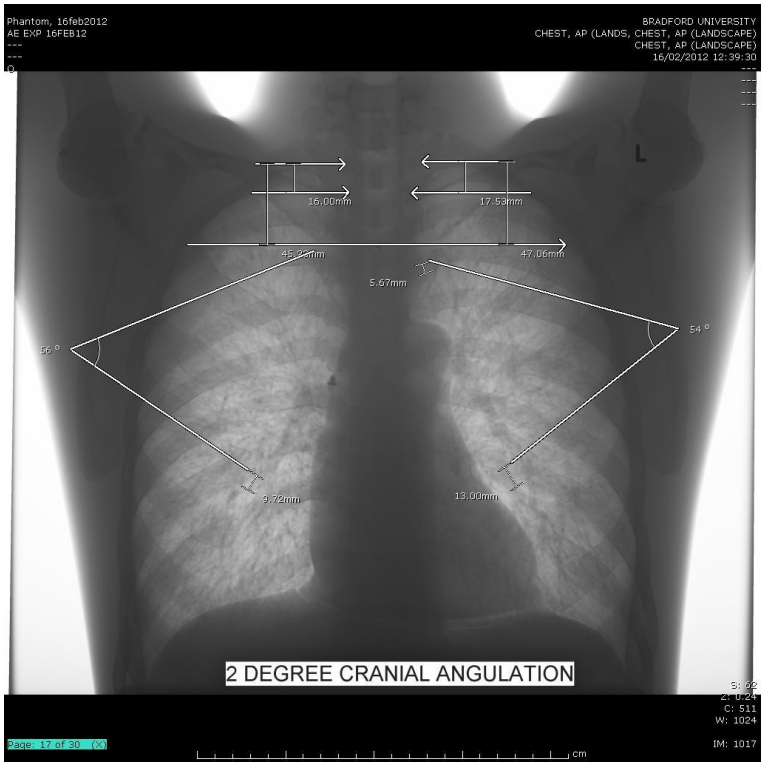
Phantom, 16feb2012
AE EXP 16FEB12
BRADFORD UNIVERSITY
CHEST, AP (LANDS, CHEST, AP (LANDSCAPE)
CHEST, AP (LANDSCAPE)
16/02/2012 12:39:30
16.00mm
17.53mm
47.06mm
5.67mm
54 °
56 °
9.72mm
13.00mm
2 DEGREE CRANIAL ANGULATION
C: 511
W: 1024
IM: 1017
cm

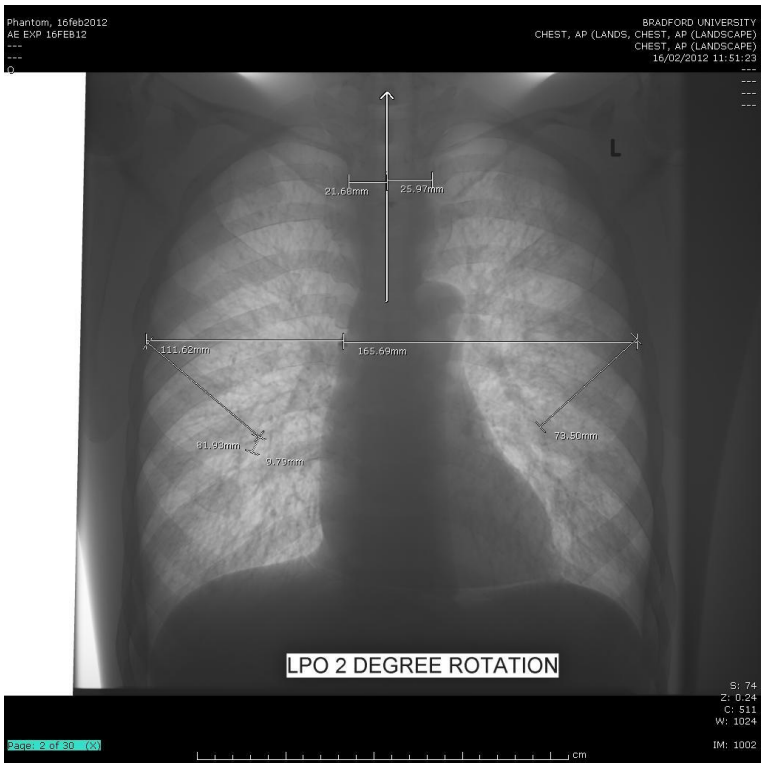
Phantom, 16feb2012
AE EXP 16FEB12
BRADFORD UNIVERSITY
CHEST, AP (LANDS, CHEST, AP (LANDSCAPE)
CHEST, AP (LANDSCAPE)
16/02/2012 11:51:23
L
21.68mm
25.97mm
111.62mm
165.69mm
81.99mm
9.79mm
78.58mm
LPO 2 DEGREE ROTATION
S: 74
Z: 0.24
C: 511
W: 1024
IM: 1002
Page: 2 of 30 (X)
cm

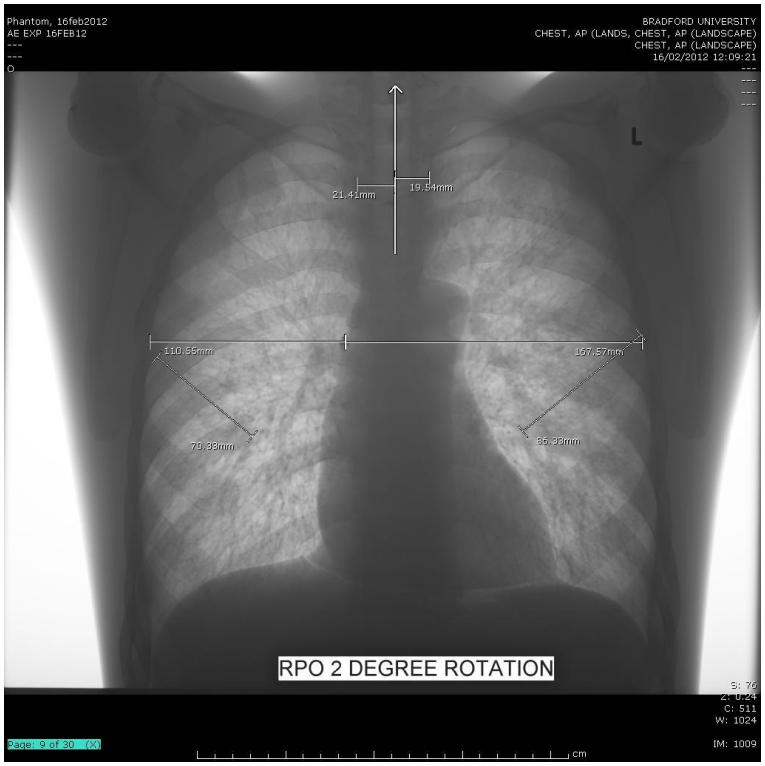
Phantom, 16feb2012
AE EXP 16FEB12
BRADFORD UNIVERSITY
CHEST, AP (LANDS, CHEST, AP (LANDSCAPE)
CHEST, AP (LANDSCAPE)
16/02/2012 12:09:21
L
21.41mm
19.84mm
110.56mm
167.57mm
79.33mm
86.38mm
RPO 2 DEGREE ROTATION
C: 511
W: 1024
IM: 1009
Page: 9 of 30 (X)
cm

Regression output of rotation measurements of clavicles and spinous process, and the log ratio of the fourth anterior rib length:

Regress lncmspr angle

```
      Source |       SS       df       MS              Number of obs =      11
-------------+------------------------------           F(  1,     9) =   76.27
       Model |  3.92361263     1  3.92361263           Prob > F      =  0.0000
    Residual |  .462994913     9  .051443879           R-squared     =  0.8945
-------------+------------------------------           Adj R-squared =  0.8827
       Total |  4.38660754    10  .438660754           Root MSE      =  .22681

------------------------------------------------------------------------------
     lncmspr |      Coef.   Std. Err.      t    P>|t|     [95% Conf. Interval]
-------------+----------------------------------------------------------------
       angle |   .1245549   .0142621     8.73   0.000     .0922917    .1568181
       _cons |  -.0621941   .1220832    -0.51   0.623    -.3383654    .2139772
------------------------------------------------------------------------------
```

Regress lncmspr angle, noconstant

```
      Source |       SS       df       MS              Number of obs =      11
-------------+------------------------------           F(  1,    10) =  237.75
       Model |  11.3249546     1  11.3249546           Prob > F      =  0.0000
    Residual |  .476346123    10  .047634612           R-squared     =  0.9596
-------------+------------------------------           Adj R-squared =  0.9556
       Total |  11.8013008    11  1.07284552           Root MSE      =  .21825

------------------------------------------------------------------------------
     lncmspr |      Coef.   Std. Err.      t    P>|t|     [95% Conf. Interval]
-------------+----------------------------------------------------------------
       angle |   .1185361   .0076877    15.42   0.000      .101407    .1356653
```

Regress bcwrat angle

```
      Source |       SS       df       MS              Number of obs =      15
-------------+------------------------------           F(  1,    13) =  326.17
       Model |  .144289232     1  .144289232           Prob > F      =  0.0000
    Residual |  .005750787    13  .000442368           R-squared     =  0.9617
-------------+------------------------------           Adj R-squared =  0.9587
       Total |  .150040019    14  .010717144           Root MSE      =  .02103

------------------------------------------------------------------------------
      bcwrat |      Coef.   Std. Err.      t    P>|t|     [95% Conf. Interval]
-------------+----------------------------------------------------------------
       angle |  -.0071078   .0003936   -18.06   0.000    -.0079581   -.0062576
       _cons |       1.488   .0054306   274.00   0.000     1.476268    1.499732
------------------------------------------------------------------------------
```

Regression output of kyphosis and lordosis measurements

Regress clavicle_apex_mean angle

```
      Source |       SS       df       MS              Number of obs =      13
-------------+------------------------------           F(  1,    11) =  499.26
       Model |  1585.24746     1  1585.24746           Prob > F      =  0.0000
    Residual |  34.9271496    11  3.17519542           R-squared     =  0.9784
-------------+------------------------------           Adj R-squared =  0.9765
       Total |  1620.17461    12  135.014551           Root MSE      =  1.7819

------------------------------------------------------------------------------
clavicle_a~n |      Coef.   Std. Err.      t    P>|t|     [95% Conf. Interval]
-------------+----------------------------------------------------------------
       angle |  -.9935181   .0444644   -22.34   0.000    -1.091384   -.8956526
       _cons |   19.28231   .4942123    39.02   0.000     18.19455    20.37006
```

Regress rib_angle_mean angle

```
    Source |       SS       df       MS              Number of obs =      13
-------------+------------------------------           F(  1,    11) =  853.19
       Model |  1961.78394     1  1961.78394           Prob > F      =  0.0000
    Residual |  25.2929878    11  2.29936253           R-squared     =  0.9873
-------------+------------------------------           Adj R-squared =  0.9861
       Total |  1987.07692    12  165.589744           Root MSE      =  1.5164

------------------------------------------------------------------------------
rib_angle_~n |      Coef.   Std. Err.      t    P>|t|     [95% Conf. Interval]
-------------+----------------------------------------------------------------
       angle |   -1.10523   .0378382   -29.21   0.000    -1.188512   -1.021949
       _cons |   56.88462   .420564    135.26   0.000     55.95896    57.81027
------------------------------------------------------------------------------
```

Regress radio_opaque_ball_mean angle

```
    Source |       SS       df       MS              Number of obs =      13
-------------+------------------------------           F(  1,    11) =  353.46
       Model |  124.411337     1  124.411337           Prob > F      =  0.0000
    Residual |  3.87178834    11  .351980758           R-squared     =  0.9698
-------------+------------------------------           Adj R-squared =  0.9671
       Total |  128.283126    12  10.6902605           Root MSE      =  .59328

------------------------------------------------------------------------------
radio_opaq~n |      Coef.   Std. Err.      t    P>|t|     [95% Conf. Interval]
-------------+----------------------------------------------------------------
       angle |  -.2783282   .0148043   -18.80   0.000    -.3109122   -.2457442
       _cons |   46.72308   .1645462   283.95   0.000     46.36091    47.08524
------------------------------------------------------------------------------
```

Appendix: 3 observer study

The image assessment template

This template to be completed by the observers to evaluate the examined images by scoring the images according to European Guidelines on the Quality Criteria for Diagnostic Radiographic Images and the included part related to chest tubes and lines. Each image will have the two algorithms applied in random order. For each image two presets algorithms will be applied 1- standard 2- invert.

- **Observer No: …….**
- **Image No: ……**
- **Algorithm No: ……..**

Image quality scoring of the chest radiograph according to the European Guidelines on Quality Criteria for Diagnostic Radiographic images.

Scoring each criterion by using ordinal scale as follows:

0	1	2	3	4	5	6	7

Extremely poor **moderate** **extremely good**

Anatomic region	**Enter score**
1- Visualization of the retrocardiac lung and the mediastinum.	☐
2- Visualization of the spine through the heart shadow.	☐
3- Reproduction of the whole rib cage above the diaphragm.	☐

4- Visually sharp reproduction of the vascular pattern in the whole lung, particularly the peripheral vessels. ☐

5- Visually sharp reproduction of the trachea and proximal bronchi. ☐

6- Visually sharp reproduction of the borders of the heart and aorta. ☐

7- Visually sharp reproduction of the diaphragm and lateral costophrenic angles.

Image details

Small round details in the lung and retrocardiac areas.

8- 0.7 mm, high contrast. ☐

9- 2 mm, low contrast. ☐

Linear and reticular details to the lung periphery.

10- 0.3 mm, high contrast. ☐

11- 2 mm, low contrast. ☐

Rate the image quality for identification of tubes/line position:

12- **Central venous catheter**:

0	1	2	3	4	5	6	7

Extremely poor **moderate** **extremely good**

13- **Swan-Ganz catheter:**

0	1	2	3	4	5	6	7

Extremely poor **moderate** **extremely good**

14-**Thoracostomy tube**:

0	1	2	3	4	5	6	7

Extremely poor **moderate** **extremely good**

15- **Nasogastric tube:**

0	1	2	3	4	5	6	7

Extremely poor **moderate** **extremely good**

16- **Endotracheal tube:**

0	1	2	3	4	5	6	7

Extremely poor **moderate** **extremely good**

4- Is the tube/line correctly positioned?

17- Central venous catheter:

0	**1**	**2**	**3**
Definitely not	**Probably not**	**Probably is**	**Definitely is**

18- Swan-Ganz catheter:

0	**1**	**2**	**3**
Definitely not	**Probably not**	**Probably is**	**Definitely is**

19- Thoracostomy tube:

0	**1**	**2**	**3**
Definitely not	**Probably not**	**Probably is**	**Definitely is**

20- Nasogastric tube:

0	1	2	3
Definitely not	Probably not	Probably is	Definitely is

21- Endotracheal tube:

0	1	2	3
Definitely not	Probably not	Probably is	Definitely is

Repeated measures regression mixed model:

```
. xi: xtreg q1 i.algorithm, i(image)
i.algorithm      _Ialgorithm_1-2     (naturally coded; _Ialgorithm_1 omitted)

Random-effects GLS regression                Number of obs     =        98
Group variable: image                        Number of groups  =        17

R-sq:  within  = 0.0000                      Obs per group: min =         4
       between = 0.0000                                     avg =       5.8
       overall = 0.0000                                     max =         6

                                             Wald chi2(1)      =      0.00
corr(u_i, X)   = 0 (assumed)                 Prob > chi2       =    1.0000

------------------------------------------------------------------------------
          q1 |      Coef.   Std. Err.      z    P>|z|     [95% Conf. Interval]
-------------+----------------------------------------------------------------
_Ialgorithm_2 |  -8.74e-17   .1521056    -0.00   1.000    -.2981215    .2981215
       _cons |   1.071078   .3359264     3.19   0.001     .4126745    1.729482
-------------+----------------------------------------------------------------
     sigma_u |  1.3113538
     sigma_e |  .75277265
         rho |  .75214851   (fraction of variance due to u_i)
------------------------------------------------------------------------------

. graph box q2, over(algorithm) over(image)
```

```
. xi: xtreg q2 i.algorithm, i(image)
i.algorithm      _Ialgorithm_1-2     (naturally coded; _Ialgorithm_1 omitted)

Random-effects GLS regression                Number of obs      =       102
Group variable: image                        Number of groups   =        17

R-sq:  within  = 0.0000                      Obs per group: min =         6
       between = 0.0000                                     avg =       6.0
       overall = 0.0016                                     max =         6

                                             Wald chi2(1)       =      0.33
corr(u_i, X)   = 0 (assumed)                 Prob > chi2        =    0.5631

------------------------------------------------------------------------------
          q2 |      Coef.   Std. Err.      z    P>|z|     [95% Conf. Interval]
-------------+----------------------------------------------------------------
_Ialgorithm_2 |   .1176471   .2034335     0.58   0.563    -.2810752    .5163694
       _cons |   1.901961   .3049111     6.24   0.000     1.304346    2.499576
-------------+----------------------------------------------------------------
     sigma_u |  1.1084805
     sigma_e |  1.0272887
         rho |  .53796037   (fraction of variance due to u_i)
------------------------------------------------------------------------------

. graph box q3, over(algorithm) over(image)

. xi: xtreg q3 i.algorithm, i(image)
i.algorithm      _Ialgorithm_1-2     (naturally coded; _Ialgorithm_1 omitted)

Random-effects GLS regression                Number of obs      =       101
Group variable: image                        Number of groups   =        17

R-sq:  within  = 0.0180                      Obs per group: min =         5
       between = 0.0091                                     avg =       5.9
       overall = 0.0139                                     max =         6

                                             Wald chi2(1)       =      1.56
corr(u_i, X)   = 0 (assumed)                 Prob > chi2        =    0.2110

------------------------------------------------------------------------------
          q3 |      Coef.   Std. Err.      z    P>|z|     [95% Conf. Interval]
-------------+----------------------------------------------------------------
_Ialgorithm_2 |   -.316112   .2527137    -1.25   0.211    -.8114217    .1791977
       _cons |   4.218073   .2147222    19.64   0.000     3.797225    4.638921
```

```
-------------+----------------------------------------------------------------
    sigma_u |   .4869092
    sigma_e |  1.2745111
        rho |  .12736277   (fraction of variance due to u_i)
------------------------------------------------------------------------------

. graph box q4, over(algorithm) over(image)

. xi: xtreg q4 i.algorithm, i(image)
i.algorithm      _Ialgorithm_1-2     (naturally coded; _Ialgorithm_1 omitted)

Random-effects GLS regression                   Number of obs     =       100
Group variable: image                           Number of groups  =        17

R-sq:  within  = 0.0000                         Obs per group: min =         4
       between = 0.0000                                        avg =       5.9
       overall = 0.0071                                        max =         6

                                                Wald chi2(1)      =      0.80
corr(u_i, X)   = 0 (assumed)                    Prob > chi2       =    0.3707

------------------------------------------------------------------------------
          q4 |      Coef.   Std. Err.      z    P>|z|     [95% Conf. Interval]
-------------+----------------------------------------------------------------
_Ialgorithm_2 |       -.24   .2681178    -0.90   0.371    -.7655013    .2855013
       _cons |   3.910253   .2281434    17.14   0.000      3.4631    4.357406
-------------+----------------------------------------------------------------
    sigma_u |  .52315563
    sigma_e |  1.3429733
        rho |  .13175559   (fraction of variance due to u_i)
------------------------------------------------------------------------------

. graph box q5, over(algorithm) over(image)

. xi: xtreg q5 i.algorithm, i(image)
i.algorithm      _Ialgorithm_1-2     (naturally coded; _Ialgorithm_1 omitted)

Random-effects GLS regression                   Number of obs     =       102
Group variable: image                           Number of groups  =        17

R-sq:  within  = 0.0000                         Obs per group: min =         6
       between = 0.0000                                        avg =       6.0
       overall = 0.1593                                        max =         6
```

```
                                Wald chi2(1)      =     33.11
corr(u_i, X)   = 0 (assumed)                Prob > chi2       =    0.0000

------------------------------------------------------------------------------
        q5 |      Coef.   Std. Err.      z    P>|z|     [95% Conf. Interval]
-------------+----------------------------------------------------------------
_Ialgorithm_2 |  -1.333333    .231707    -5.75   0.000    -1.787471   -.8791959
      _cons |   2.784314   .2992635     9.30   0.000     2.197768    3.370859
-------------+----------------------------------------------------------------
     sigma_u |  1.0325441
     sigma_e |  1.1700631
         rho |  .43780779   (fraction of variance due to u_i)
------------------------------------------------------------------------------

. graph box q6, over(algorithm) over(image)

. xi: xtreg q6 i.algorithm, i(image)
i.algorithm       _Ialgorithm_1-2     (naturally coded; _Ialgorithm_1 omitted)

Random-effects GLS regression                Number of obs      =        99
Group variable: image                        Number of groups   =        17

R-sq:  within  = 0.0196                      Obs per group: min =         4
       between = 0.0052                                     avg =       5.8
       overall = 0.0100                                     max =         6

                                Wald chi2(1)      =      1.66
corr(u_i, X)   = 0 (assumed)                Prob > chi2       =    0.1982

------------------------------------------------------------------------------
        q6 |      Coef.   Std. Err.      z    P>|z|     [95% Conf. Interval]
-------------+----------------------------------------------------------------
_Ialgorithm_2 |  -.3372326   .2621154    -1.29   0.198    -.8509693    .1765041
      _cons |   3.212502   .3502828     9.17   0.000      2.52596    3.899044
-------------+----------------------------------------------------------------
     sigma_u |  1.2351721
     sigma_e |  1.3111312
         rho |  .47019538   (fraction of variance due to u_i)
------------------------------------------------------------------------------

. graph box q7, over(algorithm) over(image)

. xi: xtreg q7 i.algorithm, i(image)
i.algorithm       _Ialgorithm_1-2     (naturally coded; _Ialgorithm_1 omitted)
```

```
Random-effects GLS regression                   Number of obs     =        97
Group variable: image                           Number of groups  =        17

R-sq:  within  = 0.0095                         Obs per group: min =         4
       between = 0.0145                                        avg =       5.7
       overall = 0.0019                                        max =         6

                                                Wald chi2(1)      =      0.75
corr(u_i, X)   = 0 (assumed)                    Prob > chi2       =    0.3855

------------------------------------------------------------------------------
          q7 |      Coef.   Std. Err.      z    P>|z|     [95% Conf. Interval]
-------------+----------------------------------------------------------------
_Ialgorithm_2 |    -.18065   .2081529    -0.87   0.385    -.5886221    .227322
        _cons |   3.112836   .4281823     7.27   0.000     2.273614    3.952058
-------------+----------------------------------------------------------------
     sigma_u |  1.6622698
     sigma_e |  1.0280866
         rho |  .72331583   (fraction of variance due to u_i)
------------------------------------------------------------------------------

. graph box q8, over(algorithm) over(image)

. xi: xtreg q8 i.algorithm, i(image)
i.algorithm       _Ialgorithm_1-2     (naturally coded; _Ialgorithm_1 omitted)

Random-effects GLS regression                   Number of obs     =        66
Group variable: image                           Number of groups  =        17

R-sq:  within  = 0.0271                         Obs per group: min =         2
       between = 0.0073                                        avg =       3.9
       overall = 0.0169                                        max =         6

                                                Wald chi2(1)      =      1.36
corr(u_i, X)   = 0 (assumed)                    Prob > chi2       =    0.2438

------------------------------------------------------------------------------
          q8 |      Coef.   Std. Err.      z    P>|z|     [95% Conf. Interval]
-------------+----------------------------------------------------------------
_Ialgorithm_2 |  -.5069377   .4349202    -1.17   0.244    -1.359366    .3454903
        _cons |   1.387837   .3748999     3.70   0.000     .6530463    2.122627
-------------+----------------------------------------------------------------
     sigma_u |  .85507325
```

```
    sigma_e |  1.7518839
        rho |  .19239543   (fraction of variance due to u_i)
------------------------------------------------------------------------------

. graph box q9, over(algorithm) over(image)

. xi: xtreg q9 i.algorithm, i(image)
i.algorithm      _Ialgorithm_1-2     (naturally coded; _Ialgorithm_1 omitted)

Random-effects GLS regression                Number of obs      =        62
Group variable: image                        Number of groups   =        17

R-sq:  within  = 0.0305                      Obs per group: min =         2
       between = 0.0829                                     avg =       3.6
       overall = 0.0265                                     max =         6

                                             Wald chi2(1)       =      1.63
corr(u_i, X)   = 0 (assumed)                 Prob > chi2        =    0.2013

------------------------------------------------------------------------------
          q9 |      Coef.   Std. Err.      z    P>|z|     [95% Conf. Interval]
-------------+----------------------------------------------------------------
_Ialgorithm_2 |  -.5270833   .4125062    -1.28   0.201    -1.335581    .281414
       _cons |    1.09375   .2869428     3.81   0.000     .5313525    1.656147
-------------+----------------------------------------------------------------
     sigma_u |         0
     sigma_e |  1.6542519
         rho |         0   (fraction of variance due to u_i)
------------------------------------------------------------------------------

. graph box q10, over(algorithm) over(image)

. xi: xtreg q10 i.algorithm, i(image)
i.algorithm      _Ialgorithm_1-2     (naturally coded; _Ialgorithm_1 omitted)

Random-effects GLS regression                Number of obs      =        60
Group variable: image                        Number of groups   =        17

R-sq:  within  = 0.0171                      Obs per group: min =         2
       between = 0.0230                                     avg =       3.5
       overall = 0.0121                                     max =         6

                                             Wald chi2(1)       =      0.81
corr(u_i, X)   = 0 (assumed)                 Prob > chi2        =    0.3692
```

```
------------------------------------------------------------------------------
       q10 |      Coef.   Std. Err.      z    P>|z|     [95% Conf. Interval]
-------------+----------------------------------------------------------------
_Ialgorithm_2 |   -.389346   .4335594    -0.90   0.369    -1.239107    .4604147
      _cons |   2.206044   .3570447     6.18   0.000      1.50625    2.905839
-------------+----------------------------------------------------------------
    sigma_u |  .73537061
    sigma_e |  1.6717352
        rho |  .16212713   (fraction of variance due to u_i)
------------------------------------------------------------------------------

. graph box q11, over(algorithm) over(image)

. xi: xtreg q11 i.algorithm, i(image)
i.algorithm       _Ialgorithm_1-2     (naturally coded; _Ialgorithm_1 omitted)

Random-effects GLS regression                   Number of obs      =        60
Group variable: image                           Number of groups   =        17

R-sq:  within  = 0.0016                         Obs per group: min =         2
       between = 0.0369                                        avg =       3.5
       overall = 0.0020                                        max =         6

                                                Wald chi2(1)       =      0.12
corr(u_i, X)   = 0 (assumed)                    Prob > chi2        =    0.7327

------------------------------------------------------------------------------
       q11 |      Coef.   Std. Err.      z    P>|z|     [95% Conf. Interval]
-------------+----------------------------------------------------------------
_Ialgorithm_2 |  -.1666667   .4880566    -0.34   0.733    -1.12324    .7899067
      _cons |   1.933333   .3451081     5.60   0.000     1.256934    2.609733
-------------+----------------------------------------------------------------
    sigma_u |         0
    sigma_e |  1.9993868
        rho |         0   (fraction of variance due to u_i)
------------------------------------------------------------------------------

. graph box q12, over(algorithm) over(image)

. xi: xtreg q12 i.algorithm, i(image)
i.algorithm       _Ialgorithm_1-2     (naturally coded; _Ialgorithm_1 omitted)

Random-effects GLS regression                   Number of obs      =        77
```

```
Group variable: image                     Number of groups   =       13

R-sq:  within  = 0.0026                   Obs per group: min =        5
       between = 0.0131                                  avg =      5.9
       overall = 0.0013                                  max =        6

                                          Wald chi2(1)      =     0.17
corr(u_i, X)   = 0 (assumed)              Prob > chi2       =   0.6808

------------------------------------------------------------------------------
         q12 |      Coef.   Std. Err.      z    P>|z|     [95% Conf. Interval]
-------------+----------------------------------------------------------------
_Ialgorithm_2 |   .0582861    .141696     0.41   0.681    -.2194328    .3360051
       _cons |   5.435897   .2103008    25.85   0.000     5.023715    5.848079
-------------+----------------------------------------------------------------
     sigma_u |  .67191182
     sigma_e |  .62450377
         rho |  .53651972   (fraction of variance due to u_i)
------------------------------------------------------------------------------

. xi: xtreg q14 i.algorithm, i(image)
i.algorithm       _Ialgorithm_1-2     (naturally coded; _Ialgorithm_1 omitted)

Random-effects GLS regression             Number of obs      =       16
Group variable: image                     Number of groups   =        4

R-sq:  within  = 0.0000                   Obs per group: min =        2
       between = 0.0000                                  avg =      4.0
       overall = 0.0000                                  max =        6

                                          Wald chi2(1)      =     0.00
corr(u_i, X)   = 0 (assumed)              Prob > chi2       =   1.0000

------------------------------------------------------------------------------
         q14_ |      Coef.   Std. Err.      z    P>|z|     [95% Conf. Interval]
-------------+----------------------------------------------------------------
_Ialgorithm_2 |   5.45e-17   .4078038     0.00   1.000    -.7992807    .7992807
       _cons |   4.616053   1.081839     4.27   0.000     2.495687    6.736419
-------------+----------------------------------------------------------------
     sigma_u |  2.0749833
     sigma_e |  .81649658
         rho |  .86592179   (fraction of variance due to u_i)
------------------------------------------------------------------------------
```

```
. xi: xtreg q14 i.algorithm, i(image)
i.algorithm      _Ialgorithm_1-2     (naturally coded; _Ialgorithm_1 omitted)

Random-effects GLS regression                Number of obs     =        16
Group variable: image                        Number of groups  =         4

R-sq:  within  = 0.0000                      Obs per group: min =         2
       between = 0.0000                                     avg =       4.0
       overall = 0.0000                                     max =         6

                                             Wald chi2(1)      =      0.00
corr(u_i, X)   = 0 (assumed)                 Prob > chi2       =    1.0000

------------------------------------------------------------------------------
       q14_ |      Coef.   Std. Err.      z    P>|z|     [95% Conf. Interval]
------------+-----------------------------------------------------------------
_Ialgorithm_2 |         0   .4078038     0.00   1.000    -.7992807    .7992807
       _cons |   4.616053   1.081839     4.27   0.000     2.495687    6.736419
------------+-----------------------------------------------------------------
     sigma_u |  2.0749833
     sigma_e |  .81649658
         rho |  .86592179   (fraction of variance due to u_i)
------------------------------------------------------------------------------

. xi: xtreg q15 i.algorithm, i(image)
i.algorithm      _Ialgorithm_1-2     (naturally coded; _Ialgorithm_1 omitted)

Random-effects GLS regression                Number of obs     =        89
Group variable: image                        Number of groups  =        16

R-sq:  within  = 0.0156                      Obs per group: min =         2
       between = 0.0539                                     avg =       5.6
       overall = 0.0049                                     max =         6

                                             Wald chi2(1)      =      1.11
corr(u_i, X)   = 0 (assumed)                 Prob > chi2       =    0.2919

------------------------------------------------------------------------------
       q15_ |      Coef.   Std. Err.      z    P>|z|     [95% Conf. Interval]
------------+-----------------------------------------------------------------
_Ialgorithm_2 |   .235181   .2231502     1.05   0.292    -.2021853    .6725474
       _cons |   4.354826   .3350225    13.00   0.000     3.698194    5.011458
------------+-----------------------------------------------------------------
     sigma_u |  1.1821468
```

```
    sigma_e |  1.0542113
        rho |  .55702049   (fraction of variance due to u_i)
------------------------------------------------------------------------------

. xi: xtreg q16 i.algorithm, i(image)
i.algorithm      _Ialgorithm_1-2     (naturally coded; _Ialgorithm_1 omitted)

Random-effects GLS regression                   Number of obs     =        64
Group variable: image                           Number of groups  =        13

R-sq:  within  = 0.0299                         Obs per group: min =         1
       between = 0.0302                                        avg =       4.9
       overall = 0.0183                                        max =         6

                                                Wald chi2(1)      =      1.73
corr(u_i, X)   = 0 (assumed)                    Prob > chi2       =    0.1884

------------------------------------------------------------------------------
       q16_ |      Coef.   Std. Err.      z    P>|z|     [95% Conf. Interval]
------------+-----------------------------------------------------------------
_Ialgorithm_2 |  -.3558818   .2705947    -1.32   0.188    -.8862376    .1744741
      _cons |   4.652542   .3694873    12.59   0.000     3.928361    5.376724
------------+-----------------------------------------------------------------
    sigma_u |  1.1298017
    sigma_e |  1.0874371
        rho |  .51909992   (fraction of variance due to u_i)
------------------------------------------------------------------------------
```

Kappa statistics

```
. kap q1_1 q1_2, wgt(w)

Ratings weighted by:
  1.0000  0.8333  0.6667  0.5000  0.3333  0.1667  0.0000
  0.8333  1.0000  0.8333  0.6667  0.5000  0.3333  0.1667
  0.6667  0.8333  1.0000  0.8333  0.6667  0.5000  0.3333
  0.5000  0.6667  0.8333  1.0000  0.8333  0.6667  0.5000
  0.3333  0.5000  0.6667  0.8333  1.0000  0.8333  0.6667
  0.1667  0.3333  0.5000  0.6667  0.8333  1.0000  0.8333
  0.0000  0.1667  0.3333  0.5000  0.6667  0.8333  1.0000

           Expected
Agreement  Agreement    Kappa  Std. Err.       Z    Prob>Z
------------------------------------------------------------------
  93.14%     80.57%    0.6469     0.1053      6.14     0.0000
```

```
. kap q1_1 q1_3, wgt(w)

Ratings weighted by:
  1.0000  0.8333  0.6667  0.5000  0.3333  0.1667  0.0000
  0.8333  1.0000  0.8333  0.6667  0.5000  0.3333  0.1667
  0.6667  0.8333  1.0000  0.8333  0.6667  0.5000  0.3333
  0.5000  0.6667  0.8333  1.0000  0.8333  0.6667  0.5000
  0.3333  0.5000  0.6667  0.8333  1.0000  0.8333  0.6667
  0.1667  0.3333  0.5000  0.6667  0.8333  1.0000  0.8333
  0.0000  0.1667  0.3333  0.5000  0.6667  0.8333  1.0000

         Expected
Agreement   Agreement    Kappa   Std. Err.      Z    Prob>Z
------------------------------------------------------------------
 85.00%     75.33%    0.3919    0.1003     3.91     0.0000

. kap q1_2 q1_3, wgt(w)

Ratings weighted by:
  1.0000  0.8333  0.6667  0.5000  0.3333  0.1667  0.0000
  0.8333  1.0000  0.8333  0.6667  0.5000  0.3333  0.1667
  0.6667  0.8333  1.0000  0.8333  0.6667  0.5000  0.3333
  0.5000  0.6667  0.8333  1.0000  0.8333  0.6667  0.5000
  0.3333  0.5000  0.6667  0.8333  1.0000  0.8333  0.6667
  0.1667  0.3333  0.5000  0.6667  0.8333  1.0000  0.8333
  0.0000  0.1667  0.3333  0.5000  0.6667  0.8333  1.0000

         Expected
Agreement   Agreement    Kappa   Std. Err.      Z    Prob>Z
------------------------------------------------------------------
 83.89%     72.63%    0.4114    0.1167     3.53     0.0002

. kap q2_1 q2_2, wgt(w)

Ratings weighted by:
  1.0000  0.8000  0.6000  0.4000  0.2000  0.0000
  0.8000  1.0000  0.8000  0.6000  0.4000  0.2000
  0.6000  0.8000  1.0000  0.8000  0.6000  0.4000
  0.4000  0.6000  0.8000  1.0000  0.8000  0.6000
  0.2000  0.4000  0.6000  0.8000  1.0000  0.8000
  0.0000  0.2000  0.4000  0.6000  0.8000  1.0000

         Expected
```

```
Agreement   Agreement    Kappa   Std. Err.      Z    Prob>Z
------------------------------------------------------------------
  89.41%     77.75%    0.5241    0.0991     5.29     0.0000
```

```
. kap q2_1 q2_3, wgt(w)

Ratings weighted by:
  1.0000  0.8333  0.6667  0.5000  0.3333  0.1667  0.0000
  0.8333  1.0000  0.8333  0.6667  0.5000  0.3333  0.1667
  0.6667  0.8333  1.0000  0.8333  0.6667  0.5000  0.3333
  0.5000  0.6667  0.8333  1.0000  0.8333  0.6667  0.5000
  0.3333  0.5000  0.6667  0.8333  1.0000  0.8333  0.6667
  0.1667  0.3333  0.5000  0.6667  0.8333  1.0000  0.8333
  0.0000  0.1667  0.3333  0.5000  0.6667  0.8333  1.0000

           Expected
Agreement   Agreement    Kappa   Std. Err.      Z    Prob>Z
------------------------------------------------------------------
  75.00%     68.17%    0.2147    0.0674     3.19     0.0007
```

```
. kap q2_2 q2_3, wgt(w)

Ratings weighted by:
  1.0000  0.8333  0.6667  0.5000  0.3333  0.1667  0.0000
  0.8333  1.0000  0.8333  0.6667  0.5000  0.3333  0.1667
  0.6667  0.8333  1.0000  0.8333  0.6667  0.5000  0.3333
  0.5000  0.6667  0.8333  1.0000  0.8333  0.6667  0.5000
  0.3333  0.5000  0.6667  0.8333  1.0000  0.8333  0.6667
  0.1667  0.3333  0.5000  0.6667  0.8333  1.0000  0.8333
  0.0000  0.1667  0.3333  0.5000  0.6667  0.8333  1.0000

           Expected
Agreement   Agreement    Kappa   Std. Err.      Z    Prob>Z
------------------------------------------------------------------
  80.88%     69.29%    0.3775    0.0946     3.99     0.0000
```

```
. kap q3_1 q3_2, wgt(w)

Ratings weighted by:
  1.0000  0.8000  0.6000  0.4000  0.2000  0.0000
  0.8000  1.0000  0.8000  0.6000  0.4000  0.2000
  0.6000  0.8000  1.0000  0.8000  0.6000  0.4000
  0.4000  0.6000  0.8000  1.0000  0.8000  0.6000
  0.2000  0.4000  0.6000  0.8000  1.0000  0.8000
```

```
  0.0000  0.2000  0.4000  0.6000  0.8000  1.0000

        Expected
Agreement   Agreement    Kappa   Std. Err.      Z    Prob>Z
------------------------------------------------------------------
  75.15%     72.29%    0.1034    0.0916     1.13    0.1296

. kap q3_1 q3_3, wgt(w)

Ratings weighted by:
  1.0000  0.8333  0.6667  0.5000  0.3333  0.1667  0.0000
  0.8333  1.0000  0.8333  0.6667  0.5000  0.3333  0.1667
  0.6667  0.8333  1.0000  0.8333  0.6667  0.5000  0.3333
  0.5000  0.6667  0.8333  1.0000  0.8333  0.6667  0.5000
  0.3333  0.5000  0.6667  0.8333  1.0000  0.8333  0.6667
  0.1667  0.3333  0.5000  0.6667  0.8333  1.0000  0.8333
  0.0000  0.1667  0.3333  0.5000  0.6667  0.8333  1.0000

        Expected
Agreement   Agreement    Kappa   Std. Err.      Z    Prob>Z
------------------------------------------------------------------
  79.90%     75.14%    0.1914    0.0703     2.72    0.0032

. kap q3_2 q3_3, wgt(w)

Ratings weighted by:
  1.0000  0.8333  0.6667  0.5000  0.3333  0.1667  0.0000
  0.8333  1.0000  0.8333  0.6667  0.5000  0.3333  0.1667
  0.6667  0.8333  1.0000  0.8333  0.6667  0.5000  0.3333
  0.5000  0.6667  0.8333  1.0000  0.8333  0.6667  0.5000
  0.3333  0.5000  0.6667  0.8333  1.0000  0.8333  0.6667
  0.1667  0.3333  0.5000  0.6667  0.8333  1.0000  0.8333
  0.0000  0.1667  0.3333  0.5000  0.6667  0.8333  1.0000

        Expected
Agreement   Agreement    Kappa   Std. Err.      Z    Prob>Z
------------------------------------------------------------------
  67.68%     66.73%    0.0285    0.0628     0.45    0.3248

. kap q4_1 q4_2, wgt(w)

Ratings weighted by:
  1.0000  0.8333  0.6667  0.5000  0.3333  0.1667  0.0000
  0.8333  1.0000  0.8333  0.6667  0.5000  0.3333  0.1667
```

```
  0.6667  0.8333  1.0000  0.8333  0.6667  0.5000  0.3333
  0.5000  0.6667  0.8333  1.0000  0.8333  0.6667  0.5000
  0.3333  0.5000  0.6667  0.8333  1.0000  0.8333  0.6667
  0.1667  0.3333  0.5000  0.6667  0.8333  1.0000  0.8333
  0.0000  0.1667  0.3333  0.5000  0.6667  0.8333  1.0000

        Expected
Agreement   Agreement    Kappa   Std. Err.      Z    Prob>Z
------------------------------------------------------------------
 84.31%     77.71%    0.2962    0.0948     3.13     0.0009

. kap q4_1 q4_3, wgt(w)

Ratings weighted by:
  1.0000  0.8333  0.6667  0.5000  0.3333  0.1667  0.0000
  0.8333  1.0000  0.8333  0.6667  0.5000  0.3333  0.1667
  0.6667  0.8333  1.0000  0.8333  0.6667  0.5000  0.3333
  0.5000  0.6667  0.8333  1.0000  0.8333  0.6667  0.5000
  0.3333  0.5000  0.6667  0.8333  1.0000  0.8333  0.6667
  0.1667  0.3333  0.5000  0.6667  0.8333  1.0000  0.8333
  0.0000  0.1667  0.3333  0.5000  0.6667  0.8333  1.0000

        Expected
Agreement   Agreement    Kappa   Std. Err.      Z    Prob>Z
------------------------------------------------------------------
 72.92%     70.90%    0.0694    0.0476     1.46     0.0725

. kap q4_2 q4_3, wgt(w)

Ratings weighted by:
  1.0000  0.8571  0.7143  0.5714  0.4286  0.2857  0.1429  0.0000
  0.8571  1.0000  0.8571  0.7143  0.5714  0.4286  0.2857  0.1429
  0.7143  0.8571  1.0000  0.8571  0.7143  0.5714  0.4286  0.2857
  0.5714  0.7143  0.8571  1.0000  0.8571  0.7143  0.5714  0.4286
  0.4286  0.5714  0.7143  0.8571  1.0000  0.8571  0.7143  0.5714
  0.2857  0.4286  0.5714  0.7143  0.8571  1.0000  0.8571  0.7143
  0.1429  0.2857  0.4286  0.5714  0.7143  0.8571  1.0000  0.8571
  0.0000  0.1429  0.2857  0.4286  0.5714  0.7143  0.8571  1.0000

        Expected
Agreement   Agreement    Kappa   Std. Err.      Z    Prob>Z
------------------------------------------------------------------
 69.64%     68.39%    0.0397    0.0383     1.04     0.1501
```

. kap q5_1 q5_2, wgt(w)

Ratings weighted by:

1.0000	0.8333	0.6667	0.5000	0.3333	0.1667	0.0000
0.8333	1.0000	0.8333	0.6667	0.5000	0.3333	0.1667
0.6667	0.8333	1.0000	0.8333	0.6667	0.5000	0.3333
0.5000	0.6667	0.8333	1.0000	0.8333	0.6667	0.5000
0.3333	0.5000	0.6667	0.8333	1.0000	0.8333	0.6667
0.1667	0.3333	0.5000	0.6667	0.8333	1.0000	0.8333
0.0000	0.1667	0.3333	0.5000	0.6667	0.8333	1.0000

Agreement	Expected Agreement	Kappa	Std. Err.	Z	Prob>Z
78.43%	71.08%	0.2542	0.0860	2.96	0.0016

. kap q5_1 q5_3, wgt(w)

Ratings weighted by:

1.0000	0.8333	0.6667	0.5000	0.3333	0.1667	0.0000
0.8333	1.0000	0.8333	0.6667	0.5000	0.3333	0.1667
0.6667	0.8333	1.0000	0.8333	0.6667	0.5000	0.3333
0.5000	0.6667	0.8333	1.0000	0.8333	0.6667	0.5000
0.3333	0.5000	0.6667	0.8333	1.0000	0.8333	0.6667
0.1667	0.3333	0.5000	0.6667	0.8333	1.0000	0.8333
0.0000	0.1667	0.3333	0.5000	0.6667	0.8333	1.0000

Agreement	Expected Agreement	Kappa	Std. Err.	Z	Prob>Z
72.55%	65.48%	0.2047	0.0810	2.53	0.0058

. kap q5_2 q5_3, wgt(w)

Ratings weighted by:

1.0000	0.8333	0.6667	0.5000	0.3333	0.1667	0.0000
0.8333	1.0000	0.8333	0.6667	0.5000	0.3333	0.1667
0.6667	0.8333	1.0000	0.8333	0.6667	0.5000	0.3333
0.5000	0.6667	0.8333	1.0000	0.8333	0.6667	0.5000
0.3333	0.5000	0.6667	0.8333	1.0000	0.8333	0.6667
0.1667	0.3333	0.5000	0.6667	0.8333	1.0000	0.8333
0.0000	0.1667	0.3333	0.5000	0.6667	0.8333	1.0000

Expected

```
Agreement   Agreement    Kappa   Std. Err.      Z    Prob>Z
------------------------------------------------------------------
  80.39%     67.16%    0.4030    0.1048     3.85     0.0001

. kap q6_1 q6_2, wgt(w)

Ratings weighted by:
  1.0000  0.8333  0.6667  0.5000  0.3333  0.1667  0.0000
  0.8333  1.0000  0.8333  0.6667  0.5000  0.3333  0.1667
  0.6667  0.8333  1.0000  0.8333  0.6667  0.5000  0.3333
  0.5000  0.6667  0.8333  1.0000  0.8333  0.6667  0.5000
  0.3333  0.5000  0.6667  0.8333  1.0000  0.8333  0.6667
  0.1667  0.3333  0.5000  0.6667  0.8333  1.0000  0.8333
  0.0000  0.1667  0.3333  0.5000  0.6667  0.8333  1.0000

          Expected
Agreement   Agreement    Kappa   Std. Err.      Z    Prob>Z
------------------------------------------------------------------
  86.36%     74.18%    0.4718    0.0980     4.81     0.0000

. kap q6_1 q6_3, wgt(w)

Ratings weighted by:
  1.0000  0.8571  0.7143  0.5714  0.4286  0.2857  0.1429  0.0000
  0.8571  1.0000  0.8571  0.7143  0.5714  0.4286  0.2857  0.1429
  0.7143  0.8571  1.0000  0.8571  0.7143  0.5714  0.4286  0.2857
  0.5714  0.7143  0.8571  1.0000  0.8571  0.7143  0.5714  0.4286
  0.4286  0.5714  0.7143  0.8571  1.0000  0.8571  0.7143  0.5714
  0.2857  0.4286  0.5714  0.7143  0.8571  1.0000  0.8571  0.7143
  0.1429  0.2857  0.4286  0.5714  0.7143  0.8571  1.0000  0.8571
  0.0000  0.1429  0.2857  0.4286  0.5714  0.7143  0.8571  1.0000

          Expected
Agreement   Agreement    Kappa   Std. Err.      Z    Prob>Z
------------------------------------------------------------------
  70.98%     68.50%    0.0788    0.0563     1.40     0.0808

. kap q6_2 q6_3, wgt(w)

Ratings weighted by:
  1.0000  0.8571  0.7143  0.5714  0.4286  0.2857  0.1429  0.0000
  0.8571  1.0000  0.8571  0.7143  0.5714  0.4286  0.2857  0.1429
  0.7143  0.8571  1.0000  0.8571  0.7143  0.5714  0.4286  0.2857
  0.5714  0.7143  0.8571  1.0000  0.8571  0.7143  0.5714  0.4286
```

```
  0.4286  0.5714  0.7143  0.8571  1.0000  0.8571  0.7143  0.5714
  0.2857  0.4286  0.5714  0.7143  0.8571  1.0000  0.8571  0.7143
  0.1429  0.2857  0.4286  0.5714  0.7143  0.8571  1.0000  0.8571
  0.0000  0.1429  0.2857  0.4286  0.5714  0.7143  0.8571  1.0000

         Expected
Agreement   Agreement    Kappa   Std. Err.      Z    Prob>Z
------------------------------------------------------------------
 73.73%     68.05%    0.1778    0.0799     2.22     0.0131

. kap q7_1 q7_2, wgt(w)

Ratings weighted by:
  1.0000  0.8333  0.6667  0.5000  0.3333  0.1667  0.0000
  0.8333  1.0000  0.8333  0.6667  0.5000  0.3333  0.1667
  0.6667  0.8333  1.0000  0.8333  0.6667  0.5000  0.3333
  0.5000  0.6667  0.8333  1.0000  0.8333  0.6667  0.5000
  0.3333  0.5000  0.6667  0.8333  1.0000  0.8333  0.6667
  0.1667  0.3333  0.5000  0.6667  0.8333  1.0000  0.8333
  0.0000  0.1667  0.3333  0.5000  0.6667  0.8333  1.0000

         Expected
Agreement   Agreement    Kappa   Std. Err.      Z    Prob>Z
------------------------------------------------------------------
 79.41%     67.39%    0.3687    0.0977     3.77     0.0001

. kap q7_1 q7_3, wgt(w)

Ratings weighted by:
  1.0000  0.8571  0.7143  0.5714  0.4286  0.2857  0.1429  0.0000
  0.8571  1.0000  0.8571  0.7143  0.5714  0.4286  0.2857  0.1429
  0.7143  0.8571  1.0000  0.8571  0.7143  0.5714  0.4286  0.2857
  0.5714  0.7143  0.8571  1.0000  0.8571  0.7143  0.5714  0.4286
  0.4286  0.5714  0.7143  0.8571  1.0000  0.8571  0.7143  0.5714
  0.2857  0.4286  0.5714  0.7143  0.8571  1.0000  0.8571  0.7143
  0.1429  0.2857  0.4286  0.5714  0.7143  0.8571  1.0000  0.8571
  0.0000  0.1429  0.2857  0.4286  0.5714  0.7143  0.8571  1.0000

         Expected
Agreement   Agreement    Kappa   Std. Err.      Z    Prob>Z
------------------------------------------------------------------
 80.30%     67.76%    0.3888    0.0979     3.97     0.0000

. kap q7_2 q7_3, wgt(w)
```

Ratings weighted by:

1.0000	0.8571	0.7143	0.5714	0.4286	0.2857	0.1429	0.0000
0.8571	1.0000	0.8571	0.7143	0.5714	0.4286	0.2857	0.1429
0.7143	0.8571	1.0000	0.8571	0.7143	0.5714	0.4286	0.2857
0.5714	0.7143	0.8571	1.0000	0.8571	0.7143	0.5714	0.4286
0.4286	0.5714	0.7143	0.8571	1.0000	0.8571	0.7143	0.5714
0.2857	0.4286	0.5714	0.7143	0.8571	1.0000	0.8571	0.7143
0.1429	0.2857	0.4286	0.5714	0.7143	0.8571	1.0000	0.8571
0.0000	0.1429	0.2857	0.4286	0.5714	0.7143	0.8571	1.0000

Agreement	Expected Agreement	Kappa	Std. Err.	Z	Prob>Z
85.22%	65.35%	0.5735	0.1204	4.76	0.0000

. kap q8_1 q8_2, wgt(w)

Ratings weighted by:

1.0000	0.8000	0.6000	0.4000	0.2000	0.0000
0.8000	1.0000	0.8000	0.6000	0.4000	0.2000
0.6000	0.8000	1.0000	0.8000	0.6000	0.4000
0.4000	0.6000	0.8000	1.0000	0.8000	0.6000
0.2000	0.4000	0.6000	0.8000	1.0000	0.8000
0.0000	0.2000	0.4000	0.6000	0.8000	1.0000

Agreement	Expected Agreement	Kappa	Std. Err.	Z	Prob>Z
81.67%	74.65%	0.2767	0.1195	2.32	0.0103

. kap q8_1 q8_3, wgt(w)

Ratings weighted by:

1.0000	0.8333	0.6667	0.5000	0.3333	0.1667	0.0000
0.8333	1.0000	0.8333	0.6667	0.5000	0.3333	0.1667
0.6667	0.8333	1.0000	0.8333	0.6667	0.5000	0.3333
0.5000	0.6667	0.8333	1.0000	0.8333	0.6667	0.5000
0.3333	0.5000	0.6667	0.8333	1.0000	0.8333	0.6667
0.1667	0.3333	0.5000	0.6667	0.8333	1.0000	0.8333
0.0000	0.1667	0.3333	0.5000	0.6667	0.8333	1.0000

Agreement	Expected Agreement	Kappa	Std. Err.	Z	Prob>Z

```
------------------------------------------------------------------
 31.25%     31.25%    0.0000    0.0000        .         .

. kap q8_2 q8_3, wgt(w)

Ratings weighted by:
  1.0000  0.7500  0.5000  0.2500  0.0000
  0.7500  1.0000  0.7500  0.5000  0.2500
  0.5000  0.7500  1.0000  0.7500  0.5000
  0.2500  0.5000  0.7500  1.0000  0.7500
  0.0000  0.2500  0.5000  0.7500  1.0000

         Expected
Agreement   Agreement    Kappa   Std. Err.      Z    Prob>Z
------------------------------------------------------------------
 29.17%     29.17%    0.0000    0.0000      0.00     0.5000

. kap q9_1 q9_2, wgt(w)

Ratings weighted by:
  1.0000  0.8000  0.6000  0.4000  0.2000  0.0000
  0.8000  1.0000  0.8000  0.6000  0.4000  0.2000
  0.6000  0.8000  1.0000  0.8000  0.6000  0.4000
  0.4000  0.6000  0.8000  1.0000  0.8000  0.6000
  0.2000  0.4000  0.6000  0.8000  1.0000  0.8000
  0.0000  0.2000  0.4000  0.6000  0.8000  1.0000

         Expected
Agreement   Agreement    Kappa   Std. Err.      Z    Prob>Z
------------------------------------------------------------------
 75.83%     75.83%    0.0000    0.0000        .         .

. kap q9_1 q9_3, wgt(w)

Ratings weighted by:
  1.0000  0.6667  0.3333  0.0000
  0.6667  1.0000  0.6667  0.3333
  0.3333  0.6667  1.0000  0.6667
  0.0000  0.3333  0.6667  1.0000

         Expected
Agreement   Agreement    Kappa   Std. Err.      Z    Prob>Z
------------------------------------------------------------------
 33.33%     33.33%    0.0000        .         .         .
```

```
. kap q9_2 q9_3, wgt(w)

Ratings weighted by:
  1.0000  0.5000  0.0000
  0.5000  1.0000  0.5000
  0.0000  0.5000  1.0000

         Expected
Agreement  Agreement    Kappa  Std. Err.      Z    Prob>Z
------------------------------------------------------------------
 16.67%    16.67%    0.0000        .        .        .

. kap q10_1 q10_2, wgt(w)

Ratings weighted by:
  1.0000  0.8000  0.6000  0.4000  0.2000  0.0000
  0.8000  1.0000  0.8000  0.6000  0.4000  0.2000
  0.6000  0.8000  1.0000  0.8000  0.6000  0.4000
  0.4000  0.6000  0.8000  1.0000  0.8000  0.6000
  0.2000  0.4000  0.6000  0.8000  1.0000  0.8000
  0.0000  0.2000  0.4000  0.6000  0.8000  1.0000

         Expected
Agreement  Agreement    Kappa  Std. Err.      Z    Prob>Z
------------------------------------------------------------------
 56.67%    48.96%    0.1510    0.0737     2.05    0.0202

. kap q10_1 q10_, wgt(w)
q10_ ambiguous abbreviation
r(111);

. kap q10_1 q10_3, wgt(w)

Ratings weighted by:
  1.0000  0.6667  0.3333  0.0000
  0.6667  1.0000  0.6667  0.3333
  0.3333  0.6667  1.0000  0.6667
  0.0000  0.3333  0.6667  1.0000

         Expected
Agreement  Agreement    Kappa  Std. Err.      Z    Prob>Z
------------------------------------------------------------------
 33.33%    33.33%    0.0000        .        .        .
```

```
. kap q10_2 q10_3, wgt(w)

Ratings weighted by:
  1.0000  0.6667  0.3333  0.0000
  0.6667  1.0000  0.6667  0.3333
  0.3333  0.6667  1.0000  0.6667
  0.0000  0.3333  0.6667  1.0000

         Expected
Agreement  Agreement    Kappa  Std. Err.      Z    Prob>Z
------------------------------------------------------------------
 33.33%    33.33%    0.0000        .       .        .

. kap q11_1 q11_2, wgt(w)

Ratings weighted by:
  1.0000  0.8000  0.6000  0.4000  0.2000  0.0000
  0.8000  1.0000  0.8000  0.6000  0.4000  0.2000
  0.6000  0.8000  1.0000  0.8000  0.6000  0.4000
  0.4000  0.6000  0.8000  1.0000  0.8000  0.6000
  0.2000  0.4000  0.6000  0.8000  1.0000  0.8000
  0.0000  0.2000  0.4000  0.6000  0.8000  1.0000

         Expected
Agreement  Agreement    Kappa  Std. Err.      Z    Prob>Z
------------------------------------------------------------------
 40.00%    39.93%    0.0012    0.0054      0.21     0.4157

. kap q11_1 q11_3, wgt(w)

Ratings weighted by:
  1.0000  0.6667  0.3333  0.0000
  0.6667  1.0000  0.6667  0.3333
  0.3333  0.6667  1.0000  0.6667
  0.0000  0.3333  0.6667  1.0000

         Expected
Agreement  Agreement    Kappa  Std. Err.      Z    Prob>Z
------------------------------------------------------------------
 33.33%    33.33%    0.0000        .       .        .

. kap q11_2 q11_3, wgt(w)
```

```
Ratings weighted by:
  1.0000  0.6667  0.3333  0.0000
  0.6667  1.0000  0.6667  0.3333
  0.3333  0.6667  1.0000  0.6667
  0.0000  0.3333  0.6667  1.0000

           Expected
Agreement   Agreement    Kappa   Std. Err.      Z    Prob>Z
------------------------------------------------------------------
  33.33%     33.33%    0.0000        .        .        .

. kap q12_1 q12_2, wgt(w)

Ratings weighted by:
  1.0000  0.7500  0.5000  0.2500  0.0000
  0.7500  1.0000  0.7500  0.5000  0.2500
  0.5000  0.7500  1.0000  0.7500  0.5000
  0.2500  0.5000  0.7500  1.0000  0.7500
  0.0000  0.2500  0.5000  0.7500  1.0000

           Expected
Agreement   Agreement    Kappa   Std. Err.      Z    Prob>Z
------------------------------------------------------------------
  83.65%     75.52%    0.3323    0.1027     3.24    0.0006

. kap q12_1 q12_3, wgt(w)

Ratings weighted by:
  1.0000  0.7500  0.5000  0.2500  0.0000
  0.7500  1.0000  0.7500  0.5000  0.2500
  0.5000  0.7500  1.0000  0.7500  0.5000
  0.2500  0.5000  0.7500  1.0000  0.7500
  0.0000  0.2500  0.5000  0.7500  1.0000

           Expected
Agreement   Agreement    Kappa   Std. Err.      Z    Prob>Z
------------------------------------------------------------------
  85.00%     75.24%    0.3942    0.1015     3.88    0.0001

. kap q12_2 q12_3, wgt(w)

Ratings weighted by:
  1.0000  0.7500  0.5000  0.2500  0.0000
  0.7500  1.0000  0.7500  0.5000  0.2500
```

```
  0.5000   0.7500   1.0000   0.7500   0.5000
  0.2500   0.5000   0.7500   1.0000   0.7500
  0.0000   0.2500   0.5000   0.7500   1.0000

         Expected
Agreement   Agreement    Kappa   Std. Err.      Z    Prob>Z
------------------------------------------------------------------
 83.00%     76.84%    0.2660    0.1276      2.08     0.0185
. kap q14_1 q14_2, wgt(w)

Ratings weighted by:
  1.0000   0.5000   0.0000
  0.5000   1.0000   0.5000
  0.0000   0.5000   1.0000

         Expected
Agreement   Agreement    Kappa   Std. Err.      Z    Prob>Z
------------------------------------------------------------------
 50.00%     43.75%    0.1111    0.1667      0.67     0.2525

. kap q14_1 q14_3, wgt(w)

Ratings weighted by:
  1.0000   0.5000   0.0000
  0.5000   1.0000   0.5000
  0.0000   0.5000   1.0000

         Expected
Agreement   Agreement    Kappa   Std. Err.      Z    Prob>Z
------------------------------------------------------------------
 50.00%     43.75%    0.1111    0.1667      0.67     0.2525

. kap q14_2 q14_3, wgt(w)

Ratings weighted by:
  1.0000   0.5000   0.0000
  0.5000   1.0000   0.5000
  0.0000   0.5000   1.0000

         Expected
Agreement   Agreement    Kappa   Std. Err.      Z    Prob>Z
------------------------------------------------------------------
 75.00%     56.25%    0.4286    0.4103      1.04     0.1481
```

. kap q15_1 q14_2, wgt(w)

Ratings weighted by:

1.0000	0.6667	0.3333	0.0000
0.6667	1.0000	0.6667	0.3333
0.3333	0.6667	1.0000	0.6667
0.0000	0.3333	0.6667	1.0000

Agreement	Expected Agreement	Kappa	Std. Err.	Z	Prob>Z
41.67%	41.67%	0.0000	.	.	.

. kap q15_1 q15_2, wgt(w)

Ratings weighted by:

1.0000	0.8000	0.6000	0.4000	0.2000	0.0000
0.8000	1.0000	0.8000	0.6000	0.4000	0.2000
0.6000	0.8000	1.0000	0.8000	0.6000	0.4000
0.4000	0.6000	0.8000	1.0000	0.8000	0.6000
0.2000	0.4000	0.6000	0.8000	1.0000	0.8000
0.0000	0.2000	0.4000	0.6000	0.8000	1.0000

Agreement	Expected Agreement	Kappa	Std. Err.	Z	Prob>Z
79.26%	70.53%	0.2961	0.1128	2.62	0.0043

. kap q15_1 q15_3, wgt(w)

Ratings weighted by:

1.0000	0.8571	0.7143	0.5714	0.4286	0.2857	0.1429	0.0000
0.8571	1.0000	0.8571	0.7143	0.5714	0.4286	0.2857	0.1429
0.7143	0.8571	1.0000	0.8571	0.7143	0.5714	0.4286	0.2857
0.5714	0.7143	0.8571	1.0000	0.8571	0.7143	0.5714	0.4286
0.4286	0.5714	0.7143	0.8571	1.0000	0.8571	0.7143	0.5714
0.2857	0.4286	0.5714	0.7143	0.8571	1.0000	0.8571	0.7143
0.1429	0.2857	0.4286	0.5714	0.7143	0.8571	1.0000	0.8571
0.0000	0.1429	0.2857	0.4286	0.5714	0.7143	0.8571	1.0000

Agreement	Expected Agreement	Kappa	Std. Err.	Z	Prob>Z
81.63%	76.06%	0.2329	0.1035	2.25	0.0122

. kap q15_2 q15_3, wgt(w)

Ratings weighted by:

1.0000	0.8571	0.7143	0.5714	0.4286	0.2857	0.1429	0.0000
0.8571	1.0000	0.8571	0.7143	0.5714	0.4286	0.2857	0.1429
0.7143	0.8571	1.0000	0.8571	0.7143	0.5714	0.4286	0.2857
0.5714	0.7143	0.8571	1.0000	0.8571	0.7143	0.5714	0.4286
0.4286	0.5714	0.7143	0.8571	1.0000	0.8571	0.7143	0.5714
0.2857	0.4286	0.5714	0.7143	0.8571	1.0000	0.8571	0.7143
0.1429	0.2857	0.4286	0.5714	0.7143	0.8571	1.0000	0.8571
0.0000	0.1429	0.2857	0.4286	0.5714	0.7143	0.8571	1.0000

Agreement	Expected Agreement	Kappa	Std. Err.	Z	Prob>Z
81.77%	76.71%	0.2174	0.1083	2.01	0.0223

. kap q16_1 q16_2, wgt(w)

Ratings weighted by:

1.0000	0.8000	0.6000	0.4000	0.2000	0.0000
0.8000	1.0000	0.8000	0.6000	0.4000	0.2000
0.6000	0.8000	1.0000	0.8000	0.6000	0.4000
0.4000	0.6000	0.8000	1.0000	0.8000	0.6000
0.2000	0.4000	0.6000	0.8000	1.0000	0.8000
0.0000	0.2000	0.4000	0.6000	0.8000	1.0000

Agreement	Expected Agreement	Kappa	Std. Err.	Z	Prob>Z
74.74%	68.09%	0.2083	0.0993	2.10	0.0179

. kap q16_1 q16_3, wgt(w)

Ratings weighted by:

1.0000	0.8000	0.6000	0.4000	0.2000	0.0000
0.8000	1.0000	0.8000	0.6000	0.4000	0.2000
0.6000	0.8000	1.0000	0.8000	0.6000	0.4000
0.4000	0.6000	0.8000	1.0000	0.8000	0.6000
0.2000	0.4000	0.6000	0.8000	1.0000	0.8000
0.0000	0.2000	0.4000	0.6000	0.8000	1.0000

Expected

```
Agreement   Agreement    Kappa   Std. Err.      Z    Prob>Z
------------------------------------------------------------------
  76.67%     72.96%    0.1370    0.0693      1.98     0.0240

. kap q16_2 q16_3, wgt(w)

Ratings weighted by:
  1.0000  0.8333  0.6667  0.5000  0.3333  0.1667  0.0000
  0.8333  1.0000  0.8333  0.6667  0.5000  0.3333  0.1667
  0.6667  0.8333  1.0000  0.8333  0.6667  0.5000  0.3333
  0.5000  0.6667  0.8333  1.0000  0.8333  0.6667  0.5000
  0.3333  0.5000  0.6667  0.8333  1.0000  0.8333  0.6667
  0.1667  0.3333  0.5000  0.6667  0.8333  1.0000  0.8333
  0.0000  0.1667  0.3333  0.5000  0.6667  0.8333  1.0000

           Expected
Agreement   Agreement    Kappa   Std. Err.      Z    Prob>Z
------------------------------------------------------------------
  76.19%     68.93%    0.2336    0.1071      2.18     0.0146

. kap q19_1 q19_2, wgt(w)

Ratings weighted by:
  1.0000  0.0000
  0.0000  1.0000

           Expected
Agreement   Agreement    Kappa   Std. Err.      Z    Prob>Z
------------------------------------------------------------------
  50.00%     50.00%    0.0000    0.0000       .        .

. kap q17_1 q17_2, wgt(w)

Ratings weighted by:
  1.0000  0.5000  0.0000
  0.5000  1.0000  0.5000
  0.0000  0.5000  1.0000

           Expected
Agreement   Agreement    Kappa   Std. Err.      Z    Prob>Z
------------------------------------------------------------------
  51.92%     53.70%   -0.0383    0.0501     -0.77     0.7781

. kap q17_1 q17_3, wgt(w)
```

Ratings weighted by:

1.0000 0.5000 0.0000

0.5000 1.0000 0.5000

0.0000 0.5000 1.0000

Agreement	Expected Agreement	Kappa	Std. Err.	Z	Prob>Z
51.92%	51.92%	0.0000	0.0000	.	.

. kap q17_2 q17_3, wgt(w)

Ratings weighted by:

1.0000 0.0000

0.0000 1.0000

Agreement	Expected Agreement	Kappa	Std. Err.	Z	Prob>Z
92.31%	92.31%	0.0000	0.0000	0.00	0.5000

. kap q19_1 q19_3, wgt(w)

Ratings weighted by:

1.0000 0.0000

0.0000 1.0000

Agreement	Expected Agreement	Kappa	Std. Err.	Z	Prob>Z
0.00%	0.00%	0.0000	0.0000	.	.

. kap q19_2 q19_3, wgt(w)

Ratings weighted by:

1.0000 0.0000

0.0000 1.0000

Agreement	Expected Agreement	Kappa	Std. Err.	Z	Prob>Z
50.00%	50.00%	0.0000	0.0000	.	.

```
. kap q20_1 q20_2, wgt(w)

Ratings weighted by:
  1.0000  0.5000  0.0000
  0.5000  1.0000  0.5000
  0.0000  0.5000  1.0000

         Expected
Agreement   Agreement    Kappa   Std. Err.      Z    Prob>Z
------------------------------------------------------------------
  86.00%     73.52%    0.4713    0.1691     2.79    0.0027

. kap q20_1 q20_3, wgt(w)

Ratings weighted by:
  1.0000  0.5000  0.0000
  0.5000  1.0000  0.5000
  0.0000  0.5000  1.0000

         Expected
Agreement   Agreement    Kappa   Std. Err.      Z    Prob>Z
------------------------------------------------------------------
  88.46%     74.85%    0.5412    0.1661     3.26    0.0006

. kap q20_2 q20_3, wgt(w)

Ratings weighted by:
  1.0000  0.5000  0.0000
  0.5000  1.0000  0.5000
  0.0000  0.5000  1.0000

         Expected
Agreement   Agreement    Kappa   Std. Err.      Z    Prob>Z
------------------------------------------------------------------
  81.03%     71.28%    0.3395    0.1522     2.23    0.0129

. kap q21_1 q21_2, wgt(w)

Ratings weighted by:
  1.0000  0.5000  0.0000
  0.5000  1.0000  0.5000
  0.0000  0.5000  1.0000
```

```
         Expected
Agreement   Agreement    Kappa   Std. Err.      Z    Prob>Z
------------------------------------------------------------------
  78.95%     65.93%    0.3821    0.1545     2.47    0.0067
```

. kap q21_1 q21_3, wgt(w)

Ratings weighted by:

```
  1.0000   0.5000   0.0000
  0.5000   1.0000   0.5000
  0.0000   0.5000   1.0000
```

```
         Expected
Agreement   Agreement    Kappa   Std. Err.      Z    Prob>Z
------------------------------------------------------------------
  84.21%     65.93%    0.5366    0.1545     3.47    0.0003
```

. kap q21_2 q21_3, wgt(w)

Ratings weighted by:

```
  1.0000   0.0000
  0.0000   1.0000
```

```
         Expected
Agreement   Agreement    Kappa   Std. Err.      Z    Prob>Z
------------------------------------------------------------------
  72.73%     56.20%    0.3774    0.2086     1.81    0.0352
```

Appendix 4 A comparison between two methods to estimate the degree of angulation for rotation, kyphosis and lordosis on 17 mobile chest radiographs

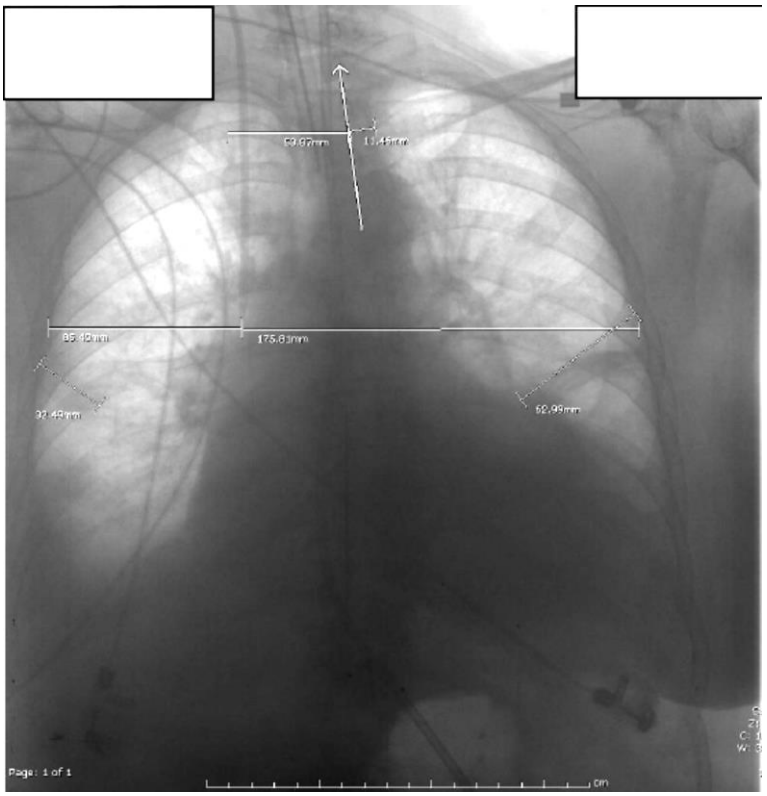

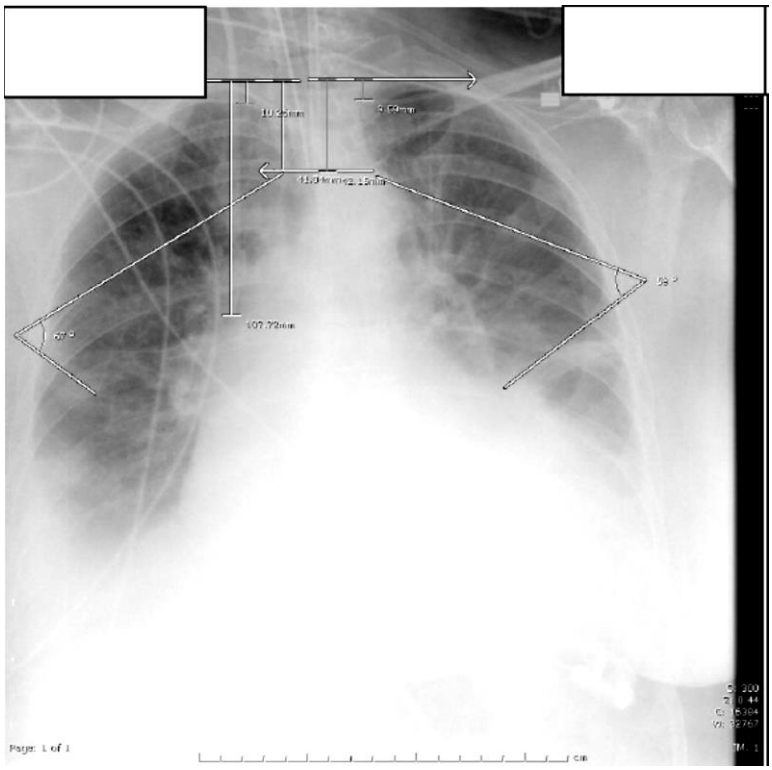

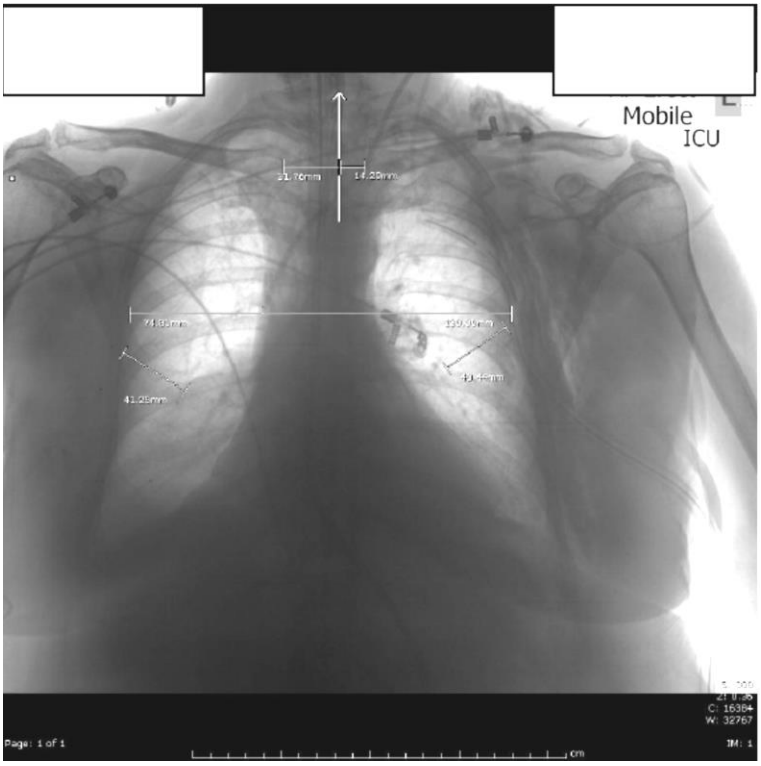
Mobile
ICU
Page: 1 of 1

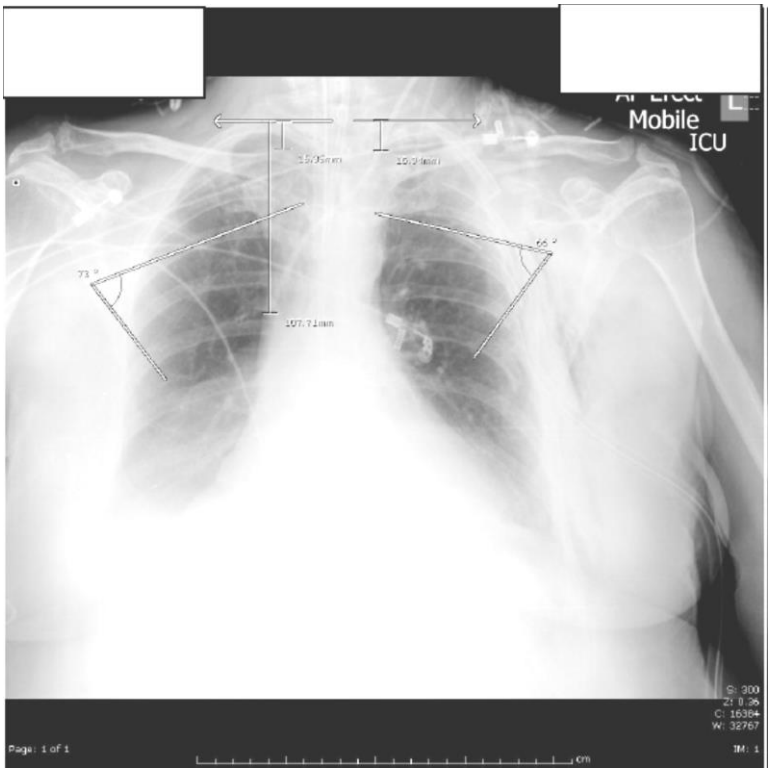
Mobile
ICU
73 °
Page: 1 of 1

Correlation coefficient output between the two methods (rotation/kyphosis/lordosis)

```
regress clavicle_sp_estimated_angle fourth_rib_angle_estimated_angle if image~=4

      Source |       SS       df       MS              Number of obs =      16
-------------+------------------------------           F(  1,    14) =    6.17
       Model |  102.854158     1  102.854158            Prob > F      =  0.0263
    Residual |  233.385825    14  16.6704161            R-squared     =  0.3059
-------------+------------------------------           Adj R-squared =  0.2563
       Total |  336.239984    15  22.4159989            Root MSE      =  4.0829

------------------------------------------------------------------------------
clavicle_sp_estimated_angle |      Coef.   Std. Err.      t    P>|t|     [95% Conf. Interval]
------------------------------------+-----------------------------------------------------------
fourth_rib_angle_estimated_angle |  -.2669831   .1074845    -2.48   0.026    -.4975145   -.0364517
                   _cons |   3.780299   1.410979     2.68   0.018     .7540505    6.806548
------------------------------------------------------------------------------


. generate adiff= clavicle_sp_estimated_angle- fourth_rib_length_estimated_angl

. summarize adiff if image~=4

    Variable |       Obs        Mean    Std. Dev.       Min        Max
-------------+--------------------------------------------------------
       adiff |        16    -1.49375    5.923169     -16.6       7.38

. generate meanangle= (clavicle_sp_estimated_angle+ fourth_rib_length_estimated_angl)/2


. generate meanlka= (clavicle_apex_estimated_angle+ fourth_rib_angle_estimated_angle)/2

. generate lkadiff= clavicle_apex_estimated_angle- fourth_rib_angle_estimated_angle

. summarize lkadiff
```

```
   Variable |      Obs       Mean    Std. Dev.       Min        Max
-------------+--------------------------------------------------------
    lkadiff |       17    6.819412    7.570039      -7.1       20.2


regress clavicle_apex_estimated_angle fourth_rib_angle_estimated_angle

      Source |       SS       df       MS              Number of obs =      17
-------------+------------------------------           F(  1,    15) =   34.26
       Model |  2041.15315     1  2041.15315           Prob > F      =  0.0000
    Residual |  893.601106    15  59.5734071           R-squared     =  0.6955
-------------+------------------------------           Adj R-squared =  0.6752
       Total |  2934.75426    16  183.422141           Root MSE      =  7.7184

------------------------------------------------------------------------------
  clavicle_apex_estimated_angle |      Coef.   Std. Err.      t    P>|t|     [95% Conf. Interval]
--------------------------------+---------------------------------------------------------------
fourth_rib_angle_estimated_angle |   1.119584   .1912692     5.85   0.000     .7119033    1.527265
                   _cons |   8.001958   2.661168     3.01   0.009     2.329812    13.6741
------------------------------------------------------------------------------
```

Regression output of the CVC to chest wall ratios and the estimated angle of rotation

```
. regress cvcrat predrat

      Source |       SS       df       MS              Number of obs =      13
-------------+------------------------------           F(  1,    11) =    1.77
       Model |    .2785042     1    .2785042           Prob > F      =  0.2107
    Residual |  1.73380326    11  .157618478           R-squared     =  0.1384
-------------+------------------------------           Adj R-squared =  0.0601
       Total |  2.01230746    12  .167692288           Root MSE      =  .39701

------------------------------------------------------------------------------
      cvcrat |      Coef.   Std. Err.      t    P>|t|     [95% Conf. Interval]
-------------+----------------------------------------------------------------
     predrat |  -4.811371   3.619566    -1.33   0.211    -12.77798    3.155241
       _cons |   8.487518   5.185502     1.64   0.130    -2.925695    19.90073
```

```
------------------------------------------------------------------------------

. regress cvcrat mean_angle

      Source |       SS       df       MS              Number of obs =      13
-------------+------------------------------           F(  1,    11) =    1.73
       Model |  .273161092     1  .273161092           Prob > F      =  0.2154
    Residual |  1.73914637    11  .158104215           R-squared     =  0.1357
-------------+------------------------------           Adj R-squared =  0.0572
       Total |  2.01230746    12  .167692288           Root MSE      =  .39762

------------------------------------------------------------------------------
      cvcrat |      Coef.   Std. Err.      t    P>|t|     [95% Conf. Interval]
-------------+----------------------------------------------------------------
  mean_angle |   .0332075   .0252638     1.31   0.215    -.0223977    .0888127
       _cons |   1.351159   .2165699     6.24   0.000     .8744919    1.827826
------------------------------------------------------------------------------
```

Regression output of the CVC/ETT to chest wall ratios and the estimated angle of kyphosis/lordosis

```
. regress cvc_apex mean_angle

      Source |       SS       df       MS              Number of obs =      13
-------------+------------------------------           F(  1,    11) =    0.00
       Model |  .197634872     1  .197634872           Prob > F      =  0.9695
    Residual |  1424.52352    11  129.502138           R-squared     =  0.0001
-------------+------------------------------           Adj R-squared = -0.0908
       Total |  1424.72116    12  118.726763           Root MSE      =   11.38

------------------------------------------------------------------------------
    cvc_apex |      Coef.   Std. Err.      t    P>|t|     [95% Conf. Interval]
-------------+----------------------------------------------------------------
  mean_angle |    .010875   .2783794     0.04   0.970    -.6018339    .6235839
       _cons |    111.708   3.463427    32.25   0.000     104.0851     119.331
------------------------------------------------------------------------------
```

```
. regress ett_apex_mean mean_angle

      Source |       SS       df       MS              Number of obs =       5
-------------+------------------------------           F(  1,     3) =    3.04
       Model |  580.230658     1  580.230658            Prob > F      =  0.1795
    Residual |  572.377419     3  190.792473            R-squared     =  0.5034
-------------+------------------------------           Adj R-squared =  0.3379
       Total |  1152.60808     4  288.152019            Root MSE      =  13.813

------------------------------------------------------------------------------
ett_apex_m~n |      Coef.   Std. Err.      t    P>|t|     [95% Conf. Interval]
-------------+----------------------------------------------------------------
  mean_angle |  -.8163697   .4681307    -1.74   0.180    -2.306171    .6734312
       _cons |   49.49412    6.42571     7.70   0.005     29.04465     69.9436
------------------------------------------------------------------------------
```

Appendix 5 Ethical approval:

CXR images - ethical consideration

Snaith Beverley <Bev.Snaith@midyorks.nhs.uk>

Thu 1/24/2013 8:17 PM

To: a.j.scally@bradford.ac.uk <a.j.scally@bradford.ac.uk>; a.m.b.elhain@bradford.ac.uk <a.m.b.elhain@bradford.ac.uk>;

Hi Andy/Ahmed

I've spoken to Jane in R&D and no issue about sharing the images so long as they are anonymised. I'm off on Monday but will get in touch Tuesday to confirm mobile here and that we are acquiring images. Can I see a copy a copy of the draft protocol before next week?

Bev

Bev Snaith

Lead Consultant Radiographer (Emergency Care)

Mid Yorkshire Hospitals NHS Trust

Tel Ext 52296 - 01924 542296 (secretary 01924 541605)

Blackberry 07712499794

Email bev.snaith@midyorks.nhs.uk